UCLouvain

epl

École polytechnique de Louvain

Coupling of Carnot Batteries with Electrolysers

Using a Dual-Source Heat Pump to Enhance Profitability

Author: **Mathis Collot**
Supervisor: **Francesco Contino**
Readers: **Yann Bartosiewicz, Antoine Laterre**
Academic year 2023–2024
Master [120] in Mechanical Engineering

Nomenclature

Abbreviations

AWE alkaline water electrolyser

$CAPEX$ capital expenditure

CB Carnot battery

COP coefficient of performance

$DSHP$ dual-source heat pump

GWP global warming potential

HE heat engine

HP heat pump

ODP ozone depletion potential

$OPEX$ operational expenditure

ORC organic Rankine cycle

PEM polymer electrolyte membrane

$PTES$ pumped thermal energy storage

PV photovoltaic

RE renewable energy

SOE solide oxide electrolyser

TES thermal energy storage

$TI-PTES$ thermally integrated-pumped thermal energy storage

$VCHP$ vapor compressed heat pump

Greek and Latin letters

ΔT temperature variation [K]

η efficiency [-]

ρ density [kWh/m^3]

e exergy [J/kg]

h enthalpy [J/kg]

m mass [kg]

p pressure [Pa]

s entropy [J/K.kg]

T temperature [K]

u speed [m/s]

Sub- and superscripts

c compressor

cd condensor

d diffuser

el electrical

$electro$ electrolyser

ev evaporator

is isentropic

mix mixing

n nozzle

$P2P$ power-to-power

p pump

Pf primary fluid

ref reference

Sf secondary fluid

sp spread

st storage

t turbine

th thermal

wh waste heat

Acknowledgments

I would like to extend my sincere gratitude to all those who have supported and guided me throughout this master thesis.

My first thanks go to my supervisor, Prof. Francesco Contino. Your advice, constant availability, and deep expertise have been crucial to the successful completion of this project.

I am also sincerely thankful to my mentor, Antoine Laterre. Your extensive experience and thoughtful guidance have been helpful. Thank you for your valuable support and advice.

I would like to extend my sincere appreciation to the department of mechanical engineering for the high quality of education and the support provided over the years.

Lastly, I am deeply grateful to my reviewers for their valuable contribution to improving this work. Their suggestions were much appreciated.

To all, thank you.

Abstract

In the future, limiting greenhouse gas emissions will be crucial. To address this, there is a strong emphasis on green production methods. For industrial processes that generate waste heat, integrating a Carnot battery with thermal integration (i.e., TI-PTES) appears to be a promising and pertinent choice. However, the main challenge is the current inability of TI-PTES to generate sufficient electricity to make their use economically viable. The main objective of this master thesis was to increase the energy and economic profitability of a Carnot battery coupled to an industrial process (i.e., electrolyser) that rejects a limited amount of waste heat and is powered exclusively by a renewable energy source. To meet this objective, we set out to demonstrated that a Dual-source heat pump (DSHP) could be a viable solution. An analysis and comparison of several promising DSHP was conducted to select the most energy-efficient one. Subsequently, an energetic and economic comparison of the coupling in its ideal configuration (i.e., DSHP with the highest COP) was carried out to assess the competitiveness of a Carnot battery compared to a lithium battery and a fuel cell. The DSHP configuration with the highest COP was the series connection of two DSHPs with open economizers. The energy comparison showed that the Carnot battery was close to the lithium battery in low demand scenarios. Economically, CAPEX in the range of [500;557] €/kW, [8;9.3] €/kWh, and [600;755] €/kW for the HP, TES and ORC respectively are needed to match the production cost of a lithium battery. While the results do not definitively determine the real profitability of the coupling, they identify the DSHP configurations that should be favored to improve the production rate and outline the CAPEX targets for the Carnot battery components needed to compete economically.

Contents

Chapter 1

Context and objectives

1.0 Thermally integrated Carnot battery and electrolysers : A judicious coupling ?

In today's industrial processes, many industries dissipate low-temperature heat into the environment, representing a direct loss of potentially valuable energy, which, depending on process efficiency, can amount to significant revenue loss. While some industries manage to reuse this heat for secondary purposes (residential heating, pool heating), this practice remains rare and often site-specific, as local demand seldom aligns with supply.

With the gradual transition towards widespread use of renewable energies, there is an need to address the crucial challenge of storing this intermittent energy. This need is particularly pressing in the context of industrial systems exclusively powered by these renewable sources, where energy availability does not always coincide with demand, and frequent fluctuations undermine the reliability, efficiency, and productivity of these systems.

It is in this context that the Carnot battery (CB) stands out as a promising solution. Indeed, this technology enables the storage of electricity in the form of thermal energy, thereby offering the possibility of converting it into electrical energy later on. Furthermore, it provides the capability to recover the low-temperature waste heat.

Although there are many industrial processes producing a significant amount of waste heat, electrolysers seem to be a particularly well-suited process for coupling with a Carnot battery.
Electrolysers represent a well-established and widely adopted technology in indus-

trial settings. Moreover, their prevalence is expected to increase further due to their ability to produce green hydrogen (see section 1.0 for further information). It's worth noting that hydrogen is a future-oriented clean energy vector with numerous potential applications (ammonia production, fuel for mobility, etc.)[1]. These electrolysers boast efficiencies, around 70% for the most common industrial technologies [11], implying that slightly under 30% of the consumed power is typically lost.
The difficulty encountered in industrial systems when it comes to recovering heat lies in how to do so without compromising system performance. However, in the case of electrolysers, the heat is in the form of hot water and must be expelled for their proper operation. Consequently, it can be easily recoverable and at low cost. This inherent characteristic makes electrolysers an attractive option for the coupling with a Carnot battery and this process will be considered in this work.
It should be noted that the choice of industrial process delivering the waste heat is not a determining variable for the majority of the results obtained in Chapter 3. They can easily be transposed to other industrial processes.

2.0 Issues and challenges involved in coupling a Ti-PTES to electrolysers

TI-PTES consists of 3 sub-systems: a heat pump (HP), a thermal storage system (TES) and an heat engine cycle. Taking the coupling shown in Figure 1.1 but considering only a single-source HP, this HP will capture the waste heat ($T \approx 75$°C) to release heat at a higher temperature set by the temperature of the TES hot tank ($T \approx 110$°C), which will be transmitted to the TES. The stored heat is then captured by the heat engine cycle and used to generate electricity.

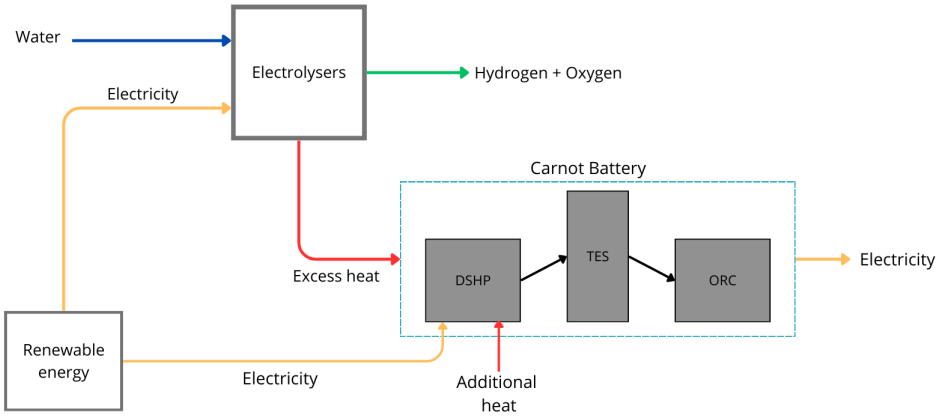

Figure 1.1: Schema of the coupling of a Carnot battery integrating a dual-source heat pump (DSHP) to an electrolyser system

In this case, as the HP captures a fixed heat flow (i.e waste heat flow) and achieves a given temperature lift, it can only transmit a limited heat flow to the TES. For illustration purpose, let's consider: (i) an electrolyser efficiency $\eta_{electro}$ of 0.7 (see 1.0); (ii) an organic Rankine cycle as heat engine cycle with an efficiency η_{ORC} of 0.105; (iii) the ratio between the heat produced by the HP and the heat captured by the HP ($\frac{Q_{produced}}{Q_{wh}}$) of 1.22 (these last two values are calculated on the basis of a hot storage temperature of 107°C); (iv) a TES efficiency of 1, the battery output power P_{out} is given by :

$$P_{out} \sim (1 - \eta_{electro}) \cdot P_{electro} \cdot \frac{Q_{produced}}{Q_{wh}} \cdot \eta_{ORC} = 0.038 \cdot P_{electro} \tag{1.1}$$

It appears that the energy produced by the CB is low or negligible (3.8% of $P_{electro}$) compared to that used by electrolysers. Therefore, the impact of using CB within the coupling will be too small to economically justify its use. One way of countering this limitation would be to use an HP capable of integrating a second heat source called a dual-source heat pump (DSHP). In this way, a larger heat flow could be transmitted to the TES, which would enable a significant amount of electricity to be converted compared with that consumed by the electrolysers. This will enable it to play a more significant role in the coupling and would therefore be more profitable.

3.0 Research objective and thesis organisation

Many different DSHP configurations currently exist, each with its own distinct characteristics. However, to the best of the author's knowledge, no study has yet looked at the comparison of several DSHP, with or without a source of heat normally lost. It is therefore impossible to know which DSHP has the best performance or even to compare the sensitivity of their performance.

In order to fill this gap, the thesis will be devoted to answer the following research question :

"What is the energy and financial efficiency of a Carnot battery coupled to an hydrogen production system using polymer electrolyte membrane?"

from which a sub-question arises :

"What dual-source heat pump configuration will maximise the efficiencies of the Carnot battery?"

To try to answer this question, this master thesis will follow a structured approach, which will begin with a review of the literature on the various components present in the coupling (electrolysers, CB, HP, TES, heat engine cycle) (Chapter 2).

In a second step, the specifications that the DSHP will have to respect in this study will be presented and the different configurations of selected DSHP will be described individually. A thermodynamic modeling of these DSHP and heat engine cycle will be proposed. The purpose of this study will be to compare the different DSHP and to analyze the sensitivity of their performance (Chapter 3).

In a third step, an energy and economic comparison between different storage technologies will be presented in a given application case. The aim will be to demonstrate and discuss the level of energy and economic competitiveness of the Carnot battery in a given situation. (Chapter 4).

Finally, the key points of this master thesis will be highlighted and last perspectives for future work will be discussed in Chapter 5.

Chapter 2

Literature review

Within this section, a literature-based review on the various types of technologies for the main components of the previously presented coupling will be conducted. This review will aim to highlight the current state of knowledge available to us and will motivate the choice of technologies considered for the coupling components in the remainder of the study.

1.0 Water electrolysis

There are currently several processes available on the market capable of producing hydrogen. In the majority of these processes (96%) [50], the energy source used comes from hydrocarbons such as coal, natural gas or liquid hydrocarbons that produce large quantities of greenhouse gases. Only 4% [50] of world production is based on the use of water electrolysis, the main obstacle being its production cost. Water electrolysis is the best-known and most widespread way of producing green hydrogen. Please, note that hydrogen is considered as "green" when it is produced entirely from a renewable energy source. However, as part of the drive to reduce global greenhouse gas emissions, a number of agencies (notably ADEME and IRENA)[75] are encouraging industries to produce more plants on a larger scale in order to cut production costs which encourages us even more to consider this industrial process for this work.

The electrolysis of water is a process during which a direct electric current passing through electrodes dissociates the water into hydrogen and oxygen. Water electrolysis is a process in which a direct electric current passing through electrodes dissociates the water into hydrogen and oxygen by means of a redox reaction.

$$H_2O_l + direct\ current \rightarrow H_{2,g} + \frac{1}{2}O_{2,g} + heat \tag{2.1}$$

This reaction is carried out in a cell consisting of an anode, a cathode and an electrolyte (i.e. conductive susbtance) which conduct ions. Hydrogen is produced and recovered at the cathode and oxygen at the anode. Each cell can be connected in series or in parallel to form a electrolyser module also called 'stacks'. The size and power of the electrolyser will thus depend on the number of cells and modules used[50].
The electrolysers will need a supply of water to function. This water will have to undergo a purification treatment beforehand and or a desalination if the water comes from the sea. In addition, the electrolysis process is exothermic which means that a thermal evacuation system must be installed.
Apart from the fact that electrolyser allows the production of hydrogen, It also has the benefit of having no moving parts, which reduces its maintenance cost, being not dependent on a specific location and having a greater hydrogen production rate with high purity[11], [83]. As mentioned in articles [83], [50], there are 3 main types of water electrolysis that are the most widespread or promising technology: the alkaline water electrolysers (AWE), the Polymer electrolyte membrane electrolysers (PME) and the solid oxide electrolysers(SOEs). Their main characteristics are listed in the comparative table 2.1

Specification	Unit	AWE	PME	SOEs
Technology maturity	-	State of the art	Demonstration	R & D
Cell temperature	°C	60-80	70-80	900-1000
Efficiency	%	62-80	67-82	81-86
SEC[1]	kWh/Nm^3	4.5–7.0	4.5–7.5	2.5–3.5
Cell pressure	bar	≤ 30	≤ 30	≤ 30
System life time	year	20-30	10-20	-
hydrogen purity.	%	≥99.8	99.999	–
Cold start up time	min.	15	≤15	≥60
Partial load range	%	20–40	0–10	–
Feed-in	-	KOH + H2O	H2O	H2O
CAPEX	€/kW	800-1300 [76]	1000-1950[76]	2000-2800[69]

Most of the data compiled from [11]
[1] Specific energy consumption

Table 2.1: Main specifications of electrolysis solutions

1.1 Alkaline water electrolysers (AWE)

Inside a AWE, the water is reduced to the level of the cathode to produce hydrogen and ions OH^-. The application of a continuous current to the terminals of the electrodes generates an electric field which displaces the OH^- ions within the

electrolyte towards the anode where it will recombine to produce oxygen.

$$Anode: \ 2OH^- \longrightarrow \frac{1}{2}O_2 + H_2O + 2e^- \tag{2.2}$$

$$Cathode: \ 2H_2O + 2e- \longrightarrow H_2 + 2OH^- \tag{2.3}$$

$$Overall: \ H_2O \longrightarrow \frac{1}{2}O_2 + H_2 \tag{2.4}$$

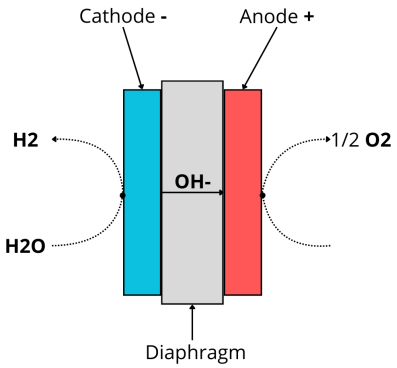

Figure 2.1: Schematic illustration of an Alkaline water electrolysers. Inspired by [83]

Alkaline water electrolyser as its name suggests uses a liquid alkaline solution as electrolyte that is usually a highly concentrated aqueous solution of potassium hydroxide KOH (25–30 %) to avoid corrosion and maximize conductivity of ions [11].

Its biggest advantage is to have a low investment cost compared to other technologies making it one of the most used technologies in commercial applications [95],[16].
Reactions can occur either under atmospheric pressure or under pressure (6 to 30 bar). The pressurized version has the advantage to reduce the energy cost of compression in post-processing but in return, the purity of the hydrogen produced is reduced. The cell temperature is typically between 60-80°C with an efficiency between 65-80% and with a investment costs in a range of 800-1300€/kW [11], [76]. Further, the alkaline electrolyser uses durable components which allows longer technical lifetime (20- 30 ans)[23]. Its main disadvantages are: (i) its limited current densities (below 400 mA/cm^2)[11]; (ii) its low operating pressure limited by the membrane which is no longer able to perform its function of being impermeable to gases and low partial load range (between 20-40%)[83]; (iii) it has a low reactivity

to power variations due to the inertia of ion transport in a fluid [78]. Therefore, the AWE is not the optimal technology to be coupled to an intermittent energy source.[50].

1.2 Polymer electrolyte membrane (PEM)

The water dissociation reaction in a PEM begins with the oxidation of H_2O to produce oxygen and H^+ ions (i.e. proton) at the anode. This proton then moves across the membrane to the cathode to reduce and form hydrogen. The reactions are given here under:

$$Anode: \ H_2O \longrightarrow \frac{1}{2}O_2 + 2H^+ + 2e^- \tag{2.5}$$

$$Cathode: \ 2H^+ + 2e^- \longrightarrow H_2 \tag{2.6}$$

$$Overall: \ H_2O \longrightarrow O_2 + 2H_2 \tag{2.7}$$

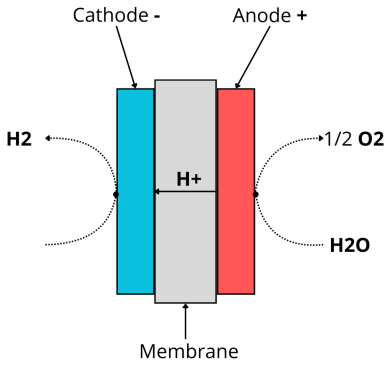

Figure 2.2: Schematic illustration of an polymer electrolyte membrane. Inspired by [83]

The main difference between AWE and PEM is the type of electrolyte used. Where AWE uses liquid solution as electrolyte, PEM uses a gas-tight thin polymer membrane. The use of this solid electrolyte will determine the longevity of the PEM equivalent to 10-20 years, and will allow the use of a wider operating pressure, as well as a consequent reduction in maintenance costs compared to the AWE [23]. The main drawback of this technology is the use of noble metals such as platinum or iridium. They considerably increase the investment cost ($\sim$ 2 times that of AWE), which is currently the main obstacle to its commercial use [11].

However, a major advantage for our application is its ability to operate even with fluctuating power levels. The use of a polymer membrane enables rapid transport of protons, resulting in a lower response time (<1s) than alkaline when faced with power fluctuations. What's more, it produces high-purity hydrogen (99.99%) and accepts a high current density (0.6-2.0), enabling it to remain compact [11].
Despite its high investment cost, this technology has some promising characteristics (high current density accepted, high operating pressure and high operating dynamics) that are motivating research aimed at reducing production costs while maintaining the same efficiency to enable it to be marketed in the near future [100].

As we will consider RE as an energy source, it is necessary that the electrolyser be able to quickly adapt to current intermittences. Based on the above information, we can consider PEM as a good technology choice for this study. In addition, these PEM will operate at atmospheric pressure because, as specified in [30], coupling pressurized electrolysers with intermittent energy sources presents less reliability due to various issues such as increased cross-permeation phenomena, corrosion, hydrogen embrittlement, and a narrower operating range, in contrast to PEM electrolysers operating at atmospheric pressure.

1.3 Solid oxide electrolysers (SOEs)

The solid oxide electrolyser is an advanced technology concept operating at high temperature and pressure and using a solid electrolyte. Water in vapour form is fed to the cathode where it is reduced to produce hydrogen and O^{2-} anions. These anions will pass through the electrolyte to the anode where they will recombine to form oxygen. The reactions are given here under:

$$Anode: \ O^{2-} \longrightarrow \frac{1}{2}O_2 + 2e^- \tag{2.8}$$

$$Cathode: \ H_2O + 2e- \longrightarrow H_2 + O^{2-} \tag{2.9}$$

$$Overall: \ H_2O \longrightarrow \frac{1}{2}O_2 + H_2 \tag{2.10}$$

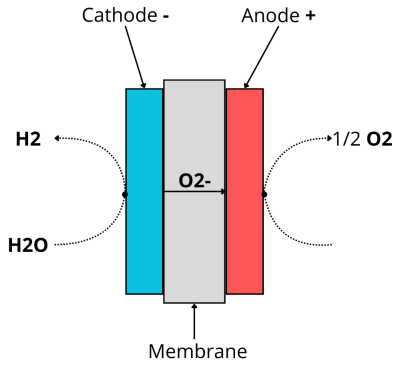

Figure 2.3: Schematic illustration of an solid oxide electrolysers. Inspired by [83]

Although still in the research and development phase, this technology offers better performance (80-90%) than the other two technologies presented and a reasonable investment cost [11]. This is because it dissociates water at high temperature (900-1000°C), which reduces the energy required for molecular decomposition. This allows to avoid the use of noble catalysts (platinum or iridium) and to reduce the electrical energy required to reach the decomposition threshold [50]. As this technology requires a high-temperature heat source, it is mainly intended to be coupled with a system for which a high temperature source is available. Typically, a concentrated solar power system or a high-temperature nuclear reactor. The disadvantages comes from load changes. Indeed, this implies micro-cracks that reduce the electrolyser lifetime and increase the heat losses which make the SOEs not suitable to be coupled with intermittent renewable energy [11].
For all the reasons mentioned above, this technology cannot be considered for our application.

2.0 Carnot battery

A Carnot battery or a pumped thermal electricity storage (PTES) is a type of energy storage system that enables electricity to be stored in the form of thermal energy. During the charging phase, the electricity is used to increase the exergy of an available heat source, which is then stored in a thermal storage system. During the discharge phase, the previously stored heat is used in a heat engine cycle to release electricity.

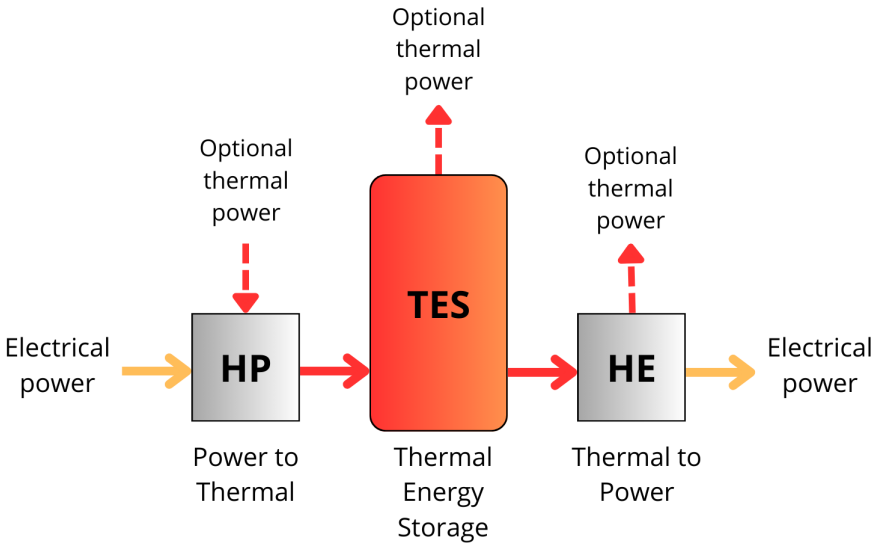

Figure 2.4: Simplified scheme of a typical Carnot battery system where HP and HE stands for heat pump and heat engine respecitevly

PTES can be divided into two main categories: PTES based on direct and inverse Brayton systems and PTES based on heat pump and Rankine cycle power systems [36],[35],[40]. For these two categories, different thermal integrations of the Carnot battery are possible and are presented in section 2.3.

2.1 Brayton based PTES

The Brayton based PTES (see Fig.2.5) is based on two sensitive heat thermal reservoirs (HT and LT). During the charging mode, the heat is transferred from the LT to the HT using the compressor and during the discharge mode, thanks to the difference of pressure and temperature, the fluid go throw an expander towards the LT. A gas (usually argon or air [36]) is used as a working fluid. It operates at a higher temperature than the other two cycles and requires a hot storage temperature of typically 200-300°C. Efficiency is highly sensitive to the polytropic efficiency of the compressor and expander. Therefore, a roundtrip efficiency of 60-70% can be achieve but at a price of a very high polytropic efficiency of 90% while a roundtrip efficiency of 10% is achieve with a polytropic efficiency of 80% [36],[99],[56],[42].

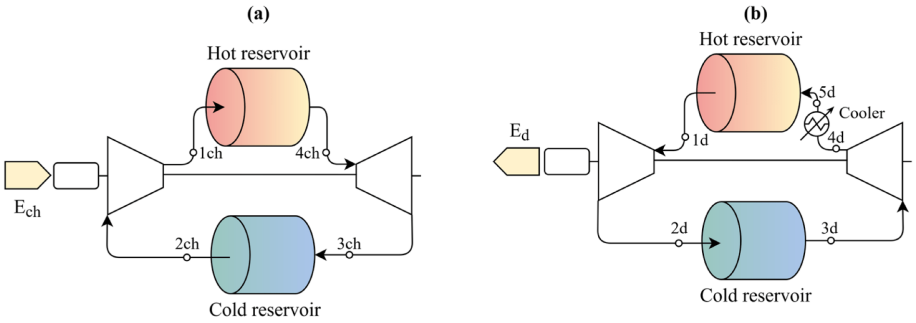

Figure 2.5: Brayton PTES system (a) charge system; (b) discharge system with E_{ch} and E_d matches with the charge and discharge electric energy respectively. Source: [42]

The Brayton system is interesting for its high level of energy density (up to 200 kW_{th}/m^3) however due to the high hot temperature tank, the thermal integration of low temperature waste heat is difficult. This does not make it a viable option for our application.

2.2 Rankine based PTES

Rankine PTES systems are good alternatives to Brayton cycles when low-temperature heat resources are available. Rankine PTES offers higher energy densities and lower temperature energy storage (100-200°C [36]) which also means lower heat loss and easier integration of low-grade waste heat. During the charging phase, the heater unit can either be a vapor compressed heat pump or an electrical heater while the discharging phase is performed by a Rankine cycles as heat engine cycle. An other possibility could be to only use one Rankine cycle (RC) for the charge and discharge cycle. In this particular case, we talk about a reversible HP/RC power system. It is mainly used for small-scale installations and can considerably reduce investment costs, as it uses a single machine instead of a combination of a HP and an RC [36]. within a Rankine cycle, a working fluid in liquid form will undergo a rise in pressure as it passes through a pump. It then heats up and passes in gaseous form through an evaporator, before expanding through an expander to the saturation pressure for condensation, thereby producing work. Finally, it is cooled by a condenser to start the cycle again. Its cycle, integrated into a PTES, is shown on the figure below 2.6.

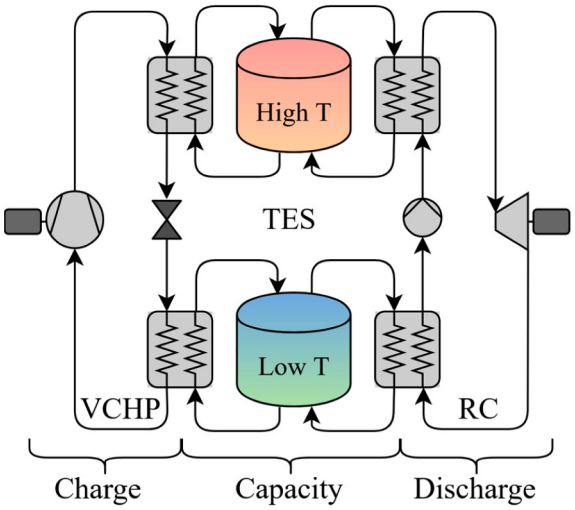

Figure 2.6: Scheme of a Rankine based PTES using a vapor compressed heat pump. Source: [41].

Two types of cycle can be envisaged for the HP and RC: transcritical cycles and subcritical cycles.

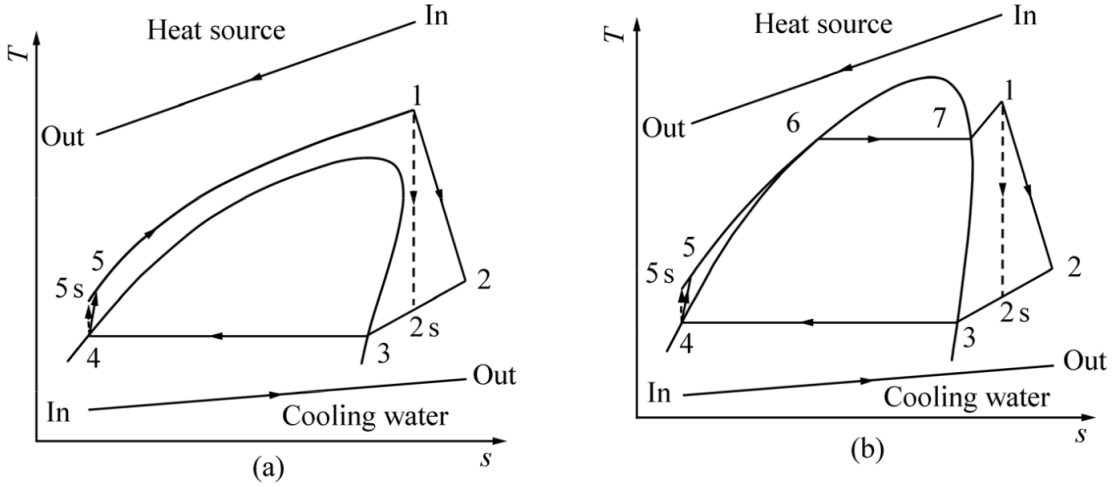

Figure 2.7: Diagram showing the differences between a transcritical and subcritical cycle for an ORC system. Source: [104].

In the case of transcritical cycle, the pump will have to work more in order to stay outside the saturation bell. As the fluid does not undergo a phase change, its heating curve is closer to the heat-source cooling curve (for sensible heat storage).

As a result, there is less irreversibility. However, no direct conclusion can be drawn on the use of one cycle rather than another and a case-by-case study should be investigated for each temperature and pressure range considered [104].

The subcritical cycle will be studied hereafter because it does not require the use of components capable of withstanding high pressures or a high-performance pump capable of producing a large pressure lift, which reduces the cost of the installation. In addition, modelling a transcritical cycle is more complex because, at the condenser, the working fluid is in the supercritical phase and it can be shown that, for a certain temperature, several pressures correspond. It is then necessary to carry out an optimisation to find the most appropriate pressure.
To eliminate the need for bulky and costly degassing equipment, fluids capable of functioning under atmospheric pressure at room temperature are employed. As a result, HP and organic Rankine cycles (ORC) often utilize organic fluids or refrigerants which strongly influence their efficiency [41]. The Rankine-base PTES and more particularly the combination HP/ORC power system remains the most optimal choice for our application as it allows better integration of the waste heat and maximum efficiency similar to that of the Brayton system (62-65% [36]).

2.3 Thermal integration of the Carnot battery

There are three different types of thermal integration of the Carnot battery. The first consists of using two insulated tanks: one at high temperature and the other at low temperature. In this configuration, the HP and HE respectively charge and discharge the high-temperature reservoir and vice versa for the low-temperature reservoir. In the other two configurations, only one tank (high-temperature or low-temperature) is retained, the other being replaced by two heat sources with different temperatures. This is known as a thermally integrated PTES (TI-PTES) [56], [36].

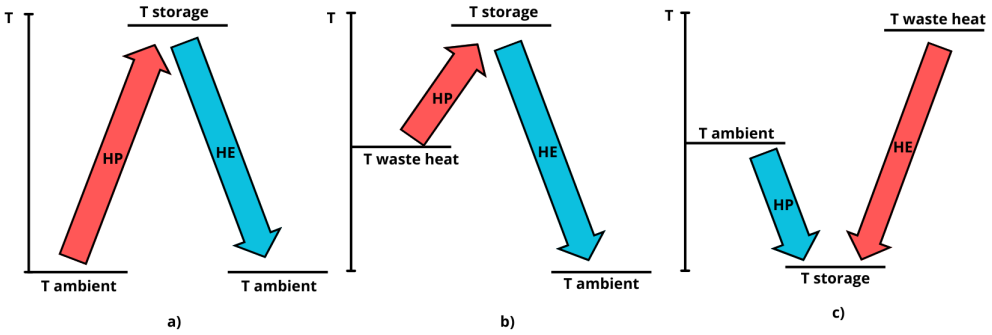

Figure 2.8: Temperature level for PTES (a), TI-PTES with one hot storage (b) and one cold storage (c). Inspired by [36]

The most common configuration of TI-PTES is obtained by integrating a low-grade heat sources (i.e waste heat source) with hot thermal storage. It has the advantage of improving the performance of the battery (power-to-power efficiency) as the temperature lift operated by the heat pump decrease which enhance its COP [41]. This is the configuration considered in this study.

In general, TI-PTES are investigated for their ability to relate to the use of both heat and electricity. Most of the studies focus almost entirely on the thermodynamic and technical aspects of the application but very few details are provided about the actual technology use. According to Frate Guido [41], one way to use the TI-PTES would be to integrate it into a system consisting of an RE source, one or more heat production systems (waste heat, solar heat, etc.), a seasonal thermal storage system and a district heater network. Within this system, the TI-PTES would play 2 different roles. Either it would uses the heat present in the seasonal storage to produce electricity or it would produces more heat to charge the seasonal storage and less electricity. Its operation being determined by the electrical or thermal production/demand. its integration would allows more efficient consumption of electricity produced by RE. Note that the seasonal storage system play an important role as it solves the issue due to temporal mismatch between the heat availability and the electric production and demand. Without this storage, the TI-PTES would not always be able to operate at the right time. Still according to [41], for its use to be economically efficient, the heat source and the electricity source must already be present before its integration. The ideal economical case would arise if the processes were already exploiting the heat source and the TI-PTES would just flow as an extension and adaptation to the existing system. Consequently, we can conclude that for now, since the TI-PTES requires preexisting energy production and distribution systems, it cannot be considered as a geographically independent electric storage technology. Therefore, the practicality

of implementing TI-PTES is situational and highly context-dependent.

3.0 Working fluid

Working fluids can greatly affect the efficiency of the Carnot battery. In general, there is no one fluid to be preferred and it will be necessary to compare/optimise with several different fluids to find the one that maximises the efficiency of the system (i.e HP and HE) for a given temperature and pressure range. Fluids can be classified according to the shape of their saturation bell: dry, wet and isentropic fluids.

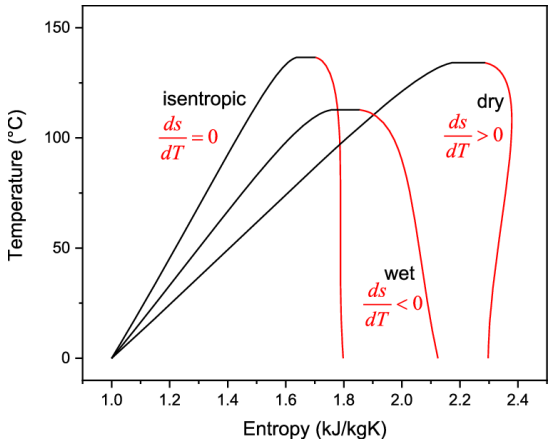

Figure 2.9: Saturation curve for the 3 types of working fluids (wet, dry, isentropic). Source: [57]

Each class has characteristics that are more or less well suited to certain configurations. For example, in the case of an ORC with a subcritical cycle, due to the steam quality constraint at the expander inlet and outlet, wet fluids will have to achieve a minimum superheat (i.e. >3K) necessary to meet the expander outlet quality constraint, unlike dry and isentropic fluids where a superheat higher than the value used to follow the rule of good practice (i.e. 3K) is not mandatory. However, depending on the temperatures and pressures considered at the evaporator, the choice of the optimum superheat is not straightforward and requires a case-by-case study. On the other hand, as presented in article [65], a few trends can be considered as a rule of good practice in the absence of a recuperator: when the fluid is dry, a minimum superheat (i.e 3K) is to be preferred and when the fluid is wet, either maximise the superheat if its effect is beneficial to the efficiency of the ORC, otherwise a minimum superheat is preferred.
In ORC, it is conceivable to use a heat recuperator at the expander outlet to heat

the fluid before it enters the evaporator. This recuperator will be particularly beneficial for a dry fluid, which has a greater temperature difference between the expander outlet and the condenser inlet. More details about the recuperator can be found in the thermodynamic chapter 3.

In addition to the impact of the working fluid on performance, there are other constraints to consider, such as its impact on the environment, its safety factor and technical constraints. Indeed, CFC and HCFC fluids are now banned because they have a too large ozone-depleting potential (ODP). These include R-11, R12 and R-502, which belong to the CFC class, and R-22, which belongs to the HCFC class. Other regulations also attack the global warming potential of fluids (GWP) and the use of fluids with too high a GWP is prohibited. These days, we prefer to use HFC-type fluids (i.e. purely fluorinated) or natural gases/liquids with low GWP and ODP [80].
Care must also be taken to avoid fluids with hazardous properties such as high flammability, high toxicity or corrosiveness, which correspond to the third class according to ASHRAE [92].
Finally, it is important to use a fluid that allows to meet the technical constraints of the application. These could include, for example, the need for good miscibility between the fluid and the oil to ensure good lubrication, or the use of a fluid that can operate over an acceptable pressure range and above atmospheric pressure to avoid leaks.

4.0 Heat pump

There are two main families of HP: absorption heat pumps and vapor compressed heat pumps.

4.1 Absorption heat pumps

In an absorption pump, mechanical compression is replaced by compression thermochemical.

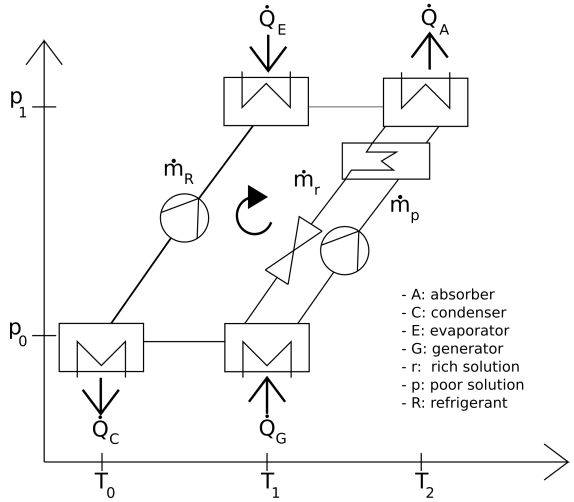

Figure 2.10: Absorption heat pump cycle scheme. Source: [29]

The principle is based on the affinity of a refrigerant for another liquid, for example ammonia for water or water for lithium bromide. The absorption heat requiring a hot source to operate, it has so far been most often used to produce cold, but it presents interesting possibilities for producing heat at lower temperatures (useful for heating sanitary water). However, it will not be useful for our application because it requires a source of heat at higher temperature than the one delivered.

4.2 Vapor compressed heat pumps (VCHP)

A typical vapor compressed heat pump consists of an evaporator through which heat is captured by the working fluid. The working fluid is then compressed through a compressor which increase in the same time the temperature of the fluid before passing through the condenser, where it delivers its heat to the fluid to be heated (i.e to the TES for a Carnot battery). The fluid then passes through an expansion valve in which it will be expanded at evaporator pressure to start the cycle again. The performance of a VCHP (i.e coefficient of performance COP) is defined as:

$$COP = \frac{Q_{cd}}{W} \tag{2.11}$$

where Q_{cd} is the useful heat supplied by the VCHP at the condenser and W is the net work used by the VCHP. It is mainly related to the lift temperature that it must perform since the work of the compressor will increase proportionally with the lift (see eq. 2.12 and fig. 2.13). In addition, as with the ORC, the choice of working fluid is very important for the correct operation and efficiency of the HP

and must be based on the temperature range between which the HP works while respecting other constraints as mentioned in the working fluid section.

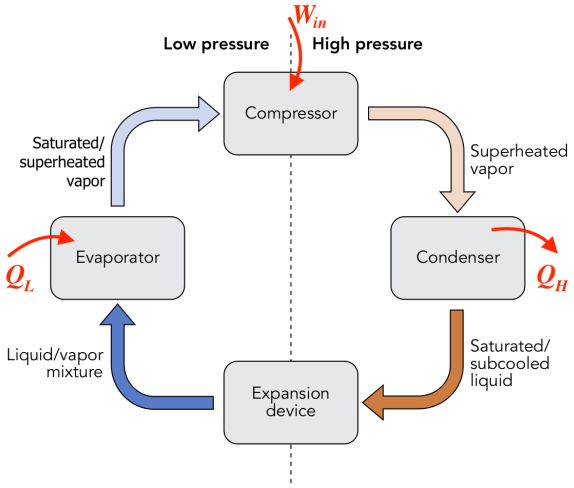

Figure 2.11: Scheme of a typical Vapor compressed heat pump (VCHP). Source: [101]

Typical T-s and p-h diagrams of a Vapor compressed heat pump are shown below.

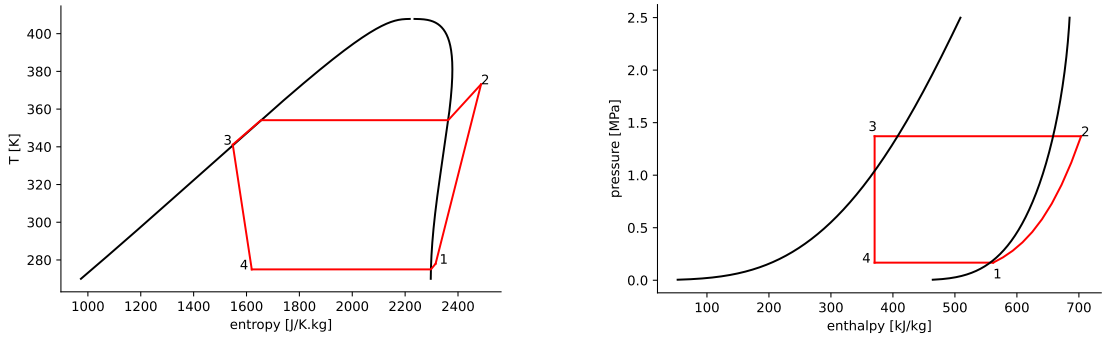

Figure 2.12: T-s (left) and p-h (right) diagrams of an typical HP with R600a as working fluid.

There are several possible ways of improving the COP of a HP depending on the operating conditions. For example, when the temperature lift is significant, we may want to use two refrigeration cycles placed in cascade. Another configuration, known as enhanced vapour injection (EVI), would be to inject the intermediate pressure vapour leaving the condenser directly into the compressor in order to

reduce the compressor's specific workload and increase the COP. Finally, another way of doing this would be to add an internal heat exchanger to the HP in order to heat the fluid entering the compressor via the still hot fluid leaving the condenser. All these configurations are not explained in more detail here above as they will be presented in the thermodynamic chapter 3.

4.3 Integration of a HP into a TI-PTES

In a TI-PTES, the goal is to use a heat source whose temperature is higher than that of the sink temperature (i.e ambient temperature) to increase the overall performance of the CB by decreasing the temperature lift that the HP must perform [41]
On the other hand, it is found that the additive heat provided by the HP (=energy provided by the compressor to the working fluid) is a function of the temperature lift it achieves (i.e. the difference between the hot storage temperature and the temperature of the heat source). Indeed, as shown in the graph below 2.13, the smaller the lift, the greater the specific heat absorbed by the evaporator and the smaller the specific heat delivered at the condenser. The two being linked thanks to energy conservation:

$$W_m = Q_{OUT} - Q_{IN} \tag{2.12}$$

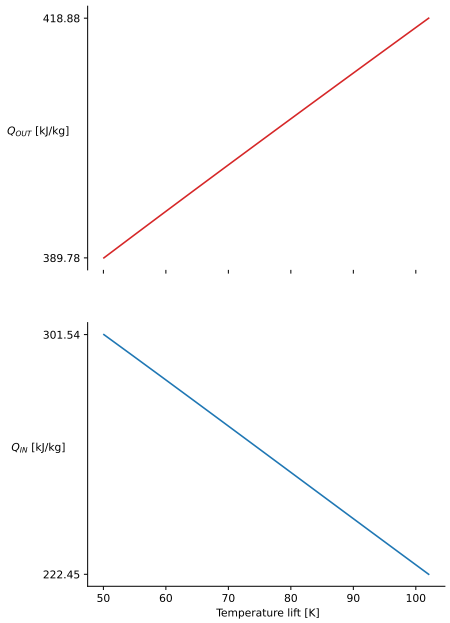

Figure 2.13: Evolution of the specific heat used by the HP at the evaporator Q_{IN} and supplied by the HP at the condenser Q_{OUT} in relation to the lift temperature between the saturation temperature of the condenser and the evaporator

The specific energy provided by the HP is therefore reduced compared to PTES. In the case where the heat source is available only in limited quantities (i.e a waste heat source), the heat flow transferred to the TES will also be limited. Thus, by modeling the efficiency of the ORC as constant (i.e fixed hot storage temperature and constant ambient temperature), the electricity produced by the CB is proportional to the amount of heat available at the hot source of the HP which is itself proportional to the efficiency of the industrial site producing it. However, in most cases, for an industrial plant to be economically viable (without considering the possibility of recovering waste heat), one seeks to increase its efficiency and thus reduce its waste heat. The result is that by recovering the waste heat via a TI-PTES, only a small or negligible share of electricity has to be returned in comparison with that used by the industrial site. Since the purpose of the TI-PTES is to serve as energy storage for the installation in question, the expected beneficial impact of its use will be too low than to justify the investment cost of the TI-PTES. This can be particularly limiting for RE-powered applications (particular with solar energy, see chapter 4) since the charging time (i.e when a power excess is present) is generally limited and much lower than that of discharge. To successfully charge the battery in this time, it is necessary to increase the charging power (HP power) which is not possible with an HP using only the heat source available in limited quantity.

In addition to this, when we seek to maximise the overall efficiency of the CB, it can be shown that there is a difference between the heat source temperature and the heat sink temperature $\Delta T_{hs,cs}$ (i.e $\sim$ 30K) above which the efficiency will be maximised when the COP of the HP is maximum (i.e. $T_{st,ht}$ as close as possible to T_{hs}) [6]. In other words, if we wish to elevate the round-trip efficiency of the CB to improve the electricity recovery efficiency, as the $\Delta T_{hs,cs}$ is generally greater than the tipping point in the case of a TI-PTES (e.g $T_{hot,s}$=75°C and $T_{cold,s}$=15°C), a low storage temperature will be favoured and the heat gain provided by the HP will be all the more limited as $COP_{CARNOT} = \frac{(T_{st,ht}+\Delta T)}{(T_{st,ht}+\Delta T)-T_{hs}} = \frac{Q_{produced}}{Q_{produced}-Q_{hs}}$ where the ΔT represent the heat transfer irreversibilities through the condenser.

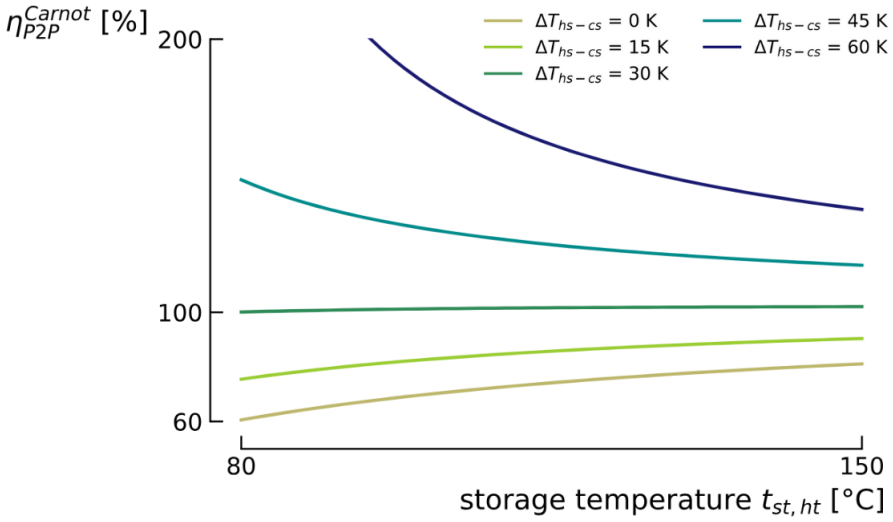

Figure 2.14: Illustration of the presence of this tipping point using Carnot efficiency of TI-PTES for different $\Delta T_{hs,cs}$ with the variation of the hot storage temperature of TES. Cold source temperature is assume equal to 20°C. Heat transfer irreversibilities are represented through ΔT (= 8°C). Source: [6].

To overcome this problem, one can imagine using the use of a storage system that would store heat outside the charge phases but it will require a very large storage capacity which means a higher cost. Not to mention the fact that the energy density will be low since the waste heat is at low temperature which will increase the cost even more. [41]. This solution is therefore not the most suitable and cost-effective solution. Another possible solution would be the use of a dual-source heat pump (DSHP). It would use another source available in larger quantities to allow a greater heat flow to the TES. In addition, the DSHP will allow greater flexibility of operation thanks to a variable load power (i.e heat flow provided by the DSHP). This will make it possible to better adapt to the fluctuations present

with renewable energies or simply to be able to adapt to different storage needs for the same installation.

4.4 Dual-source heat pump (DSHP)

Several authors have already studied some DSHP. In most cases, dual sources heat pump are used to compensate for the fluctuations in ambient air which strongly impacts the COP of the heat pump. This applies especially in winter for heat pumps (in heating mode) because the outside temperature drops. In the literature, 3 main combinations of heat sources are proposed: air-ground, air-solar, air-waste heat. However, to the best of the author's knowledge, using a dual-sourced HP with waste heat recovery remains under-researched.

4.4.1 Air-ground combination

The articles [31], [15] show that the high costs of vertical underground heat exchangers make geothermal heat pumps less competitive than air heat pumps in mild climates. Horizontal heat exchangers (FP) are less expensive to install but are quickly subject to freezing. An effective solution is the dual-source heat pump (DSHP), which alternates between air and FP heat to avoid freezing and maintain high efficiency, while reducing the initial investment compared to geothermal heat pumps. DSHPs offer an average annual thermal output four times higher and perform well in extreme conditions where air heat pumps alone would fail.The cases considered use either two separate heat pumps for each source or the two sources placed in parallel.

4.4.2 Air-solar combination

the air-solar combination was studied in several articles [19], [58],[38]. In the fist studied article [19], author analyzed multiple source arrangements: solar-air in series (SA-SHP), air-solar in series (AS-SHP), and solar-air in parallel (SA-PHP). The results indicate that SA-SHP is effective in environments with low solar irradiation and its COP varies similarly to ambient temperature changes while AS-SHP has best performances in conditions with low ambient temperature and high solar irradiation and SA-PHP achieves optimal performance at high ambient temperature or high solar irradiation.
The choice of configuration will largely depend on the climatic conditions present on the site. Overall, the study shows that the COP is always improved when the solar source is used at higher temperatures. On the other hand there is no optimal configuration for all the circumstances and it will be necessary to place the source

most likely to fluctuate (decrease in temperature or quantity) first when you want to place both sources in series to improve or maintain a good COP.
In the other two [58], [38], a thermal storage system was considered playing a buffer role for the heat produced by solar energy and thus allowing to keep a stable temperature at the source and allowing the HP to operate longer at a higher COP.

4.4.3 Air-waste heat combination

Finally, Hwan Ahn [4] focused on the study of a DSHP using air and waste heat to serve as a heating unit in an electric car. He compared the DSHP to two other configurations: one with just air as the source and the other with only waste as the source. In his study, the DSHP used two evaporators placed in parallel.
He concluded that for the waste heat-only mode, the COP and heating capacity increased with increasing waste heat amount and the performance with DSHP was higher than the other two modes. However, he noted a strong reliance on heating performance with the amount of waste heat available when the outside temperature was below -10°C because the heat absorbed at the air source was negligible due to the parallelization of the sources. To make more efficient use of the air source, he proposed a single operation mode alternating between air source only and waste heat only mode. When in air source only mode, the waste heat is stored via the refrigerant. In addition, it considered the use of an electric heater in series with the air source to boost its heat capacity during the air source only mode. This alternative mode increases the heat amount and COP by 10.5 and 4.3% respectively compared to the conventional DSHP mode with an external temperature of -10°C.

In the majority of applications using a DSHP, the two sources are often placed either in series or in parallel. In our study, we will integrate these configurations for several types of HP and for several different heat sources. Each will be described in Chapter 3.

5.0 Thermal energy storage

The thermal energy storage (TES) which is positioned between the heat pump and the power plant exists in a variety of forms/technologies as seen in article [36]. However, given that we are interested in a TI-PTES integrating a low waste heat temperature, the storage temperatures considered are between 90-140°C and therefore three technologies stand out: sensible, latent or hybrid thermal energy storage.

5.1 Sensible thermal energy storage

The sensible thermal energy storage is a storage technology which use the heat capacity of the filling material to store energy. This material can be in liquid or solid form and it is always in a single phase which implies a variation of temperature during the charging and discharging phase. For this reason, the sensible TES is made either of two separate reservoirs (i.e one hot and one cold reservoir with two heat exchangers between them) or one large reservoir using stratification of liquid material which authorizes the reduction of the size of the TES, since only one tank is required even if it entails a risk of mixing, which would reduce its performance [41]. Sensible TES can reach an efficiency in range of 50-90 % depending on the insulation [36].
In most cases, sensitive thermal storage at low-temperature will use water as the fluid to store the heat for cost reasons, because it is readily available in large quantities and has a large heat capacity (4200 J/kg.K). The reservoir will need to be pressurised when the temperature of the hot reservoir exceeds the boiling point of water at atmospheric pressure (i.e. 100°C). At intermediate temperatures (500-600°C), molten salts are used as the liquid fluid or special concretes as the solid material. For high temperatures (≈1500°C), ceramic is generally used[82].
Its main drawback is its energy density of 10-50 W_{th}/kg [36] but its investment price is of the order of $3100 - 400$ €/kW or less than or equal to 20€/kWh for sensible TES using water [82].
In this study, sensible TES with pressurised water will be considered for its low cost, low complexity and because it allows the VCHP to subcool its working fluid at the condenser, which in turn benefits the VCHP's COP. Indeed, subcooling at the condenser increases the amount of specific heat delivered to the TES for the same amount of compression work (see section 3.1.2) [41].

5.2 Latent thermal energy storage

The latent thermal energy storage use a material called phase change materials (PCM). As its name indicates, a phase change occurs during charging or discharging. So the temperature stay approximately constant. Most used Phase Change Materials (PCMs) for high-temperature latent TES are salts (eg. potassium nitrate and lithium nitrate ($LiNO_3 - KNO_3$) for 130°C storage temperature) while for low temperature ($\leq$ 0°C), the most used PCM is water ice. The latent TES have a specific energy (50-150$W_{th}h/kg$) much higher than the sensible TES however the CAPEX is also higher (6000-15000$/kW or 10-50$/kWh [36])

5.3 Hybrid thermal energy storage

Finally, the hybrid thermal energy storage is a new method developed for large scale energy storage. It combined the latent and sensible thermal energy storage systems. It can be shown (see subsection 3.1.2) that increasing the subcooling at the HP condenser increases its COP then using a combination of two different temperature profiles in the heat exchange at the HP condenser means that the difference between the hot working fluid and the TES fluid is reduced, so that energy losses are reduced. A compromise needs to be found between the complexity of hybridisation and the increase in energy efficiency.

6.0 Waste heat recovery from electrolysis

Several studies have already been carried out on the recovery of waste heat from electrolysers. This demonstrates the feasibility of the application considered in this study.
For example, the author in ref.[7] analyses the integration of waste heat recovered from water electrolysis to desalinate feedwater with membrane distillation. It demonstrates that waste recovery can purify the water and satisfy the demand of the electrolyser which increases the energy efficiency of the installation.

Another author [84] focused on optimal heat recovery in PEM electrolysers. Its aim was to find the optimal control model that would maximise the removal of heat produced by the electrolyser while maintaining stable hydrogen production. He concluded that the optimal switching control model resulted in a slightly lower specific energy consumption than a standard PEM system, which meant a slight decrease in hydrogen production (2.51kg compared with 2.56kg over a day). It also shows that heat removal reduces membrane degradation and increases membrane lifetime (+0.68 years).

Finally, the author Van Der Roest [93] set out to examine different designs for recovering waste heat from PEM electrolyser. He showed that the efficiency of the electrolyser decreases over time, leading to an increase in the available heat. Over a period of 10 years, the efficiency (HHV based) drops from 80% to 70%, resulting in an increase in recoverable heat from 20% to 30%. In his analysis, he shows that the water entering the electrolyser is preheated with the water produced. In addition, the efficiency of the electrolyser decreases with an increase in load, resulting in more waste heat at full load compared to 10% load. The stack efficiency, based on the HHV of hydrogen, drops linearly from 90% to 76% as the load increases from 10% to 100%. The heat required for this preheating is 4.5% of the recoverable heat.

He concludes that recovering and utilizing the waste heat can increase the efficiency of the electrolyser stack (based on HHV) by 15%-18% and from an economic point of view, he concludes that the economic feasibility of waste heat recovery is less evident when a heat pump (HP) is used to raise the temperature level (36.9 €/MWh heat used) compared to without an HP (8.4 €/MWh heat used). However, the Levelized Cost of Energy (LCOE) of the electrolyser heat remains at the same level or lower than that obtained for other low-temperature heat sources.

Chapter 3

Thermodynamic analysis

1.0 Introduction

In the context of this master thesis, the DSHP is used to introduce a greater quantity of heat into the Carnot battery, which makes it possible to produce a significant amount of electricity in relation to the needs (auxillaries or electrolysers) that the battery is supposed to satisfy.
In our case, We know that electricity consumption consists of usage by the electrolysers and usage by the auxiliary systems (compressor, water purification, pump,..). The idea is to use Carnot battery to supply the auxiliaries by discharging the BC when no more green electricity is available (refer to the integration case study chapter for more details on these strategies). As the Carnot battery will consume electricity to charge, the goal is to reduce this consumption for a given output power so we need to know more about its energy performance.

In addition, the choice of design and performance of the Carnot battery will have repercussions on the cost of the installation. For example, choosing a low energy density will result in a higher cost but could be beneficial for the energy performance of the CB. Just as a high COP will result in lower consumption (increased production) but could potentially require a more complex DSHP configuration which would increase cost. As the goal is to limit the total cost, we need to know more about these energy performance criteria .

Therefore, the aim is to study a Carnot battery and, more specifically, analysing the thermodynamic performance of several dual-source heat pumps to be able to compare the two options from an energy and economic point of view. In other words, we are interested to discover the performance (electricity consumption per

quantity of hydrogen produced, installation cost per unit of hydrogen produced) achievable with a Carnot battery incorporating a dual-source heat pump.

1.1 Limitations and aims of this thermodynamics section

This chapter will be devoted to the description of the dual-source HP studied, their thermodynamic characterisation and their optimisation within the Carnot battery. Finally, a parametric analysis will map the dependencies between the parameters that characterise the Carnot battery, as well as their sensitivities. The final results will help to design the set of parameters that will maximise efficiency and production for a specific integration case.

2.0 The dual-source HP

A dual-source heat pump consists of a conventional single-source heat pump with a second heat source added. This additional source can be integrated with the HP in various ways (typically in series or in parallel). In addition to these configurations, we may want to implement them in different types of single-source HP with characteristics that are well suited to certain specific temperature ranges. In our case, one of the two sources comes from waste heat recovery and the main reason for its use in our case is to increase the quantity of heat supplied to the thermal storage system (TES) of the Carnot battery.
The aim here is to find the configuration that gives the best COP while complying with the specifications specific to our application (i.e. integration within a TI-PTES with waste heat).
The method used will consist firstly of defining the specifications, then selecting a panel of DSHP configurations capable of meeting these specifications and presenting promising characteristics given the field of application (i.e. the specifications). Finally, we will compare them thermodynamically to find out their respective levels of competitiveness in terms of energy efficiency, so that we can choose the one that best meets your needs. This approach has the benefit to yields results applicable to other similar applications.

2.1 Application specifications

In order to frame the choice of DSHP configurations that will subsequently be studied, a specifications covering the areas of operation and the constraints specific to the case in question was made :

- The DSHP must supply heat at a low temperature (95-120°C)[1]. This range of temperature corresponds to the considered hot tank temperature of the sensible thermal energy storage system used in the CB for this study.
- The DSHP must use 3 energy sources, at maximum: waste heat (65-75°C)[1] and/or ambient air (5-20°C)[1] and/or electricity.
- From a thermodynamic point of view, there must be no upper limit to the thermal power delivered by the DSHP.
- The DSHP must completely use the full amount of waste heat.

2.2 Description of dual-source HP studied

On the basis of the literature and the criteria set out above (section 2.1), nine dual-source HP configurations were selected. They differ in the types of components used and the arrangement of these components. In addition, their selection was motivated either because they are a type of HP which, when used as a single source, has advantages in terms of energy efficiency for the temperature range under consideration, or because of their simplicity and low cost.
These dual-source HP can be classified into different families and sub-families as illustrated in the diagram below (Fig.3.1). Note that only families and subfamilies are represented, however, several dual-source HP can belong to the same subfamily. In the 9 dual-source HP chosen, 2 different configurations are included in the dual-source heat pump sub-family with ejector and 2 more are included in the dual-source cascade heat pump. Furthermore, an additional configuration will be presented further in this section but can not be included in only one of these subfamilies as it can be applied to all DSHPs having two evaporators.

[1]See section 3.1 for sources and justifications

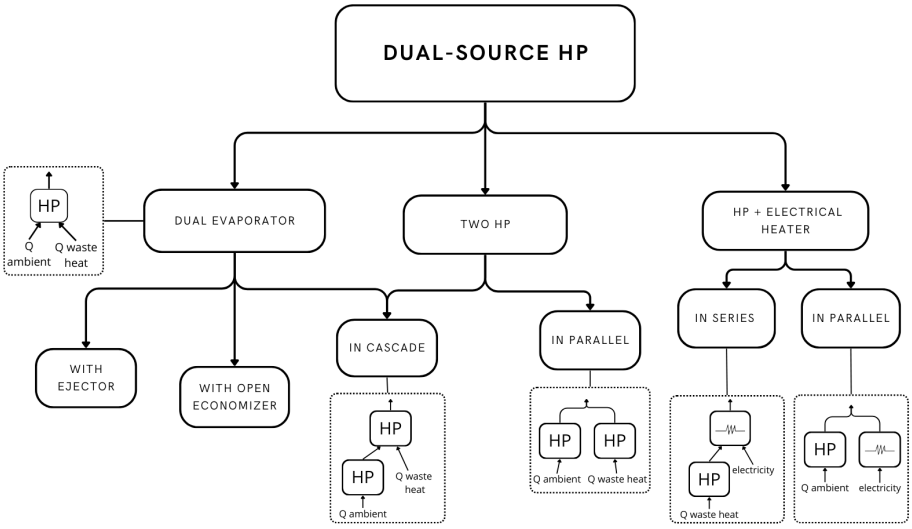

Figure 3.1: Diagram of the different dual-source HP classes and subclasses studied in this master thesis

2.2.1 Dual evaporator

Dual-source HP in cascade In a Carnot battery with Rankine cycle, the heat pump is used to increase the exergy of the heat source such that the temperature gradient between the hot storage temperature and the cold storage temperature (i.e. the environment) is sufficient to guarantee a reasonable storage energy density. In our application with TI-PTES, a hot storage temperature of the order of 95 to 120°C is considered, as well as a standard ambient temperature of 15°C. If ambient heat is to be used as an additional source, a temperature lift of 80 to 105°C is required.
Generally speaking, single stage heat pumps are unreliable when the temperature lift is large (>60°C) and its performance deteriorates (decrease in COP and in heating capacity). Cascade heat pumps are preferred to single stage HP when it is necessary to heat at a temperature greater than or equal to 60-65°C.

A cascade heat pump can be described as two heat pump circuits (a "hot" circuit and a "cold" circuit) that are mounted one behind the other in a unit and are thermally connected to each other by a central heat exchanger. This is the condenser for the first stage and at the same time the evaporator for the second stage. The waste heat source is injected into the hot circuit in parallel with the central heat exchanger.

They are preferred because under high lift temperature (>60°C), they are more reliable and allow for better maximum system performance. Indeed, for the same lift temperature, cascade pumps will have lower compressor discharge temperature, lower compression ratio and higher compressor volumetric efficiency. In addition, the cascade cycle has the advantage to have two separate closed circuits, which gives it the opportunity to have two different working fluids and to operate at two speeds regime what gives it greater flexibility during the design and allows it to have much stable water heating capacity than single stage heat pumps [53].

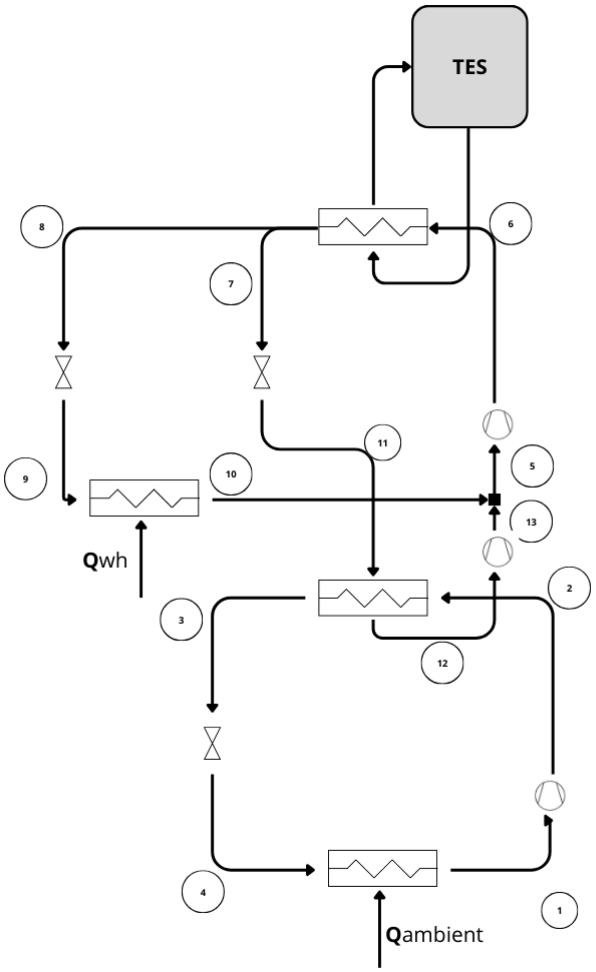

Figure 3.2: dual-source HP cycle diagram with dual-source HP in cascade with a single-source HP

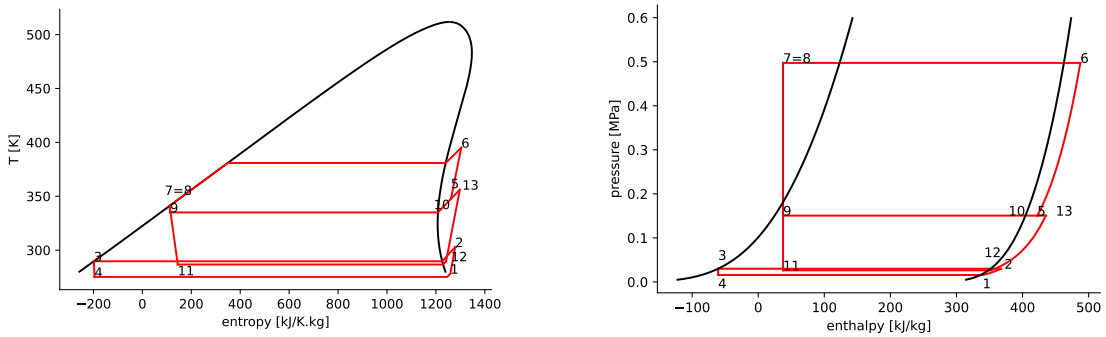

Figure 3.3: T-s (left) and p-h (right) diagrams of the cascade cycle as shown in Fig.3.2

According to Boahen [13], one way to increase the COP of a cascade heat pump could be to add a heat exchanger to cycle 1 at low temperature (i.e desuperheater). In his study, he proposed 3 different configurations for this internal heat exchanger: desuperheater mode, heater mode and parallel mode.
His results showed that the desuperheater configuration was the most efficient one. Indeed, compared with the conventional cycle, the new cascade cycle with heat exchanger in desuperheater position had a higher heating capacity and COP due to the high heat transfer within this exchanger, and a significant reduction in the energy consumption of the 'cold' circuit. The new cascade cycle with internal heat exchanger in desuperheater position showed an improvement in heating capacity and COP from 3.7 to 7.4 % and from 12.2 to 14.9 % respectively, when the OD EWT(outdoor entering water temperature) was increased from -5 ℃ to 10 ℃. For these reasons, a DSHP cascade version integrating an internal heat exchanger placed as a desuperheater was selected. Its cycle diagram is shown below (Fig.3.4).

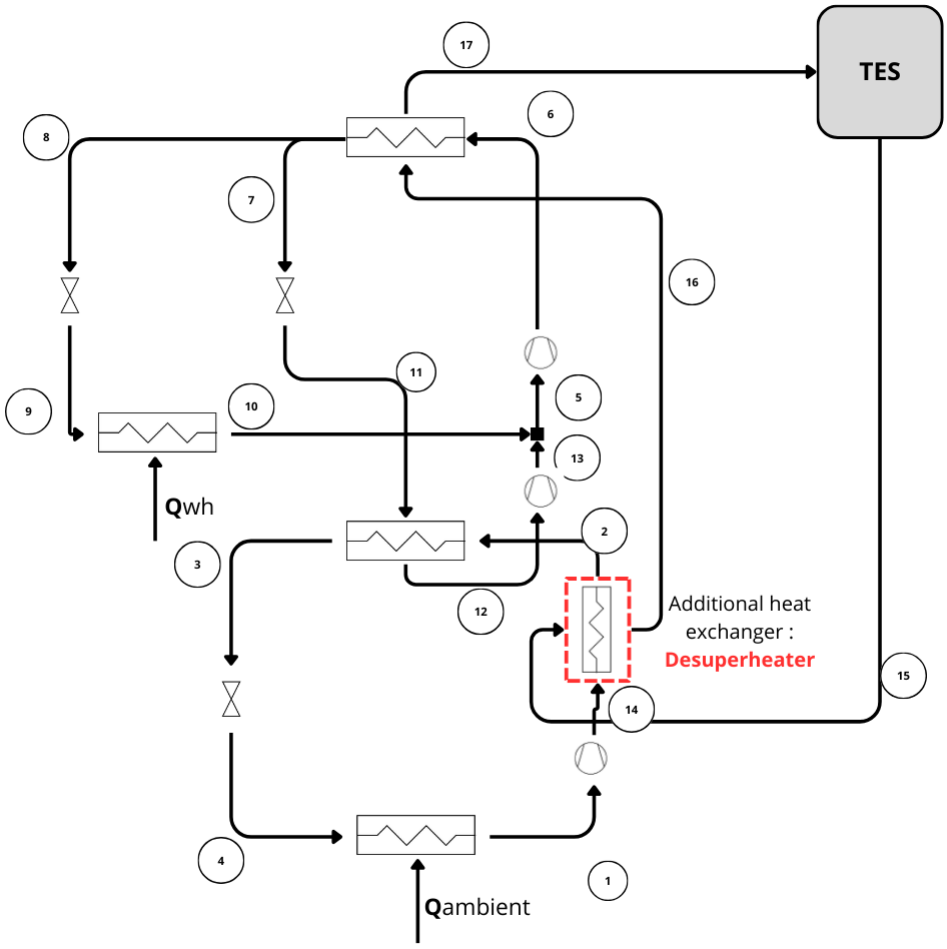

Figure 3.4: dual-source HP cycle diagram of a dual-source HP in cascade with a single source HP with desuperheater

Dual-source HP with ejector The idea behind the use of an ejector is to reduce the loss present through the expansion device. Indeed, vapour compression heat pumps commonly employ a capillary tube or throttle valve for fluid expansion. This leads to large exergetic losses as the exergy is entirely dissipated due to friction during the expansion. The ejector is a great device to recover expansion energy and used it to increase the pressure level of the compressor's inlet. Thereby, it offers the potential to enhance the COP of vapor compression cycles in general [8],[96].

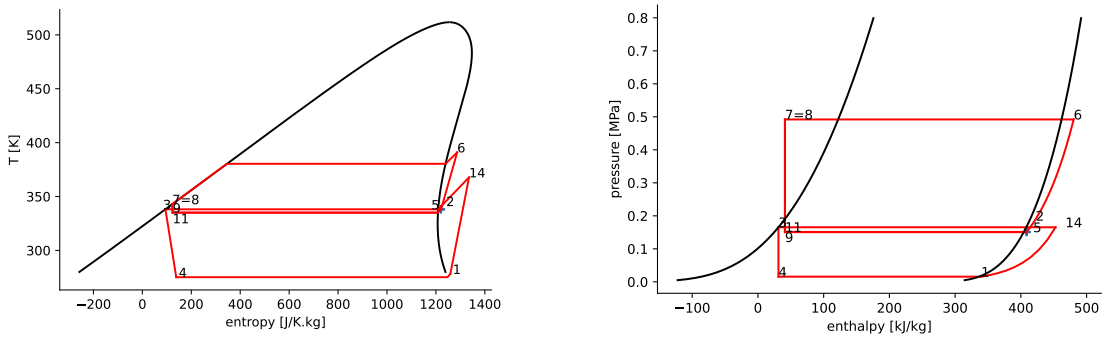

Figure 3.5: T-s (left) and p-h (right) diagrams the cascade with internal heat exchanger cycle as shown in Fig.3.4. For reasons of clarity, states 10, 12 and 13 have not been annotated directly in the diagram but are represented by a cross (close to states 5 and 2)

An ejector is a static part with three inputs (see Fig.3.6). In the first, a pressurized primary fluid (in gaseous or liquid or two-phase) is accelerated through a convergent-divergent nozzle, creating a pressure drop in the mixing chamber behind the nozzle. This pressure drop draws in the secondary (low-pressure) mixture. The two fluids mix, resulting in an increase in pressure and a decrease in speed. Finally, the remaining kinetic energy in the fluid is converted to static pressure via a diffuser. Overall, the ejector enables the secondary fluid to be compressed as the primary expands to a common pressure.

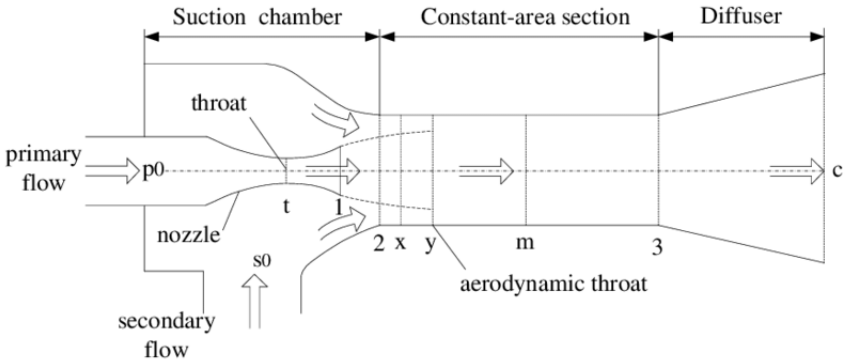

Figure 3.6: Diagram showing the various parts of an ejector [**ejector_scheme**]

The proposed system here under is inspired by a cycle from Erdinc [89]. As illustrated in Fig.3.7, the cycle employs two evaporators: one fed by ambient air and the other by waste heat. By utilizing the high-pressure refrigerant as a driving force,

the ejector elevates the pressure of the same fluid refrigerant present at low-pressure. Consequently, the total compression work of the cycle is decreased, leading to improved the COP of the dual-source heat pump. Here, the heat extracted from the waste heat source is used to evaporate the high pressure primary fluid before entering the ejector.

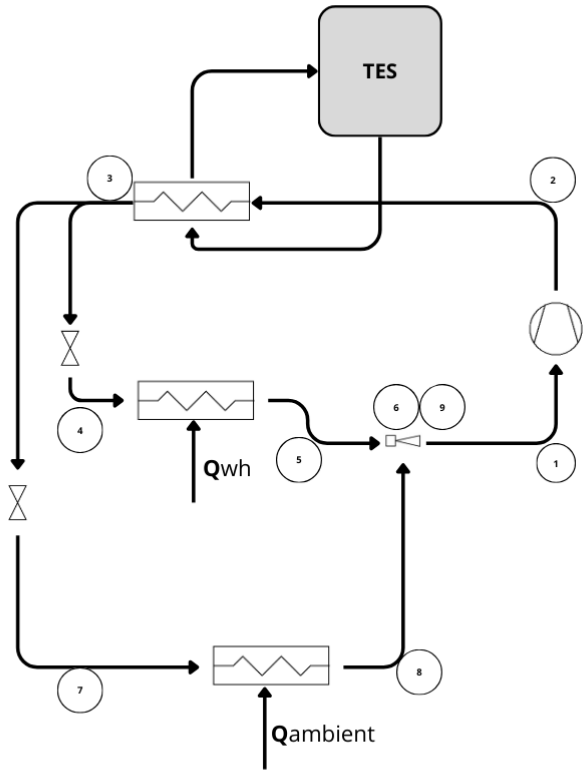

Figure 3.7: dual-source HP cycle diagram of a dual-source HP with ejector

Another variant of the ejector cycle was proposed in the [22] study. In this case, the fluid inside the ejector is saturated so there is both vapour and liquid particles. A pressure booster has been added just before the secondary fluid enters the ejector. This slightly increases the pressure of the secondary fluid, thereby boosting the

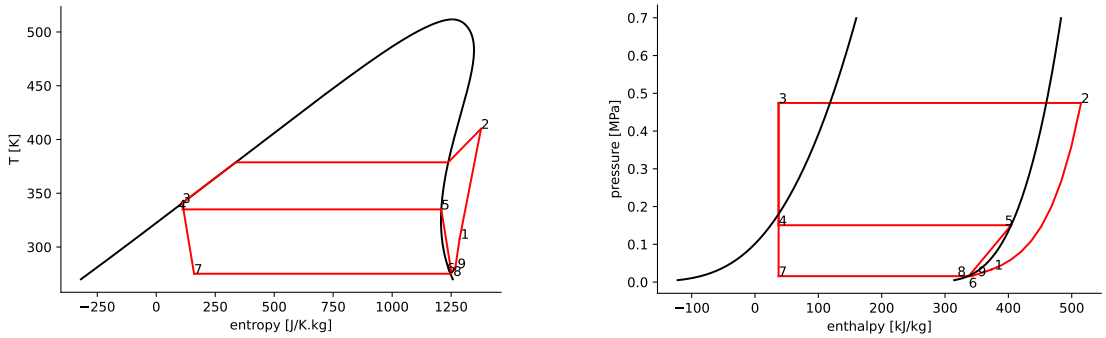

Figure 3.8: T-s (left) and p-h (right) diagrams of the HP with ejector cycle as shown in Fig.3.7

system's performance. According to the study, using the pressure dual-source HP increases performance by 25 % compared with the ejector-enhanced heat pump system without pressure boost.
The cycle used in the [22] study did not incorporate a second heat source and to ensure that the fluid at intermediate pressure was present in the form of superheated vapour at the compressor inlet (i.e. technical constraint for a compressor), an internal exchanger (i.e. sub-cooler) was used. In our case, we propose to replace this internal exchanger by integrating waste heat. The diagram of this dual heat source cycle is shown below (see Fig.3.9).

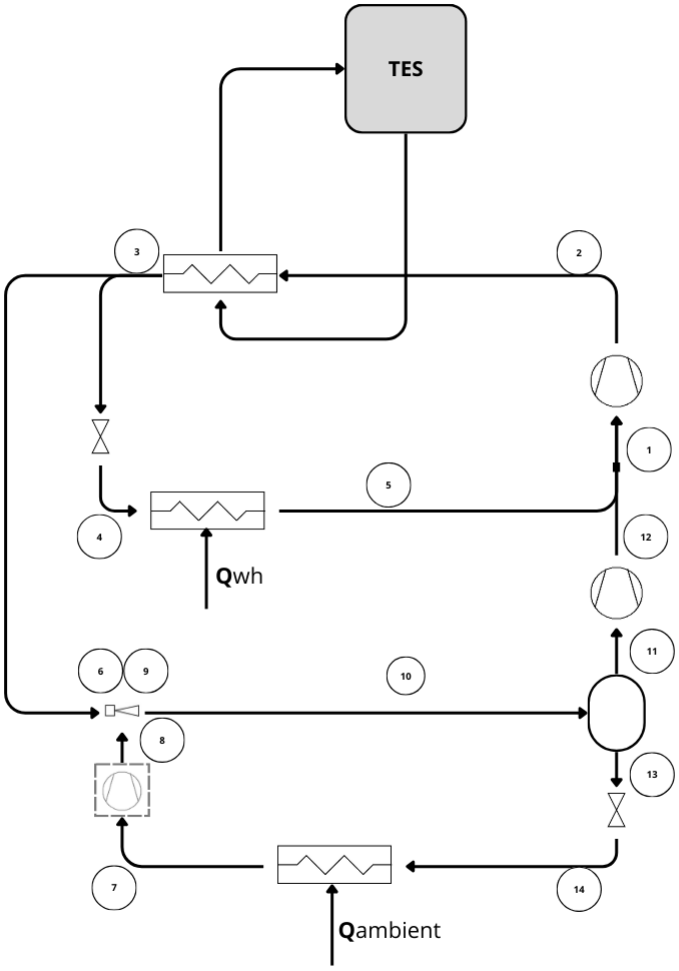

Figure 3.9: dual-source HP cycle diagram of a dual-source HP with ejector and a pressure boost

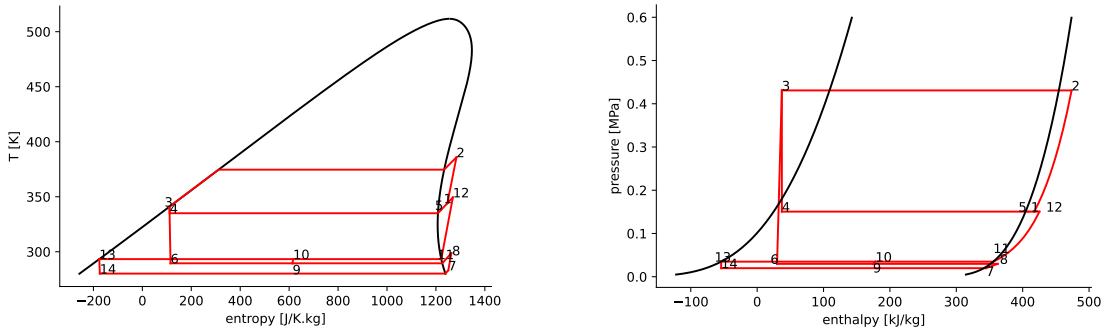

Figure 3.10: T-s (left) and p-h (right) diagrams of the HP with ejector and pressure boost cycle as shown in Fig.3.9

Dual-source HP with open-economizer As explain for the dual-source HP in cascade, a large lift temperature (>60°C) need to be achieved when ambient air is used as an additional heat source. Another alternative to cascade cycles is to use a cycle called EVI (Enhanced Vapour Injection) cycle. It consist of a classical heat pump cycle in which a fraction of the fluid flow leaving the condenser is recovered and expanded to an intermediate pressure before being reheated and injected into the compressor. Compared to a conventional HP cycle, it has the advantage of limiting the temperature at the compressor outlet (limiting superheating at the condenser inlet) for the same saturation pressure or, in other words, a higher maximum condensation temperature. As a result, it can increase its heating capacity without sacrificing energy efficiency and maintain a high COP even when the temperature lift is high (>60°C)[59].

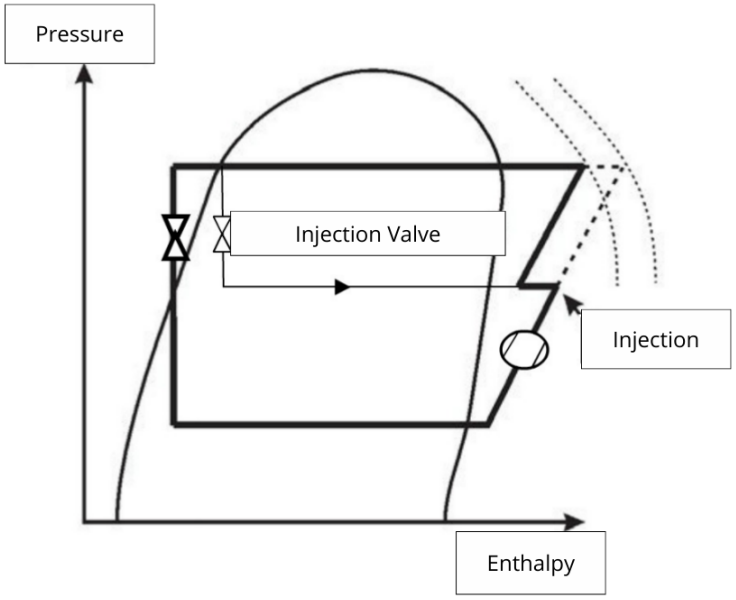

Figure 3.11: Comparison of an enthalpic diagram of a heat pump cycle with and without (dotted line) EVI (adapted from [59]).

There are mainly two ways of separating and heating the intermediate-pressure fluid fraction [10]. Here, the open economizer configuration as its name suggests integrate an open economiser placed after an initial valve (at the condenser outlet). This allows to separates the liquid part from the gaseous part. In our case, the open economiser is used to absorb heat from the waste heat source. This added heat ensures that the gaseous fluid fraction is superheated to an intermediate temperature before being injected into the compressor via an intermediate vapour injection port.
The other way would be to use a closed economizer also called "sub-cooler". It is a internal heat exchanger which uses the hot fluid leaving the condenser to superheat the fluid at intermediate pressure.
A study [10] analyzed both cases and found that the open economizer configuration was the preferred choice due to the control instabilities encountered with the closed economizer configuration.
In addition, the study [10] who studied the EVI cycle with open economizer, proposed several compressor layouts that could be used (i.e. 2 compressors in parallel, 2 serial compressors). The author showed that each configuration had similar efficiencies but the configuration with serial compressor was the most optimal

configuration from an economic and technical point of view. So when modeling this cycle, the compression was modeled by considering a first compressor that compresses the low-pressure fluid and then a second compressor that compresses the mixture at intermediate pressure.

The double source heat pump cycle with open economizer used in this study as well as its T-s and p-h diagrams that characterize it are shown below (Fig.3.12, 3.13).

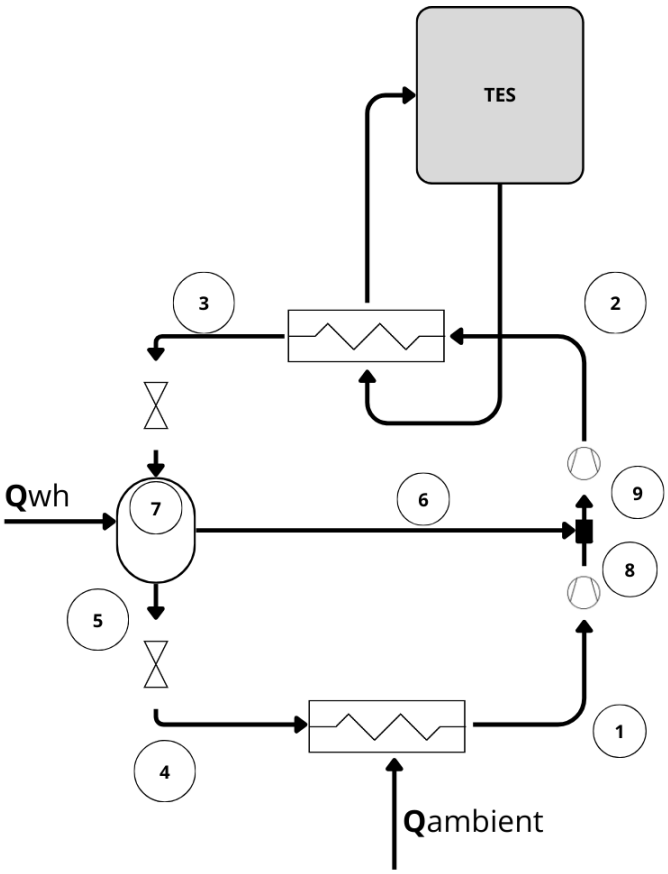

Figure 3.12: dual-source HP cycle diagram with open economizer dual-source HP. The waste heat is added directly inside the open economizer

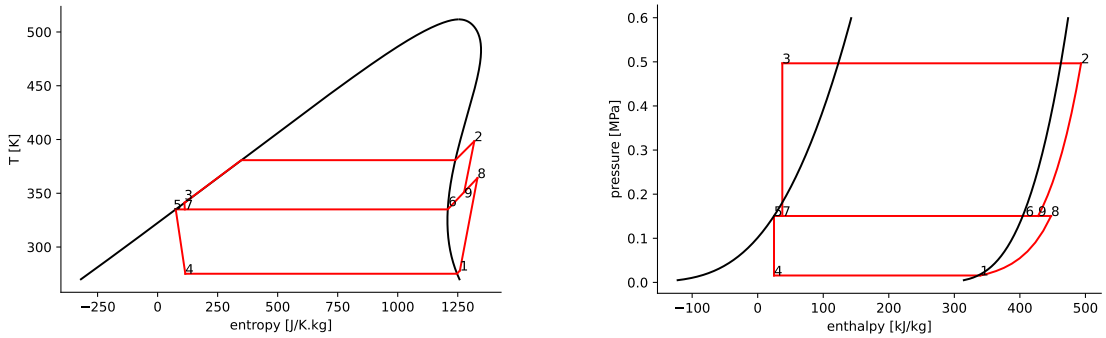

Figure 3.13: T-s (left) and p-h (right) diagrams of the HP with open-economizer cycle as shown in Fig.3.12

Two dual-source heat pumps in series The aim of this chapter is to find the DSHP configuration with the best COP. One way proposed by author Lemale [59] to improve the COP of a DSHP is to use a serialization.

The term serialization is used in this context to mean that the water from the thermal storage system passes through the two condensers and water heated from ambient heat passes through the two evaporators (from the right-hand dual-source HP to the left-hand one in the figure 3.14). This configuration reduces the temperature difference for each of the units, thus increasing the overall COP. In addition, the temperature glides at the condensers and evaporators are reduced, which reduces the temperature difference between the working fluid and the secondary fluid in the heat exchanger and thus the exergy losses through exchangers are reduced.
It can be shown that by increasing the number of HP in series, the overall COP of the installation increases logarithmically (Fig.3.17). However, it should be borne in mind that the initial investment cost will be multiplied by the number of HP, as will the maintenance cost. This is why we will limit ourselves to two HP in series. As mentioned at the beginning of this section, serialization can be applied to all DSHP with two evaporators (i.e the cycles presented above). However, the results (see section 4.0) showed that the DSHP with open economizer maximized the COP. Therefore, only the configuration of DSHP with open economizer will be presented here.

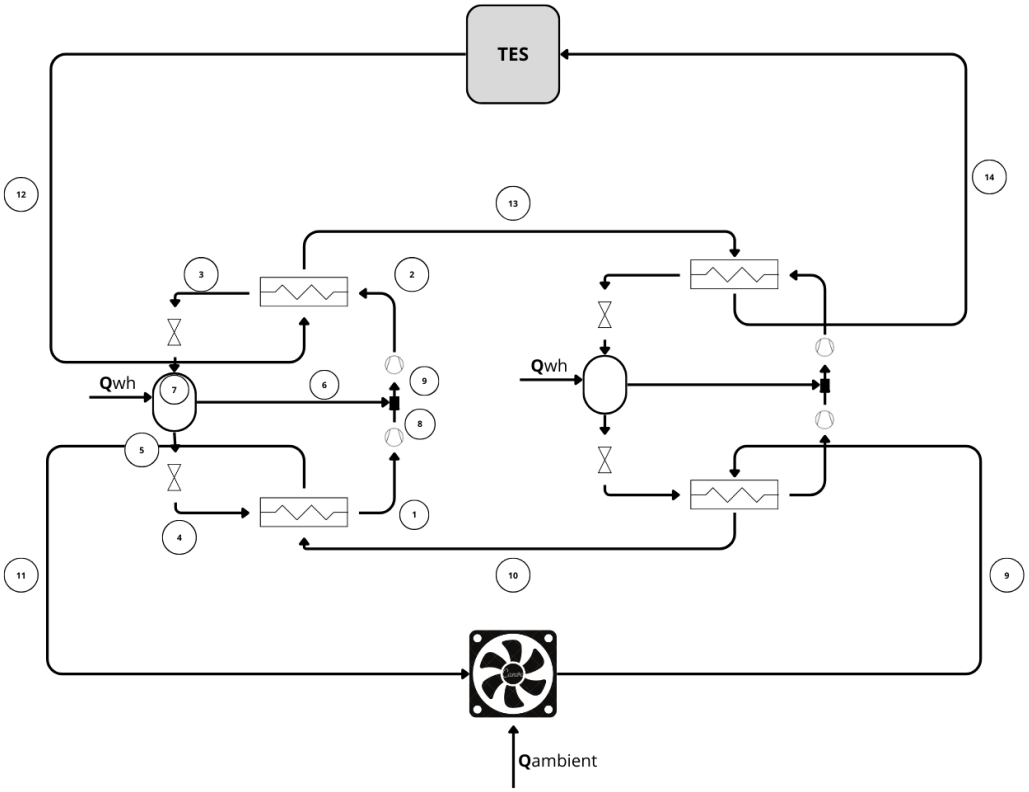

Figure 3.14: dual-source HP cycle diagram of two dual source HP with open-economizer (Fig.3.12) whose condenser and evaporator have been placed in series

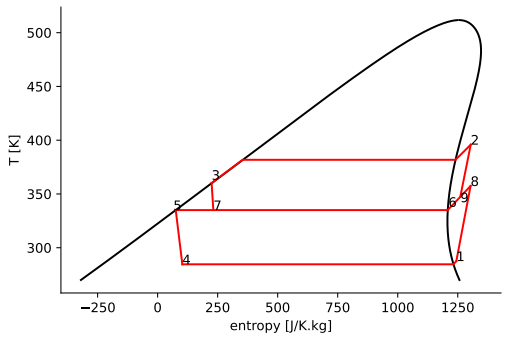

Figure 3.15: T-s diagram of the right HP cycle as shown in Fig.3.14

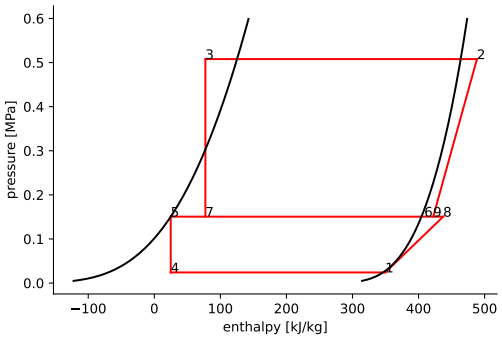

Figure 3.16: p-h diagram of the right HP cycle as shown in Fig.3.14

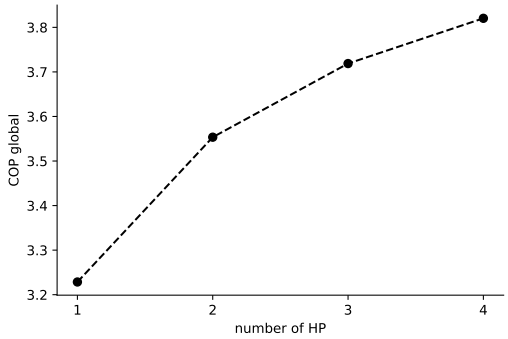

Figure 3.17: Evolution of the global COP with the number of HP in serie. The waste heat is divided equally between each HP, the hot tank temp. is $T_{st,in} = 120°C$, the cold tank temp. is $T_{st,in} = 65°C$, the cold heat source temp. is $T_{cold,in} = 15°C$ and exits at a temperature of $T_{cold,out} = 5°C$, ratio between the produced thermal energy and the waste heat energy is $E_{th,produced}/E_{th,wh} = 2.5$ and the input waste heat temperature is $T_{wh,in} = 75°C$

2.2.2 Heat pump with electrical heater

So far, we've only looked at configurations that use ambient air as a free source of heat. However, this requires a wide temperature range, which affects the COP. Another way of doing this would be to use another source of energy from a renewable source, since we want to produce green hydrogen. Therefore, the other types of energy available to us could be the electricity, biomass or solar thermal energy. Biomass has to be ruled out, as it would mean destroying exergy already stored in chemical form to transform it into thermal exergy. Solar thermal energy could be a possibility, but has not been investigated in this study as the purpose of having a second heat source is is to no longer be limited in heat, which would imply oversizing the solar thermal heat production panels. Finally, electricity seems to be the best option, as a large quantity will already be produced to supply the electrolyzers and there could be electricity produced in surplus as we are dealing with RE. Another major advantage is that an electrical heater is very simple and inexpensive component. We could imagine two configurations to integrate it with a heat pump: in series and in parallel. Both will be considered as we do not know which one is the most efficient.

In series The cycle is pretty simple and is represented on the figure 3.18. The water coming from the thermal storage system is heated by passing through the condenser of a heat pump and a heat exchanger which transfers the heat produced by an electrical resistor. The electrical resistance is placed in an electric boiler and is used to heat water to a uniform temperature using electricity. It has the

advantage of being easy to control and requires no moving parts (apart from a circulation pump).
However, its control is much complex as presented in section 3.1.3.

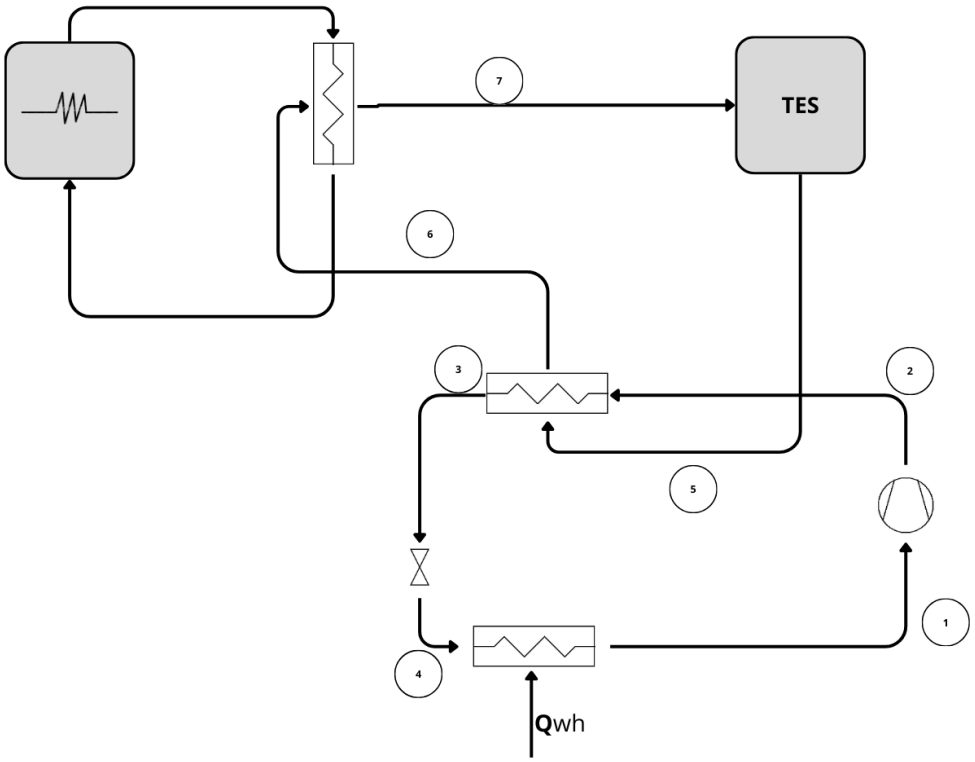

Figure 3.18: dual-source HP cycle diagram with an electric resistance heater in series with a classical HP that whose heat source is waste heat

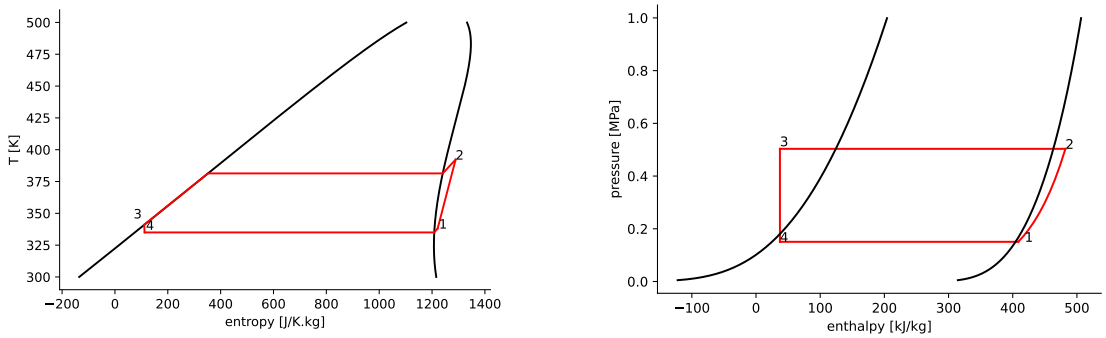

Figure 3.19: T-s (left) and p-h (right) diagrams of the HP cycle as shown in Fig.3.18.

2.2.3 In parallel

Similar to the dual-source HP in the 2.2.2 sub-section, a heat pump used the limited source of waste heat and an electrical resistor is used to increase the total heat output to the thermal storage system. The difference with the previous model 2.2.2 is that both are independently connected to the TES. The heat pump will therefore always have the same condensing temperature.

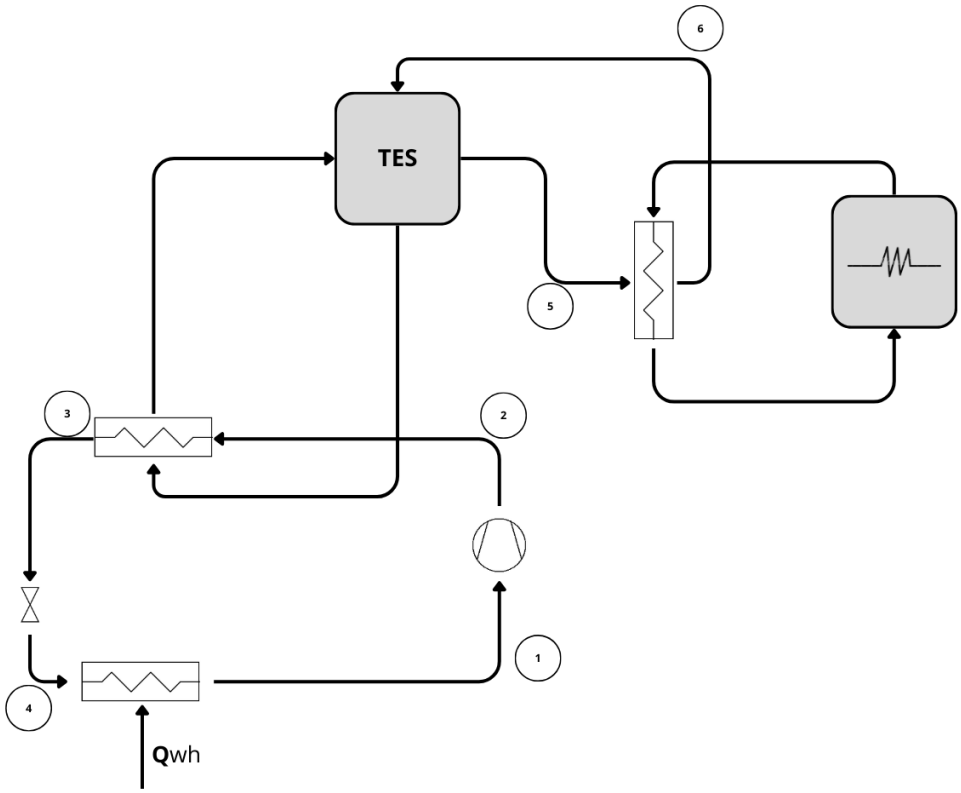

Figure 3.20: dual-source HP cycle diagram with an electric resistance heater in parallel with a classical HP whose heat source is waste heat

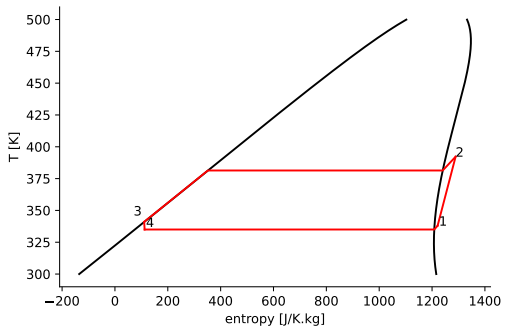

Figure 3.21: T-s diagram of the HP cycle as shown in Fig.3.20

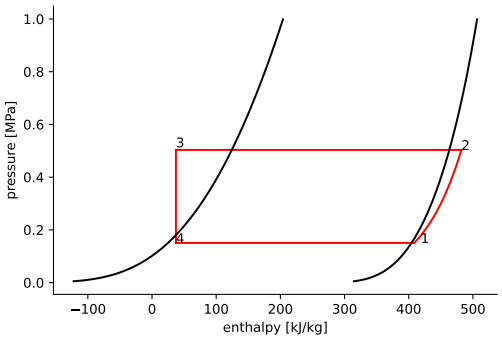

Figure 3.22: p-h diagram of the HP cycle as shown in Fig.3.20

2.2.4 Two heat pumps

Previously presented DSHP that use ambient air as heat source were all relatively complex and not yet widely available. However, it would be useful to be able to compare them to a conventional configuration and already widely used on the market in order to compare them and locate the performance gap between the configurations. Based on the results, only the case with 2HP in parallel will be studied.

In parallel Two heat pumps deliver heat independently to the TES. One uses waste heat as the heat source, while the other uses ambient heat.

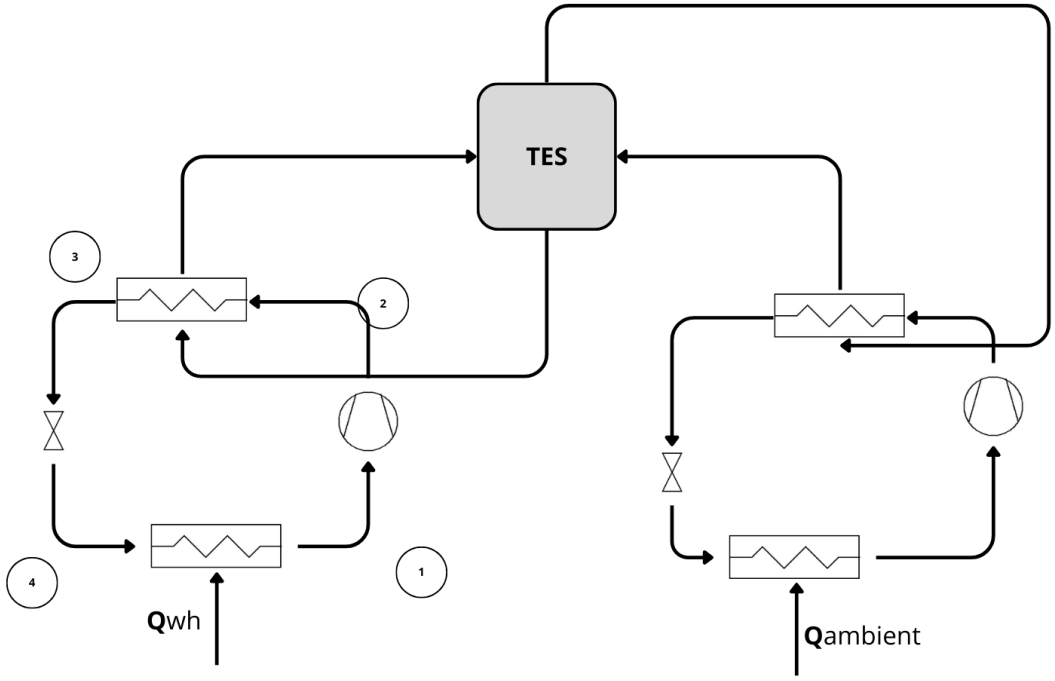

Figure 3.23: dual-source HP cycle diagram of two classical HP each independently connected to thermal energy storage systems (TES)

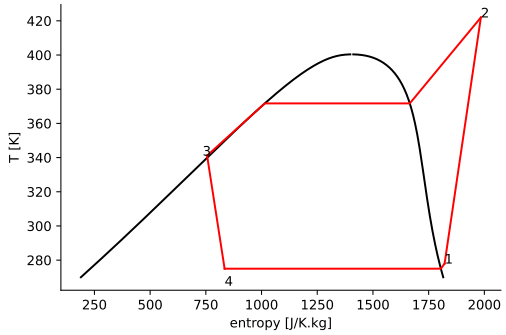

Figure 3.24: T-s diagram of the HP cycle which uses the ambient air heat source as shown in Fig.3.23. The T-s diagram for the HP which uses waste heat source is the same as the one in the dual-source HP with parallel resistance, see Fig.3.21

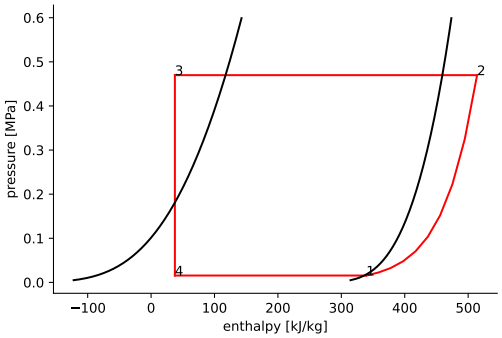

Figure 3.25: p-h diagram of the HP cycle which uses the ambient air heat source as shown in Fig.3.23. The p-h diagram for the HP which uses waste heat source is the same as the one in the dual-source HP with parallel resistance, see Fig.3.22

3.0 Model and method

Through this section, we will explain the method used to thermodynamically model the Carnot battery with thermal integration comprising a DSHP as heat pump, a sensitive thermal storage system and an ORC as heat engine. Here, we want to fully model the Carnot battery in order to see the scope of DSHP performance on it. This type of Carnot battery configuration, also known as TI-PTES, is shown in the figure below.

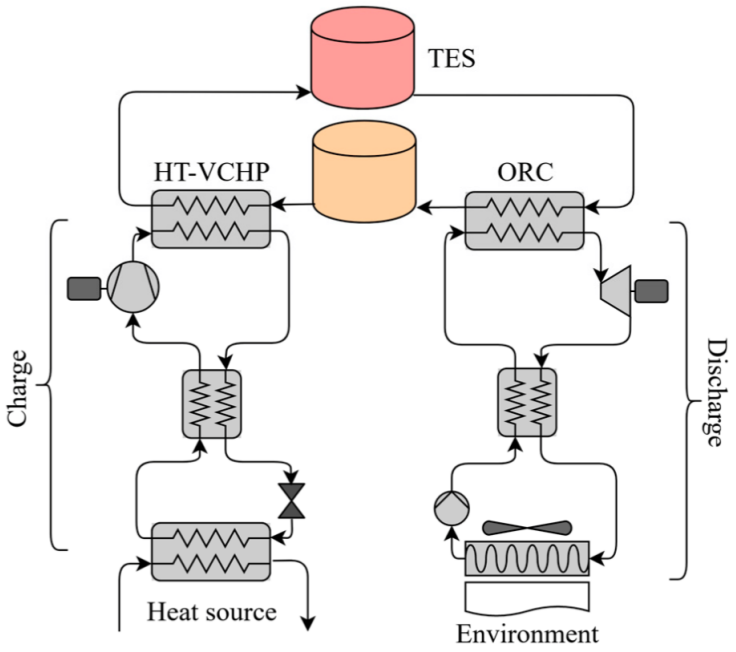

Figure 3.26: TI-PTES configuration used with sensible thermal energy storage. Source: [41].

3.1 Modelling dual-source heat pumps and ORC

Each of the cycles presented above plus the ORC were modelled numerically using the Python programming language and with the help of COOLPROP [2]. In this section, the limitations adopted during modelling will be listed and the energy evaluation of each component will be described. In addition more details will be provided on the method used to model DSHP with electrical heater placed in series and DSHP set in series .

3.1.1 Considered presumptions

To simplify the modelling, assumptions have been made:

- The system operate at steady-state operation
- the valve is considered isenthalpic
- all components except heat exchangers are considered adiabatic
- no heat loss to the environment is considered in heat exchangers

- pressure losses through heat exchangers and tubes are neglected
- potential and kinetic energy variations are not considered
- superheating of 3 [K] is assumed at the inlet of the compressor and at the outlet of the expander in order to protect the compressor and the expander from any fluid liquid particles

3.1.2 Component energy evaluation

Each component present in each cycle must respect the conservation of mass and energy defined as follows:

$$\sum \dot{m}_{in} = \sum \dot{m}_{out} \tag{3.1}$$

$$\sum \dot{m}_{out} \cdot h_{out} - \sum \dot{m}_{in} \cdot h_{in} = \dot{Q} - \dot{W} \tag{3.2}$$

where $\dot{m}_{in}, \dot{m}_{out}$ are the mass flow rate that enter and comes out the component, h_{in}, h_{out} the intake and output sensible enthalpy of the fluid, $\dot{Q}$ the heat flow rate and $\dot{W}$ the exchange work.

Compressor To model the compressor present in each DSHP, its isentropic efficiency $\eta_{is,c}$ is used. It is defined as:

$$\eta_{is,c} = \frac{h_{is,out} - h_{in}}{h_{out} - h_{in}} \tag{3.3}$$

The value of this isentropic efficiency is given based on the values found for similar cases in the literature [62],[63],[61]. See table 3.1 for the specific value. However, the isentropic efficiency of a component can change depending on its (the compressor here) size scale and the type of technology used which are intrinsic to the power of the plant. As we consider all the possible case in this section, a sensitivity analysis will be perform on this parameters (see section 3.4).

Open economizer The open economizer or separator, present in three of the dual-source HP studied, is a sort of large balloon into which the fluid is injected and which separates the gaseous phase from the liquid phase by gravity. In addition to this function, it can also be used as a heat exchanger with an external fluid as presented in the dual-source HP section. When it is used solely for separating the two phases, its energy modelling is carried out under the assumption that one of the outlets is assumed to be in the saturated vapour state while the other outlet

is assumed to be in the saturated liquid state. Conservation of mass and energy balance still apply.:

$$\dot{m}_{in} = \dot{m}_v + \dot{m}_l \tag{3.4}$$

$$\dot{m}_v = x \cdot \dot{m}_{in} \tag{3.5}$$

$$\dot{m}_l = (1 - x) \cdot \dot{m}_{in} \tag{3.6}$$

$$\dot{m}_{in} \cdot h_{in} = x \cdot \dot{m}_{in} \cdot h_{sat,v} + (1 - x) \cdot \dot{m}_{in} \cdot h_{sat,l} \tag{3.7}$$

where x is the vapor quality, $h_{sat,v}$ and $h_{sat,l}$ are respectively the vapor and liquid saturated enthalpy.
When heat is injected into the open economiser, the mass flow distribution changes:

$$\dot{m}_{v,add} = \frac{\dot{Q}}{h_{l,v}} \tag{3.8}$$

$$\dot{m}_v = x \cdot \dot{m}_{in} + \dot{m}_{v,add} \tag{3.9}$$

$$\dot{m}_l = \dot{m}_{in} - \dot{m}_v \tag{3.10}$$

where $\dot{Q}$ is the heat flux injected and $h_{l,v}$ is the latent enthalpy of vaporisation.

DSHP Condenser One effective way of increasing the energy performance (COP) and exergy performance of a heat pump is to sub-cool the condenser outlet. This increases the heat exchanged at the condenser without increasing the workload on the compressor (Fig.3.27. In addition, exergy losses at the condenser will be reduced due to the reduced temperature difference between the two fluids throughout the heat exchanger (Fig.3.28,3.29). To caracterise the exergy efficiency at the condenser heat exchanger, we can introduce the exergertic efficiency η_{condex} which represents the ratio of what the cold fluid gained over what the hot fluid lost through heat exchange. It is defined as:

$$\eta_{condex} = \frac{\dot{m}_{st}(e_{st,out} - e_{st,in})}{\dot{m}_{cd}(e_{cd,in} - e_{cd,out})} \tag{3.11}$$

where $\dot{m}_{st}, \dot{m}_{cd}$ are the storage and condenser mass flow rate respectively, $e_{cd,in} - e_{cd,out}$ are the exergy of the hot organic fluid inside the HP entering and leaving the condenser respectively, $e_{st,out}, e_{st,in}$ are the exergy of the fluid which receives the heat and which comes from the TES.

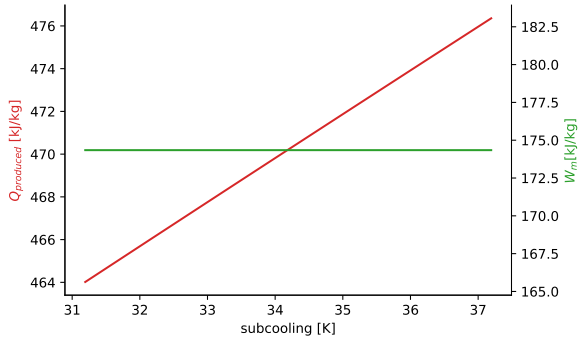

Figure 3.27: Effect of subcooling the exhaust condenser temperature of a heat pump on the heat per unit mass transmitted to the fluid to be heated for a constant work for constant compression work per unit of mass

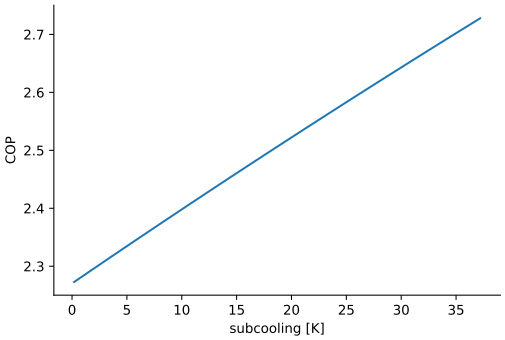

Figure 3.28: Effect of subcooling the exhaust condenser temperature of a heat pump on its COP

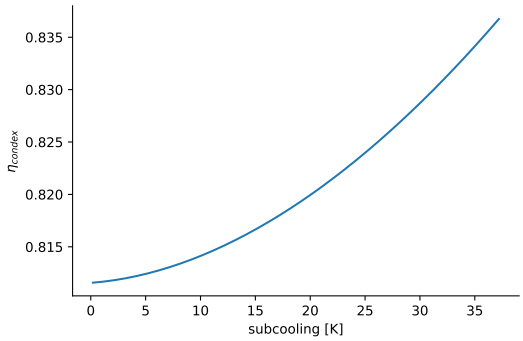

Figure 3.29: Effect of subcooling the exhaust condenser temperature of a heat pump on its condenser exergy efficiency

Therefore, the temperature at the condenser outlet for each dual-source HP is set at $T_{cd,out} = T_{st,in} + pinch$. Here, $T_{st,in} = T_{st,cold}$ is the cold temperature of the sensitive storage system and the pinch represents the irreversibility of heat transfer. The saturation pressure of the condenser is found by imposing the same pinch between the saturation temperature of the refrigerant and the temperature of the fluid receiving the heat. This is illustrated below (Fig.3.30).

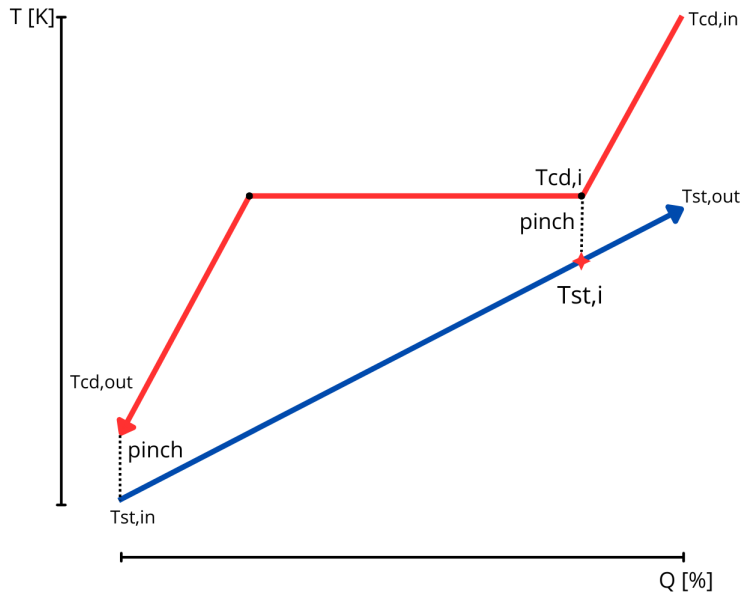

Figure 3.30: T-Q diagram showing heat exchange in a HP condenser, where the working fluid (red) is the refrigerant and the secondary fluid (blue) is the fluid from the thermal storage system.

Assuming a starting value for the saturation pressure, this allows us to find the saturation temperature $T_{cd,i}$ and via an energy balance we find the temperature $T_{st,i}$ = as a function of $h_{st,i}$:

$$h_{st,i} = \frac{\dot{m}_{cd}}{\dot{m}_{st}}(h_{cd,i} - h_{cd,out}) + h_{st,in} \tag{3.12}$$

where $h_{st,in}$ is the enthalpy of the hot reservoir. We iterate on the saturation pressure until we obtain the desired pinch.

Ejector Since the aim is not to study the ejector in detail, we will limit ourselves to calculating the thermodynamic states at the inlet, nozzle outlet, after mixing and diffuser outlet. The following model is based on the conservation of mass and the conservation of energy through a adiabatic device (= conservation of total enthalpy) [89] and assumes the following assumptions:

- the velocity at the inlets and at the outlet of the ejector is assumed equal to 0
- only 1-D flow is considered inside the ejector

- the isentropic efficiency of the ejector is defined based on the inlet, mixing region and diffuser isentropic efficiency

First, we defined the entrainment ratio μ as :

$$\mu = \frac{\dot{m}_{Sf}}{\dot{m}_{Pf}} \tag{3.13}$$

with $\dot{m}_{Sf}$ and $\dot{m}_{Pf}$ respectively the mass flow rate of the secondary fluid (low pressure's one) and the primary fluid (high pressure's one).
Then by knowing the intake state of the primary fluid and by assuming that the pressure at the exit of the nozzle is equal to that of the secondary fluid $p_n = p_{Sf}$, we can find the enthalpy at the exit of the nozzle h_n and its velocity u_n thanks to the nozzle isentropic efficiency.

$$\eta_n = \frac{h_{Pf} - h_n}{h_{Pf} - h_{n,is}} \tag{3.14}$$

where $h_{n,is} = f(p = p_{n,is}, s = s_{Pf})$.
Since we are considering an adiabatic ejector, the total enthalpy is conserved.

$$u_n = (2(h_{Pf} - h_n))^0.5 \tag{3.15}$$

By using the mixing efficiency defined as :

$$\eta_{mix} = \frac{u_{mix}^{0.5}}{u_{mix,is}^{0.5}} \tag{3.16}$$

and the fact we can defined the isentropic mixture velocity as :

$$u_{mix,is} = \frac{u_n}{1 + \mu} \tag{3.17}$$

Then the mixing velocity is given :

$$u_{mix} = u_n \cdot (\frac{\eta_{mix}}{1 + \mu})^0.5 \tag{3.18}$$

The energy equation in the mixing region can be written as:

$$h_n + \frac{u_n^2}{2} + \mu \cdot h_{Sf} = (1 + \mu) \cdot (h_{mix} + \frac{u_{mix}^2}{2}) \tag{3.19}$$

This equation allows us to find h_{mix}.
Using the same assumption of adiabaticity, we find the enthalpy and its other thermodynamic parameters at the exit of the diffuser:

$$h_d = h_{mix} + \frac{u_{mix}^2}{2} \tag{3.20}$$

$$h_{d,is} = (h_d - h_{mix}) \cdot \eta_d + h_{mix} \tag{3.21}$$

$$p_d = f(h_{d,is}, s_{mix}) \tag{3.22}$$

The temperature and entropy can be easily find using h_d and p_d.

Electrical resistance To model the electrical resistance, we assume an efficiency of 100% such that all the electricity used will be converted into heat.
The fluid heated by the resistor is pressurised water, so that it remains in liquid form. In addition, the flow rate, the temperature of the heated water and the temperature glide at the heat exchanger are all dimensioned so that the temperature profile in the heat exchanger minimises energy losses, which is equivalent to two parallel lines with constant slope running in opposite directions (Fig.3.31). To obtain this profile, the flow rates and temperature glide must be equal in both circuits. Note that in reality, the flow rates passing through the two circuits vary slightly independently. From then on, we will observe more curves.

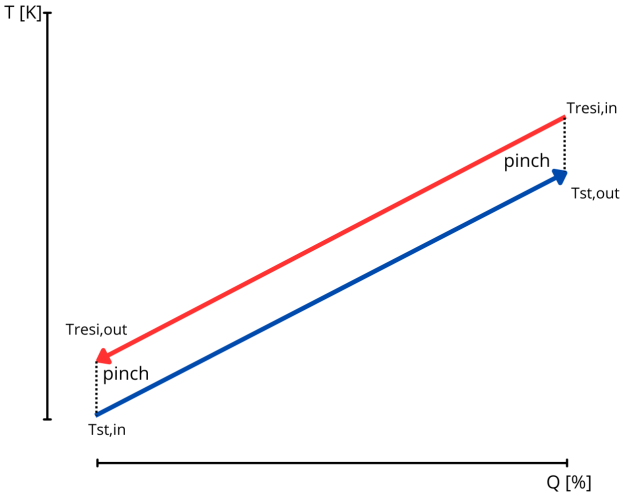

Figure 3.31: T-Q diagram of the heat exchanger between the resistance circuit (red) and the one of the thermal energy storage circuit (blue) such that it minimizes exergy losses

Turbine/expander The expansion device present in the ORC is also model thanks to its isentropic efficiency. It is defined as:

$$\eta_{is,t} = \frac{h_{in} - h_{out}}{h_{in} - h_{is,out}} \tag{3.23}$$

Its value is listed in the table 3.1.

Pump At the pump level in the ORC, we take the assumption that the pump outlet temperature is the same as the inlet one. This is a reasonable assumption, given that the compression of a fluid in liquid form is low, nearly negligible. Therefore the temperature rise associated with compression is negligible.
The pump's mechanical power of the ORC is found via its internal efficiency defined as :

$$\eta_{i,p} = \frac{\dot{m} \cdot (h_{out} - h_{in})}{\dot{W}_{pump}} \tag{3.24}$$

Model parameters and constraints The table below shows the parameters of the numerical model that calculates thermodynamic performance. Some of these are design variables and will need to be optimised (see section 3.3). The waste heat source temperature is set on the basis of the operating temperature of PEM electrolysers. For good heat integration efficiency, the thermal storage temperature must not be too high. Typically in a TI-PTES, we will find hot storage temperatures between 90-140°C [41]. In order to consider two fluids capable of maximising the performance of the DSHP and ORC respectively over the entire temperature range, we will restrict ourselves to using a hot tank temperature of between 95 and 120°C. This limitation is mainly due to the ORC, which requires a fluid with a critical temperature close to the hot storage temperature to maximise its efficiency. Increasing the spread would result in the use of a less suitable fluid for $T_{st,hot}^{min}$ and the results would therefore not represent the case of an optimal configuration. In addition, limiting the temperature above allows to limit the pressure inside the tank and therefore the cost and limiting at 95°C avoid having a too small energy density which implies a large and so more expensive storage system. The cold tank storage temperature is limited below by the output cold waste heat temperature and the storage pressure is set so that the water always remains in liquid form in the tank. Its roundtrip efficiency is assumed to be 100% in this study. The waste heat source temperature glide is limited at the top so as not to affect the correct operation of the electrolyser and to keep a consistent water flow value. The other variables have been set either based on similar applications found in the literature or arbitrarily.

Parameter	Unit	Value	Source
Reference temperature T_{ref}	$°C$	15	-
Reference pressure p_{ref}	kPa	100	-
Waste heat source temperature T_{wh}	$°C$	75	[11],[23],[50]
Waste heat source temp. glide $\Delta T_{wh,gl}$	K	10	-
Hot tank storage temperature $T_{st,hot}$	$°C$	*design var.*	-
Max. hot tank storage temperature $T^{max}_{st,hot}$	$°C$	120	-
Min. hot tank storage temperature $T^{min}_{st,hot}$	$°C$	95	[41]
Cold tank storage temperature $T_{st,cold}$	$°C$	65	-
Storage pressure p_{st}	kPa	250	-
Heat ambient source temperature T_{cold}	$°C$	15	[40]
Heat ambient source temp. glide $\Delta T_{cold,gl}$	K	10	[40]
Heat sink temperature T_{cold}	$°C$	15	[40]
Heat sink temp. glide $\Delta T_{wh,gl}$	K	10	[40]
Pinch point in exchangers ΔT_{pp}	K	3	[36],[40]
HP working fluid $fluid_{HP}$	-	*design var.*	-
ORC working fluid $fluid_{ORC}$	-	*design var.*	-
Compressor isentropic efficiency $\eta_{c,is}$	%	80	[40]
Thermal energy storage efficiency η_{TES}	%	100	
Expander isentropic efficiency $\eta_{t,is}$	%	85	[40]
Pump internal efficiency $\eta_{p,i}$	%	70	[40]
Nozzle efficiency of ejector η_n	%	85	[8],[61],[62],[63]
Mixing efficiency of ejector η_{mix}	%	90	[8],[61],[62],[63]
Diffuser efficiency of ejector η_d	%	82	[8],[61],[62],[63]

Table 3.1: Model parameters and constraints

3.1.3 HP with electrical heater in series

As presented in the description section of the DSHP with electrical heater in series, its control is more complex than the parallel configuration. Indeed, the heat pump uses waste heat as a heat source. As explained in the introduction and in the review of literature chapter, a heat pump using a limited quantity of heat will only be able to deliver a limited quantity of heat at a given condensation temperature. This is because, when all the available heat is used, the flow rate of the refrigerant passing through the heat pump is fixed and the work done by the compressor is fixed by the temperature difference between the evaporator and the condenser.
Therefore, to modify the power that will go to the thermal storage system, we need to increase the proportion of heat produced by the electrical resistance while respecting the energy balances at the exchangers. Therefore, the charging power is controlled by the temperature of the water circuit at the condenser outlet (T_6 in

figure 3.18).

3.1.4 Two dual-source HP in series

When modelling the dual-source HP with 2 HP connected in series 2.2.1, care must be taken to maintain a continuous flow in the two secondary circuits (tank circuit and cold heat source circuit). To do this, the flow rate and the intermediate temperature (between the two condensers) in the tank circuit are set respectively as a function of the heat flux received and as the average temperature of the two tanks $T_{st,int} = \frac{1}{2} \cdot (T_{st,hot} + T_{st,cold})$.
In the cold source circuit, the intermediate temperature between the two evaporators will determine the flow rate required for each HP. It is necessary to iterate on this temperature until a continuous flow through the two evaporators is obtained. Each HP receives an equivalent amount of waste heat.

3.2 Performance criteria

The proposed performance criteria assess the dual-source HP and the Carnot battery from a thermodynamic point of view. In addition, certain criteria directly affect the cost of the installation. In this section, we will explain on the basis of which criteria the dual-source HP, TES, ORC and CB will be evaluated and these criteria will be defined.
The COP coefficient of performance characterises the energy performance of an HP. In the case of a dual-source heat pump, the COP_{global} is used and allows to compare them. The COP_{global} is defined as follows :

$$COP_{global} = \frac{\sum Q_{produced}}{\sum W_m} \tag{3.25}$$

where $\sum W_m$ is the total net work carried out by the dual-source HP. The COP_{global} gives indication on the energy required to power the dual-source HP. A lower COP means that the R.E. will have to produce more electricity and so the COP is indirectly linked to the investment cost of renewable energies for a given quantity of product (hydrogen in our case).
To evaluate the ORC, we define its output η_{ORC} as :

$$\eta_{ORC} = \frac{W_{m,ORC}}{Q_{ev}} \tag{3.26}$$

where $W_{m,ORC}$ is the the net work output of the ORC or equivalently the electrical energy produced by the Carnot battery and Q_{ev} is the heat flux at the evaporator

of the ORC.
Power-to-power efficiency defined as:

$$\eta_{P2P} = COP_{global} \cdot \eta_{ORC} = \frac{W_{m,ORC}}{W_{m,DSHP}} \tag{3.27}$$

where $W_{m,DSHP}$ is the DSHP total net work input. It allows to evaluate the effectiveness of electricity recovery.
Finally, the energy density is defined as :

$$\rho_{el} = \frac{(h_{st,hot} - h_{st,cold})}{v_{st,hot} + v_{st,cold}} \cdot \eta_{ORC} \tag{3.28}$$

where $v_{st,hot}, v_{st,cold}$ are the specific volume of the hot and cold tank respectively. The density corresponds to the amount of electricity that can be discharged per unit volume of the tanks. It allows to evaluate the size of the thermal energy storage system. The larger the storage system, the more expensive it will be so the investment cost of the storage system is indirectly linked to the density.

3.3 Pursuit of peak efficiency

3.3.1 Working fluid

The working fluid in the HP of the various dual-source HP and in the ORC is a design variable that needs to be optimised. It plays a major role in the Carnot battery and must comply with environmental constraints (= low GWP, ODP and avoid eternal pollutants), technical constraints and safety constraints (= avoid as much as possible fluids that are flammable, explosive or toxic which correspond to the third class according to ASHRAE classification [92]). Furthermore, saturation pressure decreases as the critical point increases. Respecting this rule would restrict the choice of refrigerant too much. It's commonly recommended to use a pressure above 1 bar. However, strictly adhering to this guideline may overly limit refrigerant options for the large value of hot tank storage temperature investigated in this work. This is due to the decrease in saturation pressure at a given temperature as the critical point increases. The list of fluids considered for the DSHP and ORC as well as their main characteristics are shown in the table below. They are all adapted to perform with sub-critical cycles in the temperature range considered in this study.

Fluid for DSHP	Type	T_{crit} [°C]	p_{crit} [bar]	$p_{sat,15°C}$ [bar]	GWP_{100}	ASHRAE 34[1]	Shape
R717 (Ammonia)	-	132.2	113.3	7.3	N/A	B2L	wet
R600a (iso-Butane)	HC	134.7	36.3	2.6	N/A	A3	dry
R600 (n-Butane)	HC	152.0	38.0	1.8	0.006	A3	dry
R1233zd(E)	HCFO	166.5	36.2	0.9	3.88[2]	A1	dry
cyclo-Pentane	HC	238.6	45.7	0.3	N/A	N/A	dry
Fluid for ORC							
R161 (fluoroethane)	HFC	102.1	50.1	7.0	4.84[1]	N/A	wet
R152a	HFC	113.3	45.2	4.4	164[1]	A2	wet
R13I1 (CF3I)	H	123.3	39.5	3.7	0.4	A1	wet
R600a (iso-Butane)	HC	134.7	36.3	2.6	N/A	A3	dry
1-Butene	HC	146.1	40.1	2.2	N/A	N/A	dry

[1] ASHRAE Standard 34-2022, "Designation and Safety Classification of Refrigerants"
[2] Value from Table 7.SM.7 of IPCC AR6 [17]

Table 3.2: Properties of the fluids considered in this study (data from CoolProp [2])

3.3.2 Recuperator

In a HP or ORC, it is sometimes beneficial for their energy performance to incorporate a recuperator. This serves in the case of an HP to increase the temperature of the working fluid before it enters the compressor by sub-cooling the working fluid at the condenser outlet. In the case of an ORC, it serves to increase the temperature before entering the steam generator by desuperheating the working fluid at the expander outlet. The configuration of the TI-PTES with recuperator for both HP and ORC can be seen on the graph below. Here, the configuration with recuperator is given for a single-source HP. The recuperator configurations investigated for each DSHP presented can be found in the appendix.

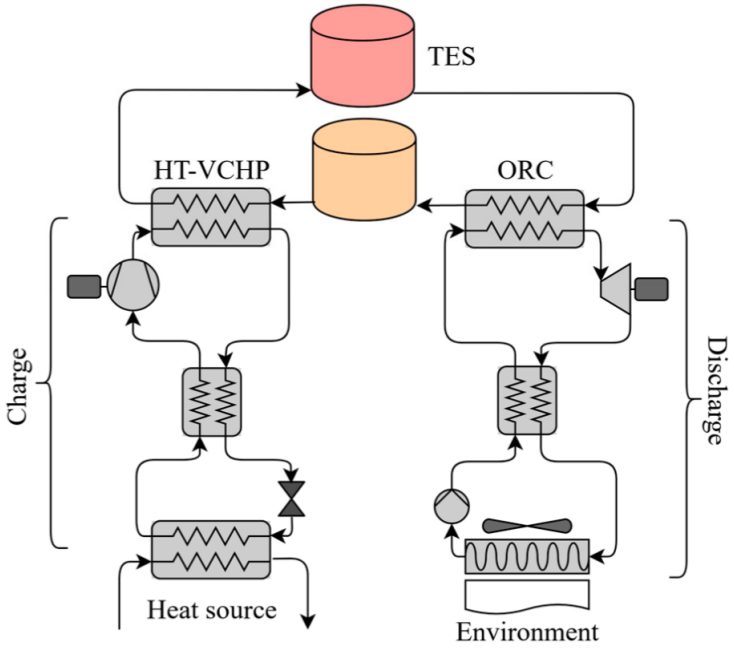

Figure 3.32: TI-PTES configuration used with recuperator integration for both HP and ORC. Source: [41].

Adding a recuperator involves additional costs. It is therefore necessary to ensure that its integration allows a clear improvement in performance. The COP_{global} and the ORC efficiency with and without recuperator for all the fluids considered and for each dual-source HP have been compared in order to find the best combination. The T-s and p-h diagrams and the cycles with recuperator for each DSHP studied are listed in the appendix.

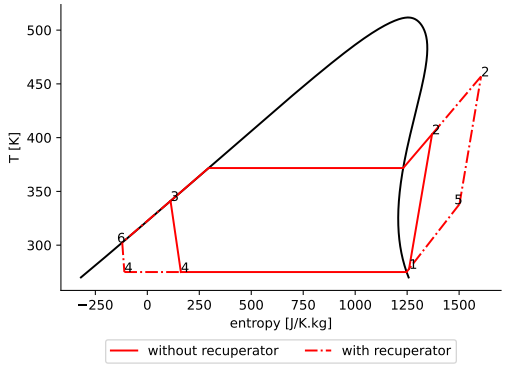

Figure 3.33

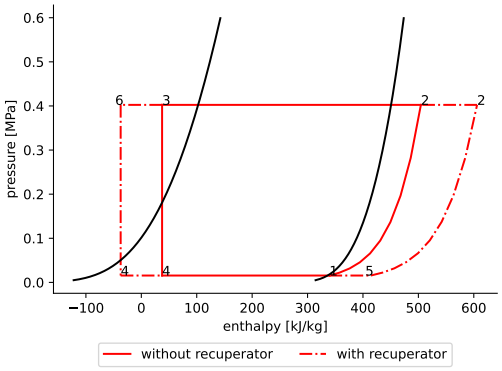

Figure 3.34

Figure 3.35: T-s (left) and p-h (right) diagrams of a classic HP with and without heat recuperator using cyclopentane as the working fluid. The COP is equal to 2.72 and 2.96 without and with recuperator respectively at $T_{st,hot} = 107°C$

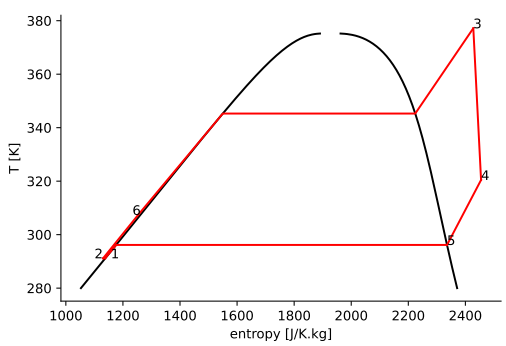

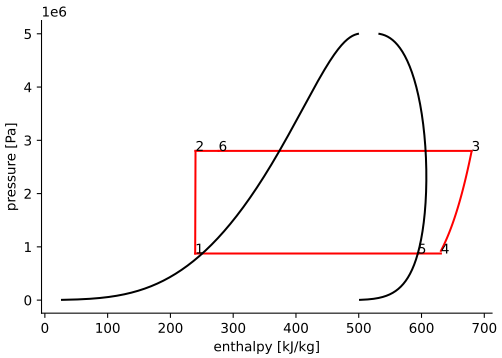

Figure 3.36: T-s (left) and p-h (right) diagrams of an ORC without and with recuperator (between states 4-5 and 2-6) using fluoroethane as the working fluid. The efficiency is equal to 0.116 and 0.1195 without and with recuperator respectively at $T_{st,hot} = 107°C$

3.3.3 Carnot battery dilemma

As demonstrated in the article [40], there is a dilemma which consists of the conflict between the power-to-power efficiency η_{P2P} and the energy density ρ_{el}. Obviously, we would like to maximise both. The objective is twofold. Firstly, we want to know the sensitivity of one to the other and secondly, to find the optimum between the two.

3.4 Parameter sensitivity analysis

Certain parameters are specific to the scale and power of the installation (i.e. $\eta_{c,is}, \eta_{t,is}, \eta_{p,i}$). As we are not restricted to a scale of magnitude, it is important to be aware of the level of sensitivity of performance to these parameters. For example, if a high level of sensitivity is detected, the parameter in question should be carefully selected for a particular case study. Other parameters have a direct influence on the cost of components and on the efficiency of the CB. Notably the temperature pinch. Indeed, given that the temperature levels within the CB are low (<120°C), we can expect to observe a strong sensitivity of the efficiency with the temperature pinch at the exchangers [35]. Furthermore, if economic considerations were not taken into account during the design phase, we would always tend to minimise this temperature pinch for reasons of energy efficiency and exergy. However, to obtain low pinch, it is necessary to have a large contact surface and high fluid velocity. These constraints increase the cost of heat exchangers and pressure losses [73].

4.0 Results & discussion

4.1 Results of the pursuit towards peak efficiency

4.1.1 Dual-source HP: configuration used to aim for peak efficiency

In all the dual-source HP, cylopentane stands out from the crowd every time. Despite its low saturation pressure at low temperature (heat sink/ambient temperature), we will still consider it in view of its performance. In the case of the two dual-source HP with cascade HP, there are two cycles with two distinct fluids. All possible combinations of fluids have been considered, but the configuration with the best COP is the one with cyclopentane in both cycles. Based on the graph below, we can see that the effect of the recuperator depends on the fluid. For butane, the effect is largely beneficial, unlike R717 (i.e ammonia), which performs better without recuperator. However, when considering the use of cyclopentane, the addition of a recuperator is largely beneficial for all the HP configurations present in the various dual-source HP.

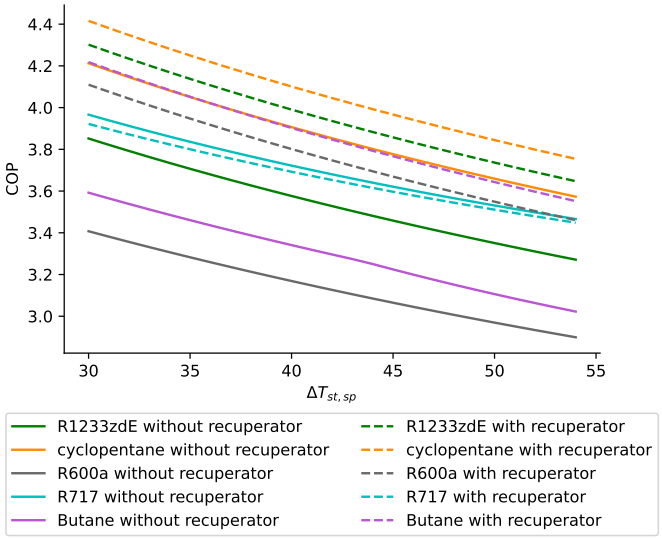

Figure 3.37: Comparison of the COP_{global} for the case of the HP dual-source HP with open economizer with the variation of thermal storage spread temperature $\Delta T_{st,sp}$ for the involved fluids with and without recuperator. A ratio $\frac{E_{th,produced}}{E_{wh}} = 2.5$ is used

There are only 2 exceptions: HPs whose only source of heat is waste heat (3.20,2.2.2,3.23) and the dual-source HP with ejector + pressure boost (3.9). HP systems that only use waste heat as a heat source have a temperature difference between the condenser and the evaporator that is too small to justify the use of a recuperator. In the dual-source HP with ejector + pressure boost, the idea of this dual-source HP is to use the heat leaving the condenser to inject it into the ejector. The greater the internal energy (=enthalpy) of the fluid leaving the condenser, the greater the pressure lift produced by the ejector. Reducing entalpy by using a recuperator would be counterproductive.

In some dual-source HP, there are free variables that need to be optimised. As soon as a parameter (external or internal to the dual-source HP) is modified, the optimum value of these variables must be recalculated. For dual-source HP with cascade HP, the free variable corresponds to the intermediate temperature (i.e. temperature at the level of the intermediate exchanger between the two HP (see states 11, 12 on the figure 3.2). This temperature sets the temperature lift of each HP and their respective work. This optimum temperature is calculated iteratively until the best COP is obtained.

In the dual-source HP with ejector + pressure boost, the pressure ratio produced by the small compressor acting as a pressure dual-source HP is also a free variable

to be optimised. This is calculated iteratively until the best COP is obtained.

4.1.2 ORC: configuration used to aim for peak efficiency

In a similar way to the optimisation of dual-source HP, each fluid has been tested with or without a recuperator. The aim is to find the configuration that optimises the ORC's efficiency in the range of the tank temperature spread considered. To do this, the optimum superheat at the expander inlet was calculated for each temperature spread and for the two configurations under consideration while maintaining a sufficient superheat at the expander outlet to ensure a constant supply of fluid in vapor form. This constraint is necessary for the expander's durability, and a good practice superheat value of at least 3K is applied. Indeed, this superheat ensure that there are no droplets in the fluid that could damage the expander.

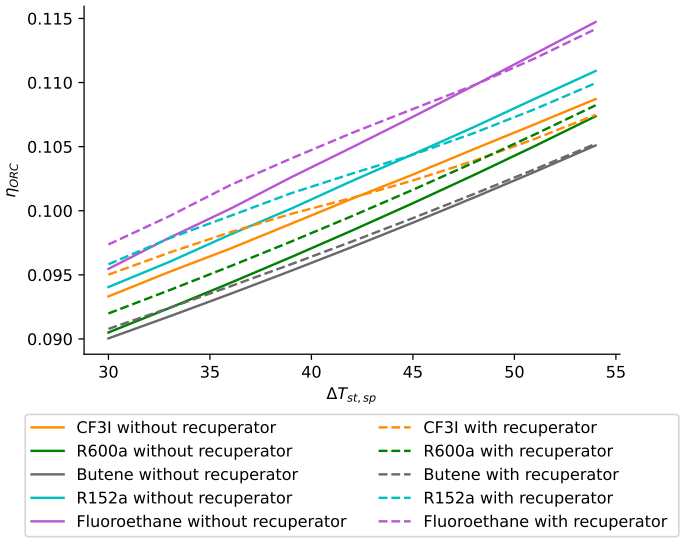

Figure 3.38: Comparison of the ORC efficiency with the variation of thermal storage spread temperature $\Delta T_{st,sp}$ for the involved fluids with and without recuperator

Based on these results, it can be seen that maximum ORC efficiency is obtained when fluoroethane is used. With regard to the gain linked to the recuperator for the case with fluoroethane, its use is beneficial only for a $\Delta T_{st,sp} \leq 48[K]$, altough the gain it brings remains minimal ($\leq 3.11\%$) and its influence on the overall performance of the Carnot battery (i.e power-to-power efficiency) will be negligible. Consequently, its use is not economically justifiable and it will not be considered in the rest of this work. Note that the fluctuations in the ORC efficiency curves

are due to the fact that the optimum superheat temperature value varies for each temperature spread considered.

4.2 Carnot battery optimisation

We know that by providing only a finite amount of heat to the heat source of a basic heat pump, it can only generate a restricted quantity of thermal energy at a specific temperature. In our case, this means that the flow of heat supplied to the TES is fixed and insufficient to load the TES in a consistent manner in a given time, which results in the production of a too small quantity of electricity compared to that of the industrial installation which reject the "waste" heat. This low ratio makes it impossible to economically justify such an installation. We have already seen that one solution for increasing this heat flow with respect to the given waste heat was to use a DSHP. However, we need to be able to define the net input work that the DSHP will have to do in return. In the lower left-hand figure, the COP is used to represent the net work to be done for a given quantity of thermal energy sent to the TES and is represented as a function of the ratio of thermal energy produced by the DSHP for a given quantity of waste heat. In other words, behind this graph lies the link between the performance of the DSHP as a function of the fraction of heat coming from the second heat source. In the case of our application, we are considering an RE source that supplies an electrolyser plant and the carnot battery intermittently. These electrolysers are characterised by an internal efficiency and a power supply. The heat flux normally lost is derived from these two terms. In addition, the carnot battery is used to satisfy a presumed known need (powering the auxiliaries or powering the electrolysers) in order to produce more hydrogen for an in. From this need comes the thermal energy ($E_{th} = E_{el,ORC}/\eta_{ORC}$) that the CB must store in order to meet the demand. Finally, the overall performance of the CB (η_{P2P}) can be compared according to a ratio that directly compares the energy produced by the CB to the main consumption of the installation (i.e the energy consumed by the electrolysers). The graph on the left is more general and can be used to design any system using one of the dual-source HP studied which incorporates a residual heat source. The graph on the right focuses on our application by concentrating on the evolution of power-to-power efficiency as a function of the amount of electricity produced by the ORC for a given amount of electricity consumed by the electrolyser system.

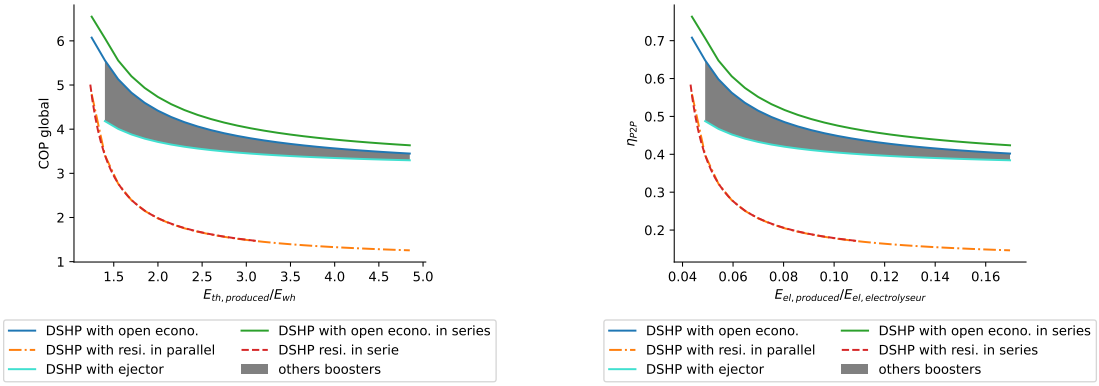

Figure 3.39: Comparison of the performance of dual-source HP (left)/ Carnot battery coupled to an electrolyser system (right) as a function of the ratio of thermal/electrical energy produced to the thermal/electrical energy characterising the size of the installation (respectively the waste heat and the power consumption of electrolyser). An efficiency of 70% for the electrolyser plant and a hot tank storage temperature $T_{st,hot}$ of 107°C have been used.

As can be seen, the COP_{global} and η_{P2P} of the resistor dual-source HP are much lower when the heat produced by them is increased. For this reason, these two dual-source HP will no longer be considered in the sensitivity analysis. Except for the dual-source HP with HP connected in series, which has a COP_{global} that clearly stands out, all the others have similar performances. However, the economic factor must be taken into account before we can say that the dual-source HP with HP in series is the best choice.

As explained above, energy density and power-to-power efficiency are important parameters for a Carnot battery. The density characterises the volume/size of the TES (and therefore its cost) while the η_{P2P} efficiency characterises the storage efficiency. By looking at the figure 3.40, we can see that the COP is inversely proportional to the density and, conversely, the ORC efficiency is directly proportional. When we combine the two, we see that power-to-power efficiency decreases with density. However, except for the dual-source HP with cascade HP + IHX (i.e internal heat exchanger), the decrease is slight. There is a compromise between these two variables, even if it is not very marked. This is good news, because we'll be able to maximise energy density without sacrificing P2P efficiency. This graph will enable us to choose the compromise based on a previously determined case study.

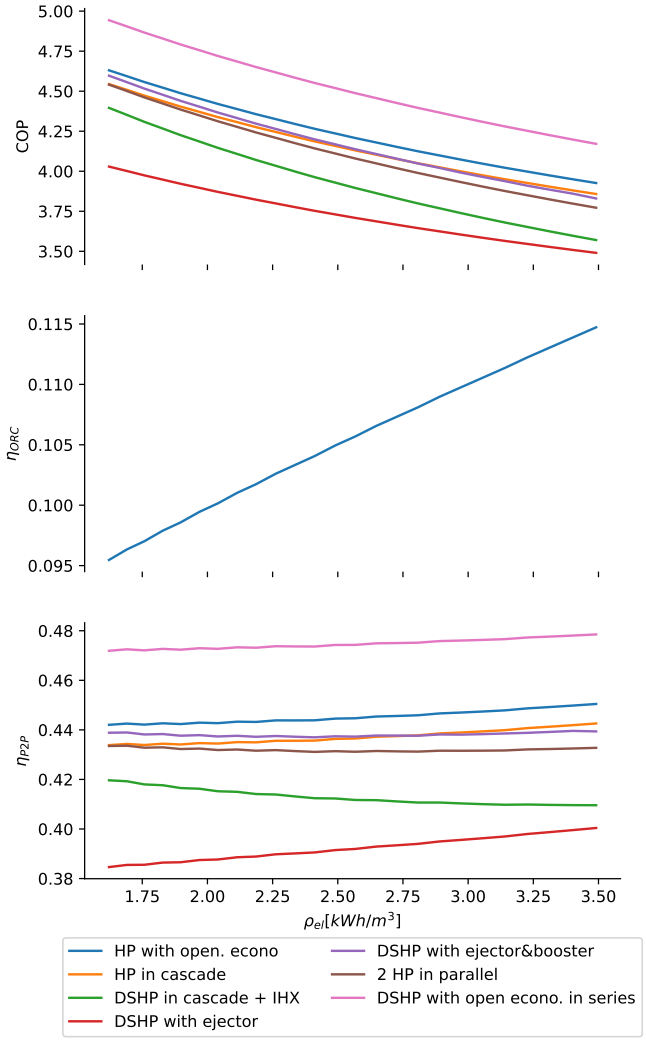

Figure 3.40: The Carnot battery dilemma for a ratio $E_{th,produced}/E_{wh}$ equal to 2.5

As mentioned above, the fluctuations in the ORC and power-to-power efficiency curves are due to the fact that the optimum superheat temperature value varies for each temperature spread considered. Note also that these curves are obtained for a given ratio $E_{th,produced}/E_{wh}$ of 2.5 arbitrarily chosen. Overall, the pattern remains the same. However, there is a slight decrease in the efficiency with the energetic density when the ratio is low (<2.1) and an increase that becomes more marked as the ratio increases. This is explained by the fact that the fraction of heat coming from the second source (i.e ambient air at lower temperature than the waste heat) increases as the ratio increases. As a result, the COP of the DSHP decreases while that of the ORC remains unchanged, showing that the influence of the ORC efficiency on the power-to-power efficiency increases with the ratio

$E_{th,produced}/E_{wh}$. The figure of the dilemma of the Carnot battery 3.40 with two other ratios (1.8 and 4) are listed in appendix.

4.3 Results of sensitivity analysis

As stated above a ratio $E_{th,produced}/E_{wh}$ of 2.5 is arbitrarily chosen for the graphs shown below but the evolution of the COP_{global} and the η_{P2P} depending on the density and the ratio $E_{th,produced}/E_{wh}$ for the different variables analysed can be found in the appendix.

4.3.1 Pinch point sensitivity analysis

The most important heat exchanges take place in the exchangers linking the dual-source HP and the TES, and between the TES and the ORC. Changing the temperature pinch at the condenser of a HP requires it to perform a greater lift temperature. Its COP is therefore affected. At the ORC evaporator, the evaporation temperature is reduced and so is its efficiency. This is why we have carried out a sensitivity analysis of these two exchangers.

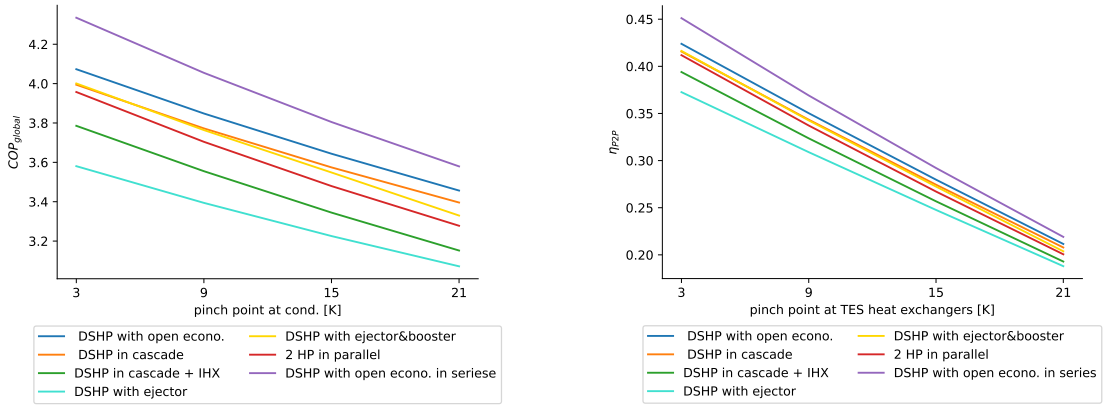

Figure 3.41: COP_{global} and η_{P2P} sensitivity to the pinch temperature with $T_{st,hot}$ = 107°C and a ratio $E_{th,produced}/E_{wh}$ of 2.5

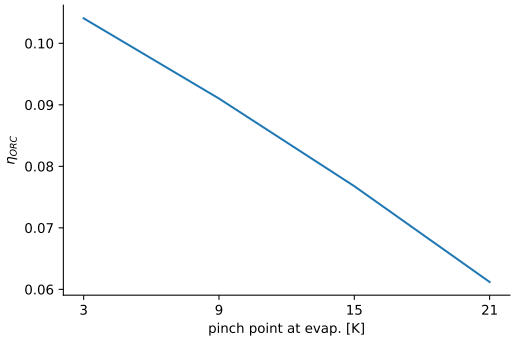

Figure 3.42: η_{ORC} sensitivity to the pinch temperature with $T_{st,hot} = 107°C$

It is see that an elevation of the pinch of 10 [K] causes a decrease of 15% of η_{P2P}. We concluded that it is important to invest in a larger exchanger as a priority in order to minimize the pinch.

4.3.2 Compressor efficiency sensitivity analysis

As stated previously, the isentropic efficiency of a compressor may depend on the size of the compressor, the type of compressor, etc. The efficiency of the compressor obviously affects only the COP within the dual-source HP.

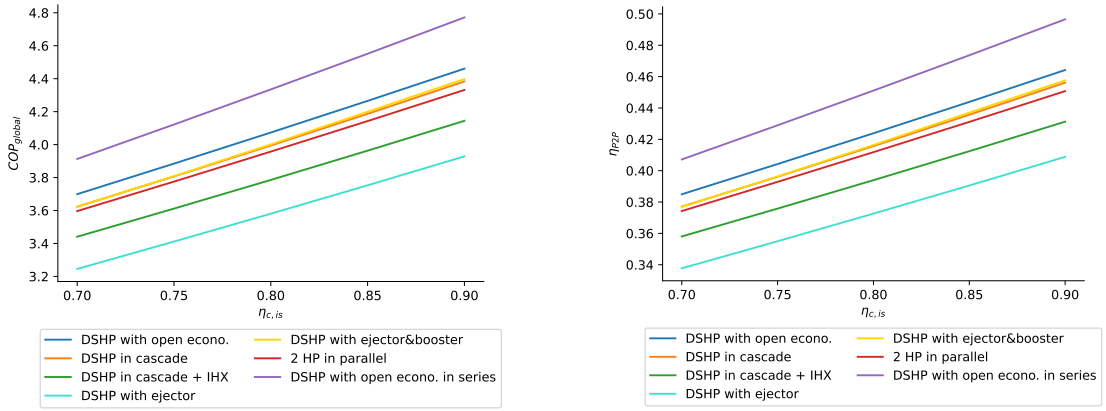

Figure 3.43: COP_{global} sensitivity of dual-source HP to the compressor's isentropic efficiency and its impact on the power-to-power efficiency with $T_{st,hot} = 107°C$ and a ratio $E_{th,produced}/E_{wh}$ of 2.5

As expected, the COP believes with $\eta_{c,is}$. It is also noted that the present performance gap between dual-source HP increases slightly with $\eta_{c,is}$. There is a η_{P2P} increase of 8,825% for a $\eta_{c,is}$ increase of 20%. It is concluded that the sensitivity remains moderate.

4.3.3 Expander efficiency sensitivity analysis

Expander efficiency affects only the ORC.

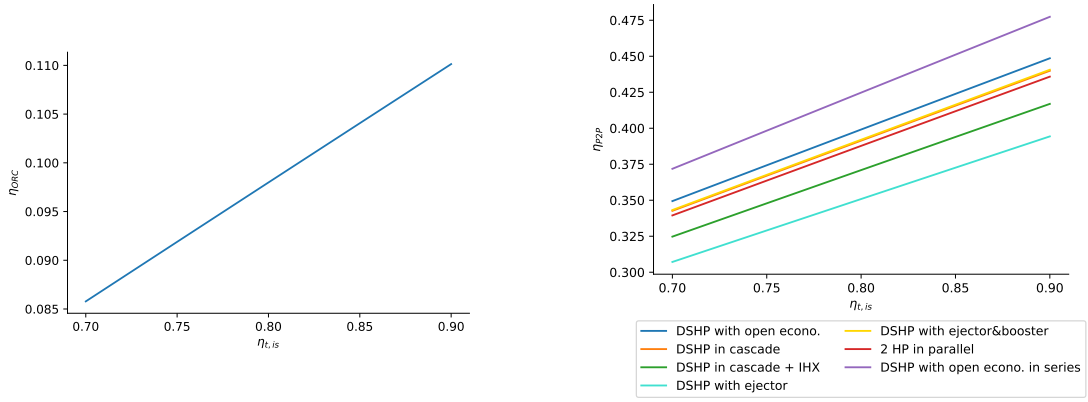

Figure 3.44: Sensitivity of ORC efficiency to the expander's isentropic efficiency and its impact on the power-to-power efficiency with $T_{st,hot} = 107°C$.

As expected, the yield increases with $\eta_{t,is}$. There is an increase of η_{P2P} of 11.25% for an increase of $\eta_{t,is}$ of 20%. It is concluded that sensitivity remains moderate but higher than $\eta_{c,is}$.

4.3.4 Pump efficiency sensitivity analysis

Pump efficiency affects only the ORC but its influence on η_{ORC} is found to be negligible. Indeed, it influences the work of the pump which is itself much lower than the work of the turbine (<2%).

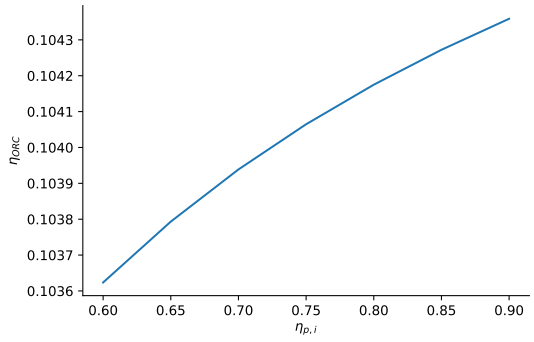

Figure 3.45: Minimal sensitivity of the ORC's performance to the pump's internal performance with $T_{st,hot} = 107°C$

5.0 Conclusion

one will retain that the majority of dual-source HP have similar energy performance. Only the dual-source HP with dual-source open economizer HPs in series and the dual-source HP with resistors stand out respectively because its COP surpasses all others and the serialization makes it possible to add an offset at the COP and because their COP drops as the share of energy produced by the resistor increases. During optimization, it is the cyclopentane fluid that clearly stands out for all dual-source HP and the recuperator is an advantage in general. For the ORC, propane stands out but the configuration varies according to the temperature spread of the TES. Finally, it should be noted that the typical trade-off between energy density and power-to-power efficiency, commonly observed in a Carnot battery, is minimally present in our case.

Chapter 4

Carnot battery integration case study with Dual-source heat pump

The chapter 3 allowed us to characterize thermodynamically the DSHP and to know the sensitivity of the CB performances for these different DSHP. However, the impact on the production performance that CB can bring within the coupling and the economic aspect of this coupling has not yet been addressed. This chapter will therefore be devoted to the analysis and comparison of the performance of an electrolyser site coupled to an energy storage system all powered by a renewable energy source (i.e green production). The second stage will involve comparing and discussing the competitiveness of the CB against the best storage options already available on the market (found in the previous step of this chapter) from an economic and technical perspective.

1.0 Description of the application case and the storage system's use

1.1 Type of renewable energy source

In the literature [54],[44],[87],[67], three cases are generally considered for the production of hydrogen via water electrolysis: the solar energy via photovoltaic (PV) panels , the wind energy using wind turbine and the mix between these two energy sources. On one other hand, the production of wind turbines on the time scale corresponding to that of thermal storage (a few hours to a few days), does not follow any trend and is not predictable. This random nature makes it impossible to consider this type of RE with the model considered in this study. On the other hand, electricity produced from PV panels is characterised by an average production pattern that repeats itself every day, which simplifies the analysis and

the comparison. Indeed, the charging and discharging cycles will be similar from day to day and will be easily identifiable (i.e day and night) over the period considered. Consequently, electricity production from PV panels will be considered in this chapter and the comparison will be based on a 1-year average daily production pattern. The irradiation dataset considered to calculate the production pattern equals to the irradiation pierced at Puertollano (Spain). This location has been selected because a 100 MW photovoltaic solar plant used to produce green hydrogen has already been implemented there [32], which means that, by deduction, the irradiation rate of this location is promising for a good profitability. The solar irradiation data used comes from National Solar Radiation Database (NSRDB) [70].

1.2 Hydrogen issues

One major issue when dealing with hydrogen is its transport. Although hydrogen has a very high mass specific energy ratio, it is a fluid which, at ambient pressure, has a very large specific volume. In order to transport it, it must therefore be compressed to a high pressure (150-200 bar) [60], which generates additional energy costs. Futhermore, hydrogen is a highly explosive and flammable fluid [20], making it even more difficult to transport. To counter these problems, hydrogen can be converted to ammonia directly on the production site. Ammonia has the advantage of having a higher energy density than hydrogen (11.5 compared to 0.010-0.011 MJ/L under standard conditions [55]) and although it is classified as toxic (B2L according to ASHRAE [92]), it is much less explosive and flammable than hydrogen. It is therefore safer and more efficient to transport. In addition, ammonia is already widely used, particularly in the agricultural sector for the production of fertilisers. Up to 45% of the world's hydrogen production is used to produce ammonia [1]. These reasons lead us to consider a case of power-to-ammonia integration (= hydrogen produced from RE will be transformed into ammonia on site).

1.3 Storage system's use

The production of green ammonia requires a renewable energy source (i.e PV panels), a hydrogen production process (i.e PEM electrolysers), an ammonia production process (i.e Haber-bosch) and auxiliaries (i.e desalination unit, pump, air separator, compressor) needed to operate the production process (the entire system is shown in figure 4.1 and describe in the following subsection).

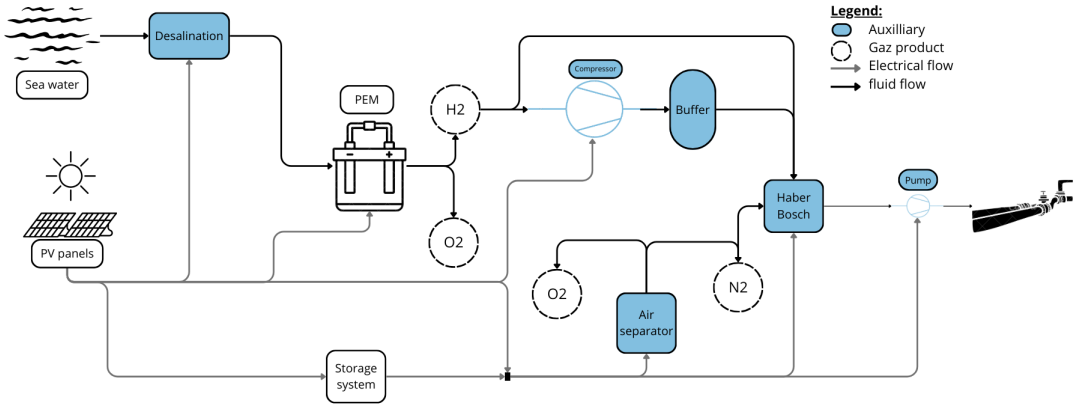

Figure 4.1: Diagram of the integration case considered in this chapter

As the whole system can only use the electricity produced by the PV panels, it must technically be able to cope with this constraint. We know that PEM electrolysers are not very sensitive to fluctuations and can operate at low load 1.0. Therefore, there are no technical constraints that would require them to be powered continuously. On the other hand, several articles [68],[94] have shown the importance of operating the ammonia production system in steady-state. In fact, a continuous process can produce more ammonia than an intermittent process, and in less time. This is why generic ammonia synthesis reactors are designed to operate continuously 330 days a year and when a mandatory shutdown occurs, it takes several days to restart the reactor. One of the reasons for this is that the process uses catalysts that are highly sensitive to fluctuations in pressure and temperature within the reactor. As we're only using PV panels, there will be no electricity production at night and as the ammonia production process has to be powered continuously, a electrical storage system as well as a buffer storage have to be used to supply the ammonia production process of electricity and hydrogen respectively.

1.4 Description of the integration case

To be able to design the storage system, we need to know the consumption of the auxiliaries that will need to be supplied during the off-peak production phase (i.e

the night). To do this, let's review the various elements present in the system (see Fig.4.1) and quantify their specific consumption. Fortunately, a study [54] has already focused on characterizing the specific consumption of components used in the production of green hydrogen and ammonia from PEM electrolyser. Therefore, we will use or adapt these results for the present case.

PEM electrolyser The most energy consuming element is obviously the PEM electrolyser. According to the study [54],[68], the mass ratio of hydrogen necessary to produce 1 kg of ammonia is equal to 0,17755:1 . Its specific consumption is equal to 4.2-5.6 $[kWh/Nm^3_{H2}]$ [23] which correspond to 50.15-66.86 $[kWh/t_{H2}]$ using hydrogen density of 83.75 kg_{H2}/Nm^3. Finally, taking the previous ammonia to hydrogen mass ratio, the specific consumption per unit of ammonia's mass is equal to 8904.5-11871.45 $[kWh/t_{NH3}]$.

Desalination unit Electrolyser needs to be supplied with water which is not always available in every locations., especially since solar panels are often placed in isolated desert regions to have greater irradiation. Desalination of water from the sea remains a viable and commonly used solution. In addition to this, electrolysers need pure water so water purification treatment is usually necessary. For that reasons and even if several desalination technologies exist, the Mechanical Vapor Compression (MVC) technology will be considered here. Based on the results of the above study, its specific energy consumption is equal to 22.8 $[kWh/t_{H2O}]$. As the electrolyser need 10 kg_{H2O} to produced 1 kg of hydrogen and reusing the previous mass ratio, the specific consumption per unit of ammonia's mass is equal to 41 $[kWh/t_{NH3}]$. Considering the foregoing, the water purification element can be neglected. As its use stipulates, desalination should only work when the electrolyser is also running

Compressor Once the hydrogen is produced, two paths open to him. Either it is sent directly into the ammonia production process, or the ammonia production process is already sufficiently fed in which case the excess hydrogen produced will have to be compressed and stored in buffer storage to be transformed into ammonia later. This compression step is necessary because, as explained above, the density of hydrogen is very low and storing it in a reasonable volume requires compression. In the study, it is assumed that the gas will be stored under a pressure of 160 bar. However, a peculiarity that has not been taken into account in their study is the fact that PEM electrolysers powered by an intermittent source are more robust when they operate at atmospheric pressure. This is why the results below need to be adapted to the new pressure lift (=160/1) considered here. The specific power found for the compressor is then equal to 630.5 $[kWh/t_{NH3}]$.

Ammonia synthesis process The ammonia synthesis loop is represented on the figure 4.2. Roughly, the process can be divided into several steps. First, hydrogen and nitrogen are injected into the feed compressor to be brought to a pressure in a range of 150-250 bar [68],[94]. They will then be mixed with the recycled stream from the reactor. This mixture will then be heated via the lost heat from the exothermic reactions within the reactor before it can be introduced into the reactor. Finally the outgoing flow of the reactor is cooled then the ammonia produced is condensed and recycled while the rest of the gas synthesis is recycled and repaints the cycle until reaching the level of sufficient purity.

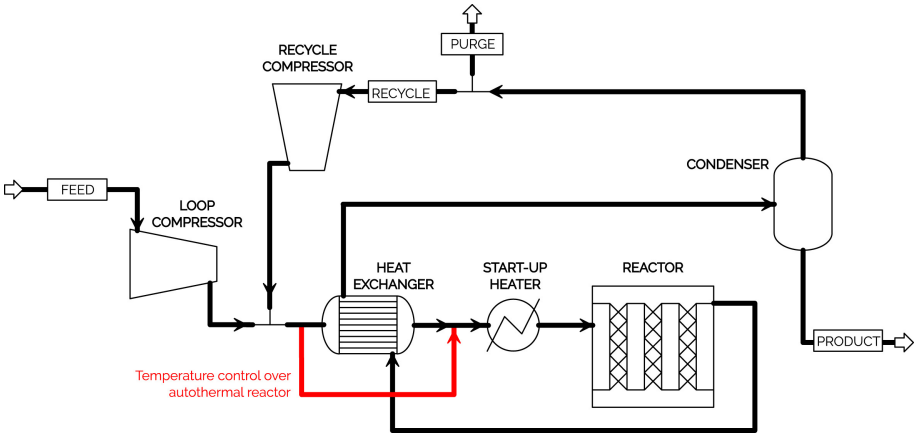

Figure 4.2: Diagram of the entire ammonia production process. Source: [94]

The main energy cost of this process is the consumption of compressors which must be added to the cost of the recycled compressor plus the cost of the refrigerant cycle used to condensed ammonia. In the study, a operating pressure of 200 bar is assumed and the energy cost of the recycled compressor is estimated assuming a pressure drop of 6 % of the process operating pressure (= 12 bar). The energy cost of the refrigerant cycle is calculated on the basis of a COP of 2.5. However, to calculate the energy consumed by the feed compressor, there are two cases that must be differentiated for our case:

1. Hydrogen consumed comes from buffer storage and is pressurized to 160 bar
2. Hydrogen consumed comes directly from the electrolyser and is at 1 bar

In the first case, the compressor need to compress the nitrogen from 1 to 200 bar and the hydrogen from 160 to 200 bar. The study shows a specific consumption for all the ammonia production process equal to 309.6 $[kWh/t_{NH3}]$.
In the second case, the compressor need to compress both nitrogen and hydrogen from 1 to 200 bar. The specific consumption, adapted from the results of the study,, correspond to 927.7 $[kWh/t_{NH3}]$.

Air separator unit The nitrogen used in the ammonia production process is produced using an air separator unit. The cryogenic distillation method is considered to separate the oxygen from the nitrogen (the oxygen can also be sold to the market but we will not consider it in this study) as it allows a high nitrogen purity necessary for the ammonia production process. The study found that the specific energy consumption driven by the consumption of the compressor present inside, is equal to 90 $[kWh/t_{NH3}]$.

Pump station Finally, for large production plant, a pipeline can usually be considered to transport the ammonia in liquid phase. The energy required to counter the pressure losses within the pipeline depends on the length, the diameter of the pipeline and the speed of the fluid transported. The study uses a very detailed approach to design the pipeline and to calculate the pressure loss for different location scenarios. However, we will consider a specific energy consumption of pressurization stations of 0.5% of the electrolyser's specific energy consumption which corresponds to the same order of magnitude as the results presented in the study.

All the consumptions of the different elements are listed in the table below:

Component	SEC $[kWh/t_{NH3}]$	Share of energy consumed [%]
PEM electrolyser	10387.75	90.29
Desalination	41	0.35
Hydrogen compression	630.5	2.46
Ammonia synthesis process	309.6 or 927.7 [1]	5.65
Air separator	90	0.78
Pump	51.9	0.45

[1] Specific consumption varies depending on whether the hydrogen used comes from the buffer under pressure or not. The share of compressed hydrogen over all hydrogen produced is 45%. The share of directly transformed hydrogen is 55%.

Table 4.1: Specific energy consumption (SEC) of all auxiliaries plus the electrolysers and their respective shares related to the total consumption on a full day

Since the electrolyser is the most energy-intensive component and the consumption of the other elements is proportional to that of the electrolyser (i.e the amount of hydrogen produced), we decided to express their consumption relative to the electrolyser's consumption. In addition, the day and night consumption is

expressed. This makes it possible to clearly show the energy flows during these two phases, as well as the proportion of energy that the battery must satisfy.

Component	Daytime consumption		Night consumption	
	$[MWh]$	[%]	$[MWh]$	[%]
PEM electrolyser	575.92	-	-	-
Desalination	1.23	0.21	-	-
Hydrogen compression	15.90	2.78	-	-
Ammonia synthesis process	27.01	4.7	7.80	1.37
Air separator	2.72	0.47	2.27	0.40
Pump	1.56	0.27	1.30	0.23
Total	624.34	98	11.38	2.00

Table 4.2: Energy consumption during the day (i.e $P \geq 0.1P_n + P_{aux}$) and night consumption (i.e $P \leq 0.1P_n + P_{aux}$) of all auxiliaries plus the electrolysers for the typical day and their respective shares related to the total consumption of the electrolyser on a full day

In conclusion, the storage system will need to supply the ammonia synthesis process at its low specific consumption (i.e the hydrogen is already pressurized), the air separator and the pump when the PV panels will no longer be able to supply them. This corresponds to 2% of the electrolysers' consumption over a typical day However, this consumption can be affected depending on how we choose to design the whole system. For example, one could decide to pressurize the nitrogen produced by the air separator unit in order to store it and thus only run it during the day which will reduce the necessary consumption of auxiliaries at night. On the other hand, one could imagine wanting to supply housing located near the site from the RE during the day and from the storage system at night which is equivalent to increasing the energy demand that the battery will have to meet.
It is therefore clear that the consumption obtained above is used to give an order of magnitude for the system presented. In order not to be limited to this configuration and to have a general/global vision, we will also consider the case where the need for auxiliaries (i.e the energy the battery has to deliver) correspond to 3% and 4% of the total consumption of electrolysers over a day.

Finally, an important parameter when considering a system powered solely by renewable energy is the load factor of the various system components. This characterises the efficiency of the components in producing or consuming energy in relation to their theoretical maximum capacity over a given period. These load factors are shown in the table below:

Component	load factor [%]
PV panels	22.7
PEM electrolyser	41.5 - 42.6
Ammonia synthesis process	91.6

Table 4.3: Load factor of the main components present in the system

The load factor of the photovoltaic panels was calculated via the system advisor model SAM software [88] and corresponds to the DC capacity factor of the installation. Concerning the load factor of the electrolysers, it will vary slightly according to the considered storage systems. Finally the load factor of the ammonia production system is calculated on the basis of the hypothesis that shutdowns due to technical failures occur, on average, 5.7 times per year. The synthesis process takes several days to return to its steady state, so it is considered to be fully operational 330 days a year. [68].

1.5 Type of storage technology

In this study, 3 storage systems will be compared: lithium battery, Carnot battery and fuel cell.

Lithium battery The lithium battery is already widespread and well installed on the market and has a storage time scale similar to that of the CB. It has a good power-to-power efficiency between 85-95% [37] and is the system commonly used to store electricity in any place when using renewable energy. Its investment costs have been falling steadily over the last few years due to the strong demand that has emerged. As a result, its cost varies greatly depending on the sources considered. In our case, we will use a cost in a range of 270-230€/kWh which seems to be the most up-to-date value for a battery system capable of storing approximately 12 MWh [45],[28]. An additional criterion to take into consideration during its design phase is the fact that the state of charge (SOC) must always remain in the range of 15-95% (= depth of discharge of 80%)[87] because full charge and discharge cycles would damage the battery too quickly. This implies to consider an additional margin for the battery capacity which impacts its cost. Another drawback with the lithium battery is that they have the characteristic of having a self-discharge (0.5-1% per month) with implies a limited life time of about 15 years [3].

Fuel cell The fuel cell is a system capable of transferring the chemical energy contained in hydrogen (in our case) to transform it into electricity. It is characterized by a investment cost in the range of 2000 - 5000 €/kW [26],[27] and a constant

efficiency between 40-65% [39] defined as:

$$\eta_F = \frac{W_{el}}{W_{H_2}} = \frac{W_{el}}{m_{H_2} LHV_{H_2}} \tag{4.1}$$

In our case, we will consider an efficiency of 49% [44].

Carnot battery The Carnot battery has already been extensively analyzed in this work. For this chapter, we will consider an TI-PTES using a DSHP with open economizer all placed in series (= DSHP configuration with the best COP found in the previous chapter) with a hot storage temperature of 107°C and a fixed ORC efficiency related to this temperature of 0.105. We will consider this temperature because, as presented in the results section of chapter 3, the power-to-power efficiency is weakly sensitive to the energy density (i.e the temperature of the hot tank). Optimization is therefore not necessarily needed. Choosing an average value makes possible to reach a simple compromise between the two.

2.0 Methodology

First, please remember that the main purpose of this chapter is to compare production with different storage systems. To ensure a fair comparison, constraints had to be imposed (see further) and the system was designed to maximise production under these constraints

The first step was to define the nominal power of the PV installation. A power of 100MW was chosen arbitrarily for that purpose. From this point, we were able to find the power profile of a day averaged over an entire year (Fig.4.3) using the SAM software [88] with reference parameters and the irradiation dataset from Puertollano (Spain) as mentioned above.

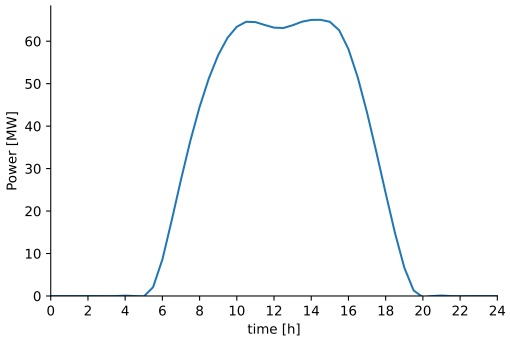

Figure 4.3: Power profile of a typical day obtained for a 100MW PV panel installation located in Puertollano.

The second step was to fix the total power consumption of the total system in order to be able to compare fairly the mass production. This limit has been set as high as possible to make the best use of the electricity available for that particular standard day. We assume that the battery will only be charged when this power level is reached. This allows the Carnot battery to benefit from maximum waste heat.
Then, we need to differentiate between cases according to the level of power available.

1. $P \geq P_{tot,used}$
2. $P_{tot,used} \geq P \geq 10\%P_{n,electro} + P_{aux}$
3. $10\%P_{n,electro} + P_{aux} \geq P \geq P_{aux}$
4. $P_{aux} \geq P$

The first case corresponds to the situation where either the battery is being charged or it is already full and the electrolyser is operating at nominal power. The second case represents the situation where all the available power is used solely to supply the auxiliaries and to supply the electrolysers with the remaining power. The third case corresponds to the situation where the power available is too low to supply the electrolysers. In our case, we considered that the PEM electrolysers could not operate below 10% of their nominal load. So the remaining power is only used to supply the auxiliaries. In the latter case, there is not enough power available to supply either the electrolysers or the auxiliaries. This is when the storage system comes into play to power the auxiliaries that need to be continuously supplied (i.e. the ammonia production process, the air separator and the pump). The power profile of the electrolysers and auxiliaries as a function of time in the case of a lithium battery, Carnot battery and fuel cell are shown in figures 4.4 and 4.5 respectively.

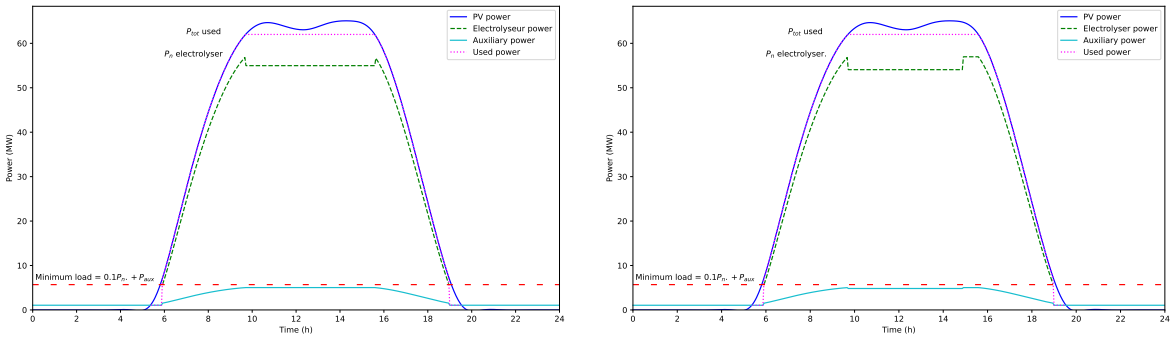

Figure 4.4: Profiles of the different powers considered in the system as a function of time on a typical day for the case with lithium battery (left) and with Carnot battery (right)

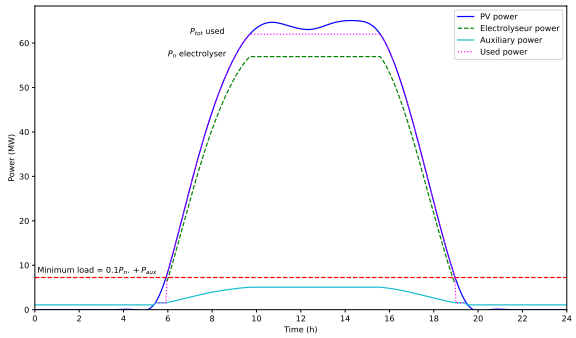

Figure 4.5: Profiles of the different powers considered in the system as a function of time on a typical day for the case with fuel cell

Given that with the BC, we always want to use all the waste heat available, this means that the electrical power delivered to the DSHP will be limited to a lower level. This explains why the electrolysers are not at full power during charging. The same applies to the case with a lithium battery for a better comparison. Futhermore, we can clearly see that the supply power of the auxiliaries is not constant over the day. This is due to the fact that the production of hydrogen is distributed unevenly over the day. The energy cost of compressing the hydrogen therefore implies an increase in the consumption of the auxiliaries for the high power loads of the electrolyser. On the opposite, their consumption is minimal during the discharge cycle as only the ammonia synthesis process, air separator unit and the pump will have to operate.

3.0 Results & discussions

A homemade python model capable of predicting the mass of NH_3 produced on a typical day was implemented on the basis of the method and assumptions described above. It will then enable us to compare the cost of ammonia production for the 3 storage systems considered.

3.1 Energy comparison

As explained above, the demand for auxiliaries is a variable that is likely to change depending on the location of the site, a particular demand present on the site or even how the production system is designed. In order to consider as many cases as possible, 3 levels of auxiliary demand(i.e energy supplied by the battery) have been analysed (respectively 2%, 3% and 4% of the total consumption of the electrolysers) in order to visualise how production evolves for these different cases. The results are shown in the figure below:

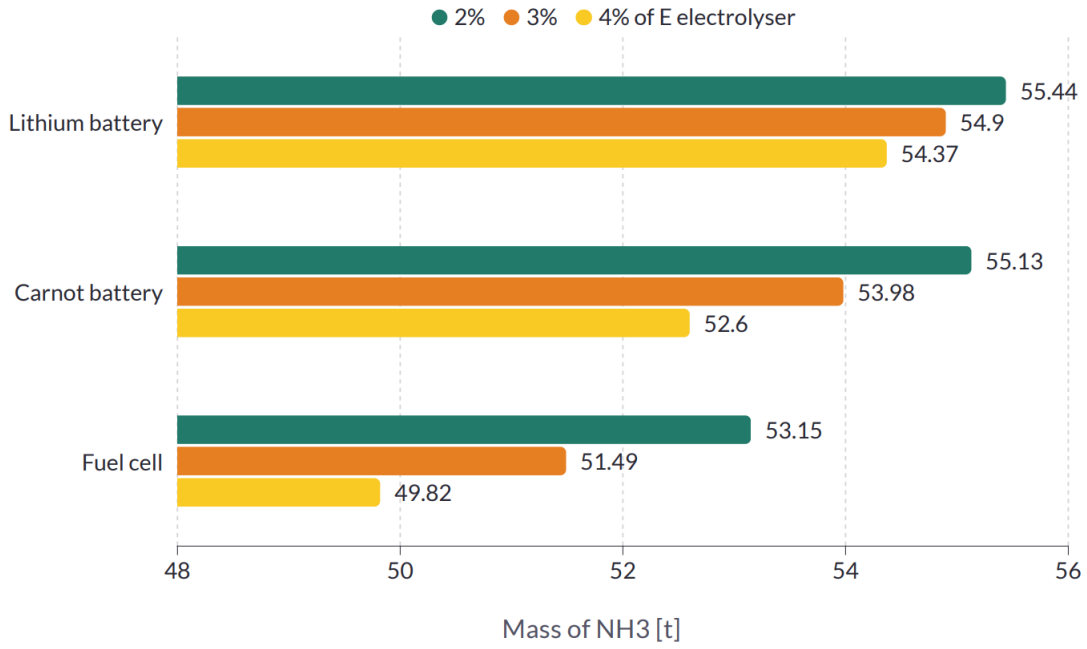

Figure 4.6: diagram comparing ammonia production for the different storage configurations under consideration and for three different auxiliary energy demands

We can see that it is with the lithium battery that production is maximised, for all 3 levels of demand while the case with fuel cell has the smallest ammonia production. The good performance obtained with the lithium battery can be

explained by the fact that it has a good power to power efficiency (90%) which reduces the losses during charging and discharging process. It is also noted that the production with Carnot battery is very close to that with lithium battery ($\Delta m_{NH3} = 0.31$ [t]) in the case of a need equivalent to 2%. However, this production differences between the lithium battery and the Carnot battery comes from the fact that the CB has a lower power-to-power efficiency so it will have to charge with greater power to satisfy the same need. In the case of lithium battery and Carnot battery, the decrease in ammonia production with the increase in demand is due to the fact that the battery will require a larger capacity so more electricity will be consumed to charge, which means that there will be less electricity available for electrolysers (=less hydrogen).

On the other hand, for fuel cell, the electrolysers will always produce in the same way no matter the level of demand but during the night, the consumption of hydrogen by the fuel cell will increase to meet demand and this in a linear way since a consequent yield is considered.

In addition, we note that the decrease between the levels of needs for the case with CB is not constant ($\Delta m_{NH3,2-3\%}$ =1.15 [t] against $\Delta m_{NH3,3-4\%}$=1.38 [t]). By making a link with the results obtained in section 4.0 of Chapter 3, we understand that this non-linearity is related to the overall COP of the DSHP. Indeed, increasing the need, increases the charging power (i.e the electrical power of the DSHP) and decreases the amount of waste heat available for the CB since the electrolysers then operate at a lower power. As a result, the $E_{th,produced}/E_{wh}$ ratio increases and the global COP as well as η_{P2P} decrease as shown in Figure 3.39. This ratio is equivalent to 1.25, 1.67, 2.27 for a demand of 2%, 3% and 4% respectively

3.2 Economic comparison

The purpose of this section is to determine the level of economic competitiveness of the Carnot battery compared to the lithium battery and fuel cell. As the lithium battery and fuel cell are already well-established technologies on the market, we are even able to find a specific investment and maintenance cost, characterizing them. On the other hand, the use of the CB is not yet sufficient to estimate a specific cost. The method used to counter this unknown is to consider a range of CAPEX for the three components of the CB (HP, TES, ORC) as their combination results in an ammonia production cost equivalent to the smallest production cost obtained through one of the other two storage systems (lithium battery or fuel cell). To characterize the economic production performance of the system, we will use the levelized cost of ammonia (LCOA). It is defined as the total cost required to install, operate and maintain the entire green ammonia production system over its lifetime divided by the total mass of ammonia produced over that lifetime. It is

calculated using the following formula:

$$LCOA = \frac{\sum_{t=1}^{T} \frac{(CAPEX_{tot}+OPEX_{tot,t})}{(1+r)^t}}{\sum_{t=1}^{T} \frac{(m_{NH3,t})}{(1+r)^t}} \tag{4.2}$$

where r is the discount rate considered equal to 5%, T is the lifetime of the system (20 years), $CAPEX_{tot}$ is the total specific investment cost of the system, $OPEX_{tot,t}$ is the total specific operational cost of the system over 1 year and $m_{NH3,t}$ is the total ammonia mass produced over 1 year. An important point to note is that the life of the lithium battery and fuel cell are less important than the life of the system. A replacement cost was therefore considered in the calculation of the LCOA. Given the clear evolution of the costs of these technologies in recent years, it is difficult to predict their cost for the near future, so we have assumed that its replacement cost will be equivalent to that of its initial cost. All CAPEX and OPEX used to calculate this LCOA are listed in Table 4.4.
The CAPEX ranges considered for CB components were therefore limited below in order to compete with the best LCOA for the case with 2% demand for auxiliaires. The high limit was based on the CAPEX found in the literature for a conventional HP and ORC as well as for a sensitive TES at low temperature ($\approx 100 - 120$°C) [91], [77],[82]. These will allow us to evaluate the order of magnitude of the specific cost reduction margin needed to compete with the best option.

Component	CAPEX	OPEX	Lifetime	
PV panels	780 €/kW	17.5 €/kW/y	25 y	[30]
PEM electrolyser	1750 €/kW	4 %[2]	80 000h[3]	[30]
HB +ASU[1]	4192 €/(kg_{NH3}/h)	436 €/(kg_{NH3}/h)/y	25 y	[21]
Desalination unit	26 €/kg_{H2O}/h	0.0003 €/kg_{H_2O}	20 y	[21]
Hydrogen storage	461 €/$kg_{H2,stored}$	1 €/$kg_{H2,stored}$/y	50 y	[21]
Lithium-ion battery	250 €/kWh	2 %[2]	15 y	[28],[77]
Fuel cell	3500 €/kW	2 %[2]	43 800h[4]	[27],[26]
DSHP	[500;1900] €/kW	2 %[2]	20 y	[91]
TES	[8;20] €/kWh	2 %[2]	25 y	[82],[51]
ORC	[600;2100] €/kW	2 %[2]	20 y	[77]

[1] Haber-bosch process (i.e ammonia synthesis process) + air separator unit
[2] Percentage of the investment cost
[3] Corresponding to 20 years for the integration case considered
[4] Corresponding to 10 years for the integration case considered

Table 4.4: Economic parameters characterising the system

The graph 4.7 show the LCOA with the total battery cost (i.e investment + operation and maintenance costs) for the three cases. Then, the LCOA of the CB (i.e the blue line) has been obtained by combining a multitude of different CAPEX for its components (i.e. range shown in table 4.4) so as to obtain a LCOA equal to or less than that of the most competitive case (i.e. the lithium battery).
Please, note that the LCOA obtained with fuel cell is much higher than with lithium battery and always greater than or equal to that obtained for the CB (with respect to the considered CAPEX range) while its total battery cost is lower than the lithium battery. This can be explain by its lower mass production of ammonia.

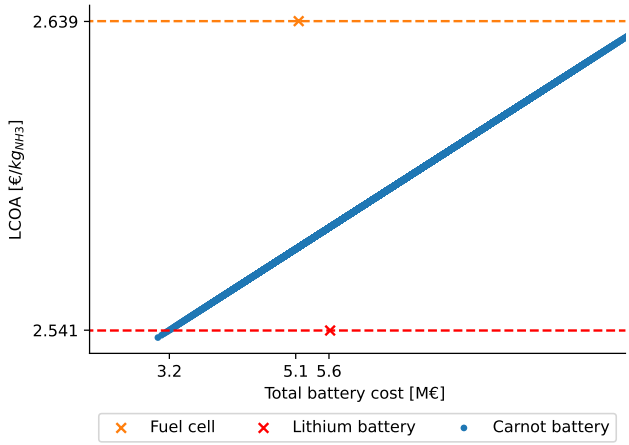

Figure 4.7: Evolution of the LCOA obtained with the CB for different combinations of CAPEX for the DSHP, TES and ORC composing the CB

Considering the total investment cost of the CB needed to compete with the system with lithium battery, one can find the combinations of HP, TES and ORC costs used to achieve it. The graph 4.8 show the evolution of the total cost of the CB with the cost of each of its components.
An additional remark that can be made by referring to graph 4.8 is that the CAPEX of the HP has a wider impact on the total cost of the Carnot battery compared to the other two. This is the consequence of a large load power since the load is done in a reduced time range (when $P > P_{tot,used}$) and the cost of the HP is proportional to its load power $Cost_{HP,tot} = CAPEX \cdot P_{charge}$. So when you are in a situation where the electrical power is limited and where the CB must be sufficiently loaded to meet a fixed need (as in our case) , it is necessary to choose a wise compromise between a large CAPEX for the HP in order to have a high performance heat pump (= large COP) which will limit the load power needed or a more limited CAPEX but reduced performance and therefore greater load power.

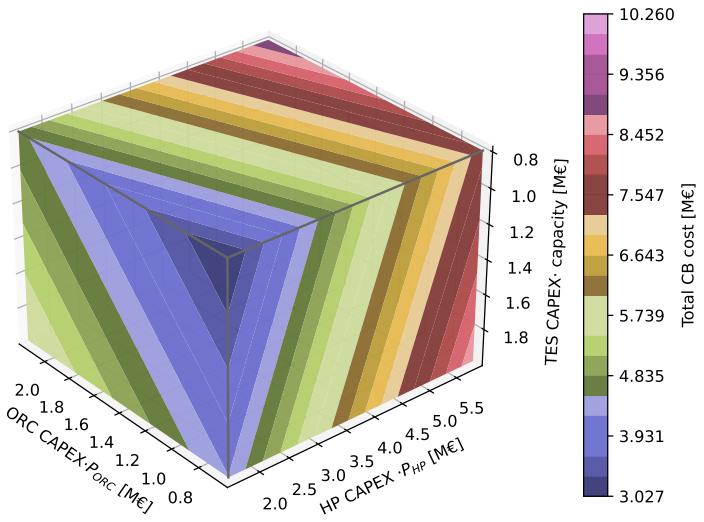

Figure 4.8: Evolution of the total cost of the Carnot battery for different investment cost of its components(i.e DSHP, TES, ORC)

To compete with the lithium battery, the total battery cost found for the CB is equal to 3.2 M€. By knowing the HP and ORC power and the capacity of the TES, the range of CAPEX of these components are finally found. These are listed in the table below4.5.

Component	Total Cost [M€]	CAPEX
DSHP	[1.5;1.73]	[500;557] €/kW
TES	[0.8;0.93]	[8;9.3] €/kWh
ORC	[0.62;0.78]	[600;755] €/kW

Table 4.5: List of target costs for Carnot battery components

It can be concluded from the above that a reduction between 50% and 70% for each component of the CB would be necessary to be competitive with the lithium battery. The margin of reduction of the CAPEX of these components in the coming years is obviously debatable since it depends on a lot of factors that are still unknown to us as the evolution of the future demand for these components, technical developments,.... We can nevertheless point out that the margin achievable for the TES will be less since its cost is mainly related to the purchase cost of its materials already widely spread and little margin for technical improvement seems to be achievable. On the other hand, HP and especially ORC are much less widespread in trade and one could imagine a sharp decrease in their specific costs in the coming years if an overall increase in their use would occur.

Finally, we can compare how the LCOA evolves with the need for auxiliaries. The 3 graphs below correspond respectively to the case with a demand of 2%, 3%, 4% relative to the daily consumption of the elecrolysers. The same range of CAPEX were considered in each case. We can conclude from this that the greater the need, the lower the CAPEX required to compete with lithium batteries. We also note that the differences between LCOA and between the total investment costs for the different storage systems increase, which is explained in the same way as for the production differences observed above.

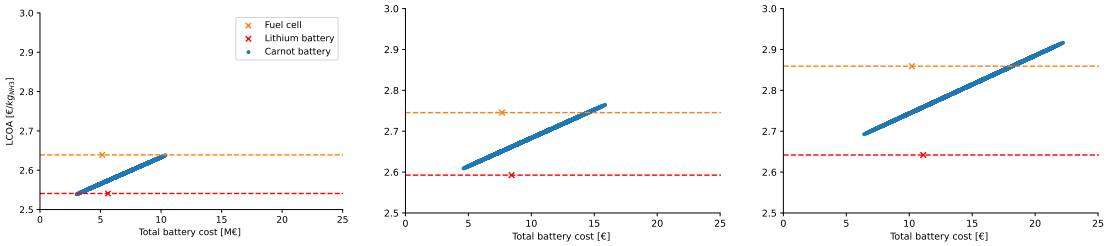

Figure 4.9: Evolution of the LCOA specific to the 3 storage systems considered with a demand relative to the daily consumption of the elecrolysers of 2, 3, 4% for the first, second and third graph respectively

3.3 Discussions

For now, it goes without saying that the Carnot battery is less energetic and is less economical compared to the lithium battery but could be interesting compared to a fuel cell. On the basis of the results obtained in this chapter, it can be shown that one of the situations which will favour the competitiveness of the CB would correspond to a case where a long load and discharge of the CB is carried out at low power. Indeed, we know that the more we increase the load power for a given case, the more the COP of the DSHP will be affected. On the other hand, it is also known that the cost of the Carnot battery is mainly related to the HP and the ORC and as their cost is proportional to their power, charged and discharged at low power will also promote a lower cost.

Even if the Carnot battery is not the best solution from an economic and energetic point of view, that does not mean it does not have a future. If we take an holistic view of things, the CB may have other characteristics that give it an advantage over a lithium battery. In particular, it has a reduced risk of ignition, unlike a lithium battery. It also has the advantage of having a decorrelation between power and storage, which makes it highly modular and capable of covering a wide range of applications (from 100kW to +100MW) [41]. Finally, the CB will stands

out from the lithium battery due to the materials used. In the case of lithium battery, rare and critical minerals are present (including lithium, nickel, cobalt, manganese). From the moment a gap between prospective production and demand appears, the production of the batteries will be limited which reduces the scaling up of lithium batteries [34]. In the case of the Carnot battery, it does not use critical materials. Another drawback of using these rare materials is that they often require energy-intensive extraction processes, which are mostly bad for the environment and are responsible for 80% of the carbon footprint of lithium batteries (=77 to 221 kg CO2e/ kWh) [12]. Thus, the Carnot battery allows a good durability in environmental terms (an optimistic reduction of 7 to 30 times, depending on the size of the installation, is announced for the CB compared with electrochemical batteries according to [86]).

Chapter 5

Conclusion and future work

The main objective of this master thesis was to 'increase the energy and economic profitability of a Carnot battery (i.e. TI-PTES) coupled to an industrial process (i.e. electrolyser) rejecting a limited amount of waste heat and powered exclusively by a renewable energy source.

To meet this objective, we have shown that DSHP could be a solution. An analysis and comparison of several promising DSHPs was then carried out in order to select the most energy-efficient one. Then, an energetic and economic comparison of the coupling in its ideal configuration (i.e. DSHP with the highest COP) was carried out to find out the level of competitiveness of a CB compared with a lithium battery and fuel cell.

As a result, the DSHP configuration that achieves the highest COP is the series connection of 2 DSHP with open economizers, using cylopentane as the working fluid. It has a COP ranging from 4.7 to 3.95 for a hot storage temperature of 95°C to 120°C and ranging from 6.55 to 3.64 for an $E_{th,produced}/E_{wh}$ ratio ranging from 1.25 to 4.8. The energy comparison of the coupling showed that the CB was close to the lithium battery (i.e. best case) in the case of low demand, with a 1-day production of 55.13 , 53.98, 52.6 t_{NH3}/day for a demand of 2, 3, 4% of the electrolyser consumption compared with aa 1-day production of 55.44, 54.9, 54.37 t_{NH3}/day with a lithium battery respectively. In economic terms, however, we found that a CAPEX in a range of [500;557] €/kW, [8;9.3] €/kWh, [600;755] €/kW for the DSHP, TES and ORC had to be achieved in order to produce a specific production cost identical to that obtained with a lithium battery.

The results do not allow us to determine the real profitability of the coupling, but they do show the DSHP configurations that should be favoured to improve the production rate and present the CAPEX objectives of the CB components to be

achieved in the near future if we wish to be able to compete economically with the competition.

Despite certain limitations, such as the operating conditions selected, this study opens the way for future research into the recovery of low-temperature waste heat based on the use of DSHP. In addition, future research could focus on the technical-economic study of the components of a CB in order to know the current CAPEX of a CB and to estimate their future projections. Analysing the robustness of such a coupling by considering the operational uncertainties also seems necessary to estimate the technically achievable energy performance.

In conclusion, this study makes an additional contribution to the understanding and application of a Carnot battery integrating a heat source, considered to be a promising technology for the evolution of tomorrow's energy systems.

Master thesis written with the help of deepL and chatGPT for translation and reformulation

Appendix A

Configuration of DSHP with recuperator

The DSHP with recuperator can be seen below. As stated previously, we do not consider the use of a recuperator for the DSHP with ejector+pressure booster and the single-source HP using the waste heat source.

1.0 DSHP in cascade

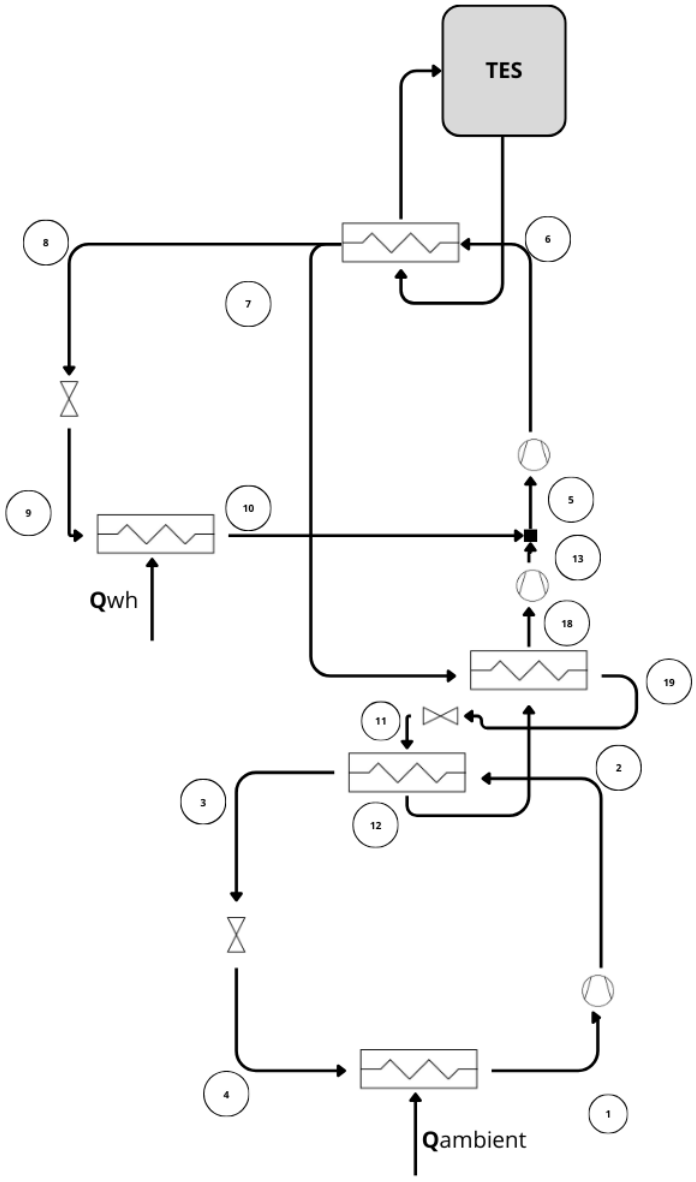

Figure A.1: Scheme of the DSHP in cascade with recuperator

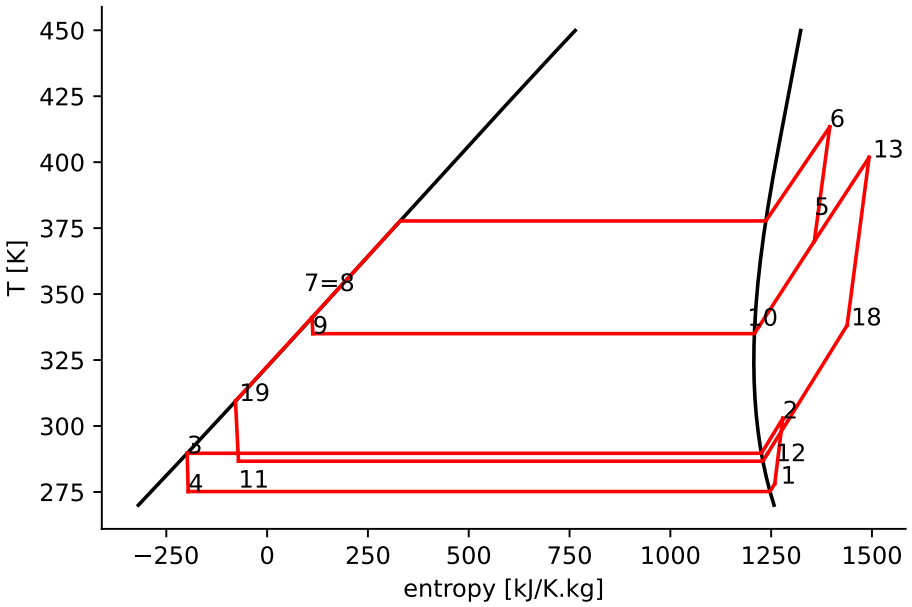

Figure A.2: T-s diagram of the cycle with recuperator

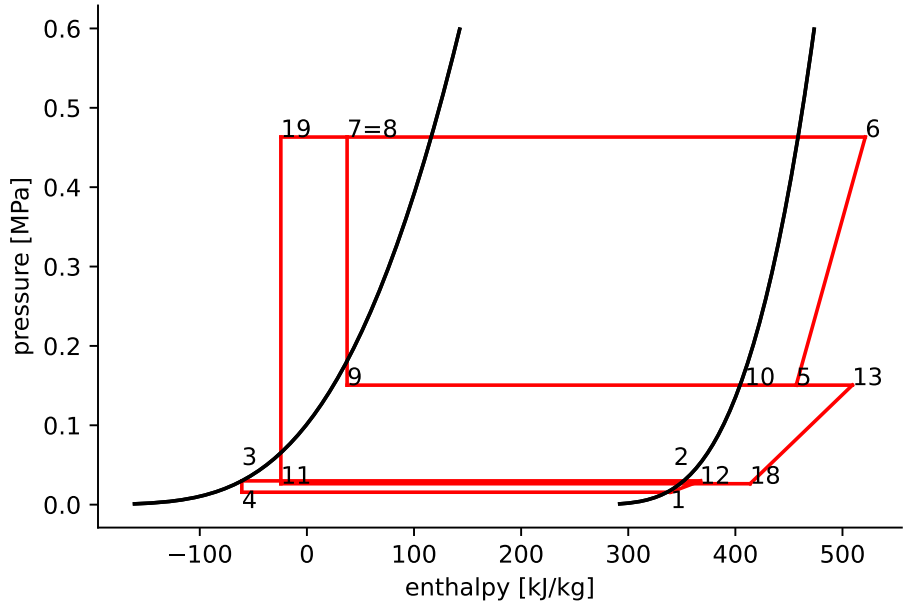

Figure A.3: p-h diagram of the cycle with recuperator

2.0 DSHP in cascade + IHX

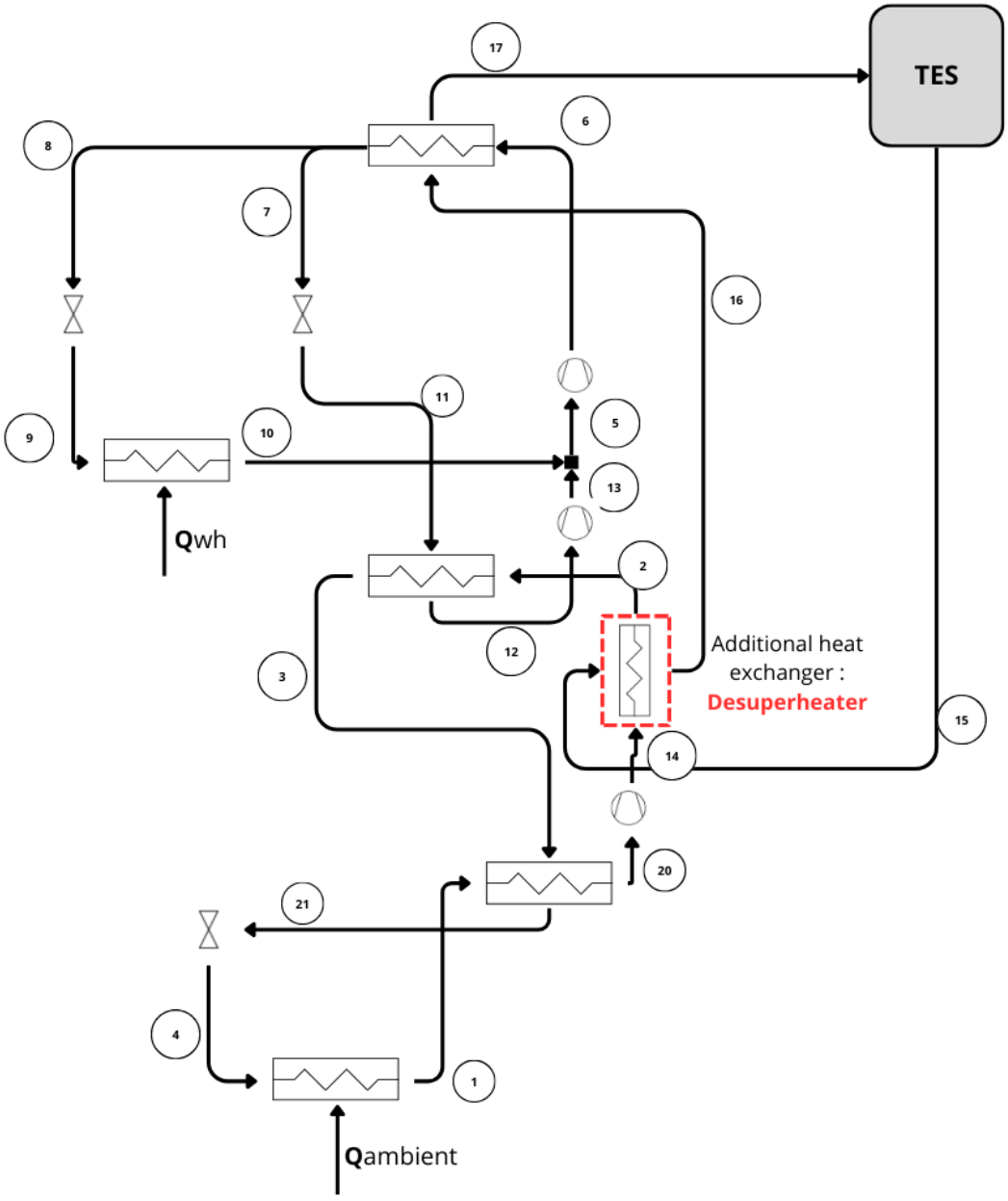

Figure A.4: Scheme of the DSHP in casacde +IHX with recuperator

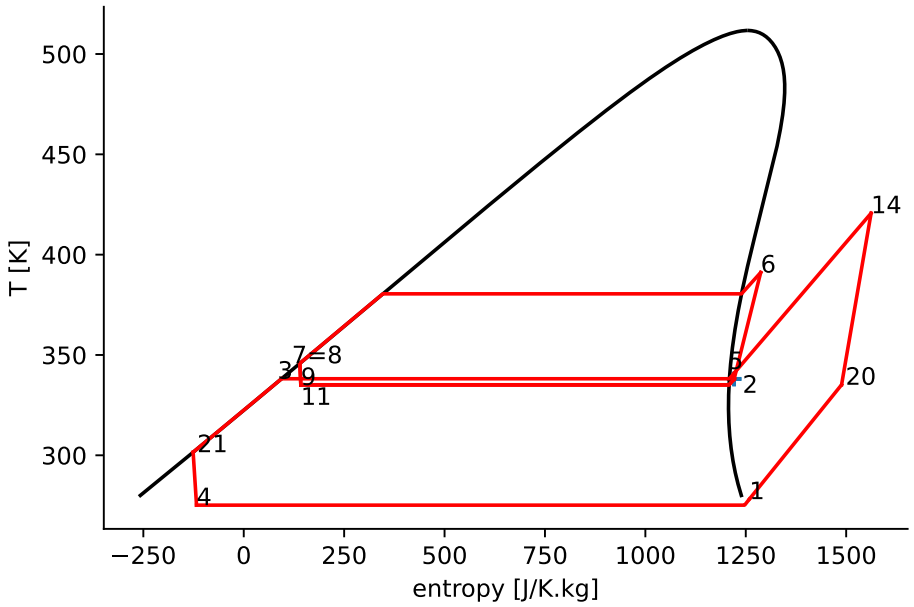

Figure A.5: T-s diagram of the cycle with recuperator

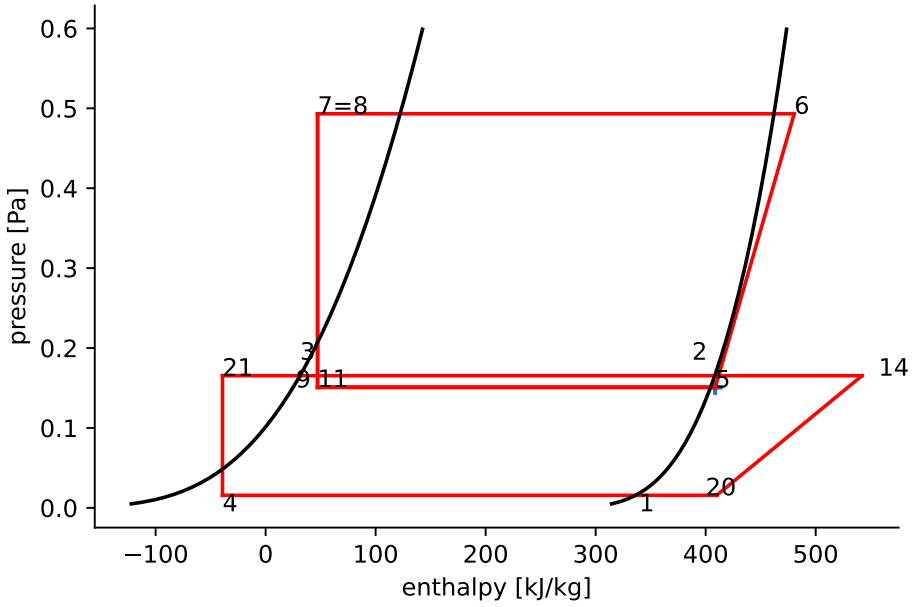

Figure A.6: p-h diagram of the cycle with recuperator

3.0 DSHP with ejector

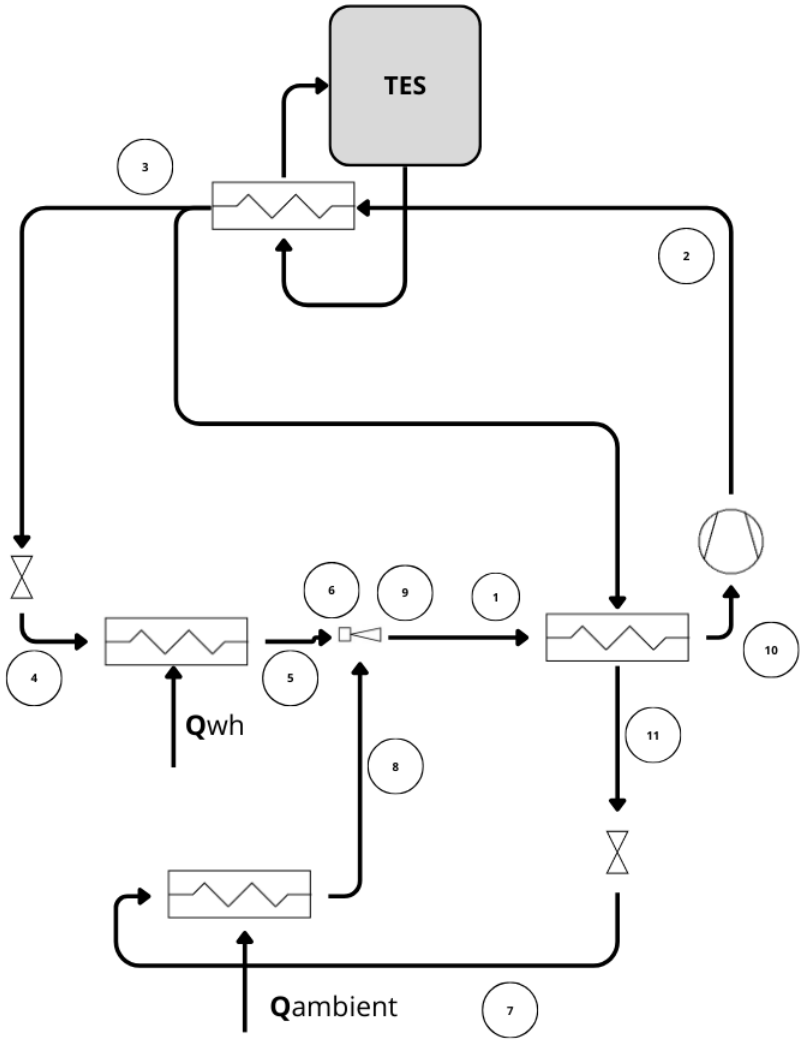

Figure A.7: Scheme of the DSHP with ejector and recuperator

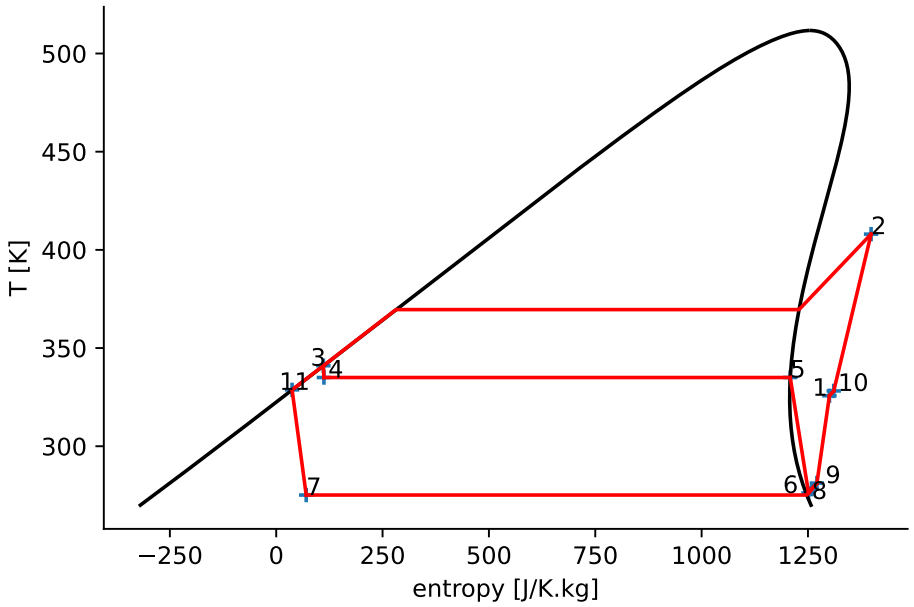

Figure A.8: T-s diagram of the cycle with recuperator

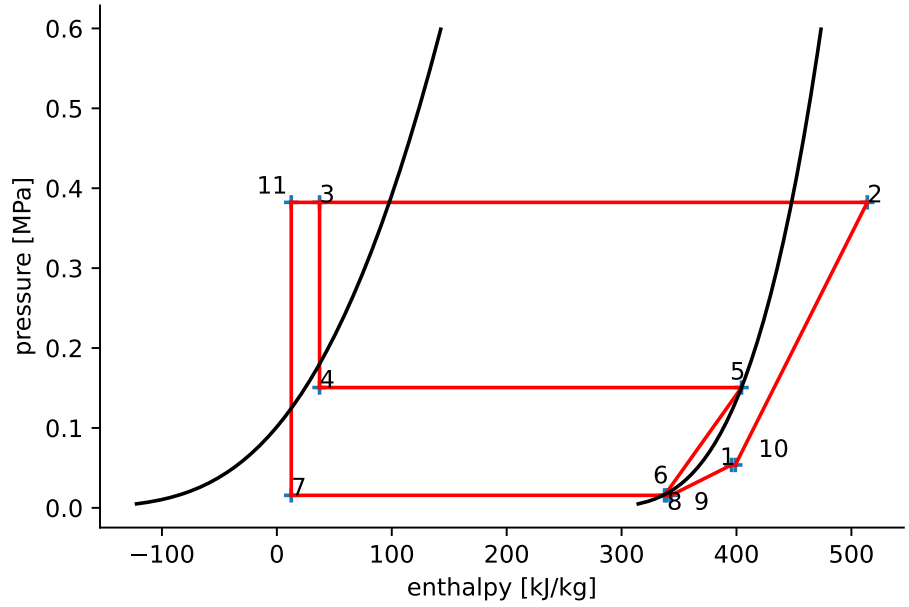

Figure A.9: p-h diagram of the cycle with recuperator

4.0 DSHP with open economizer

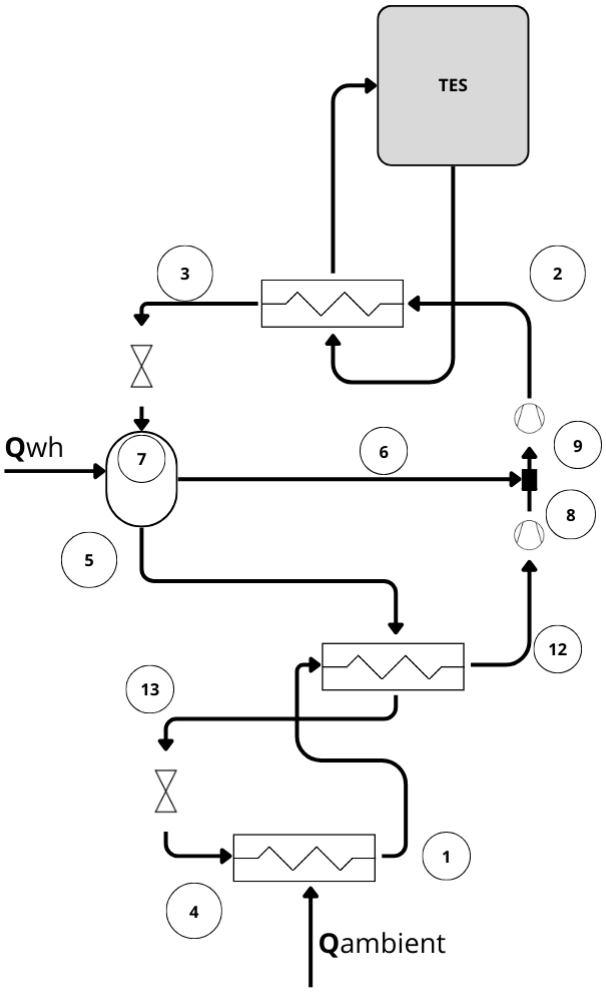

Figure A.10: Scheme of the DSHP with open economizer and recuperator

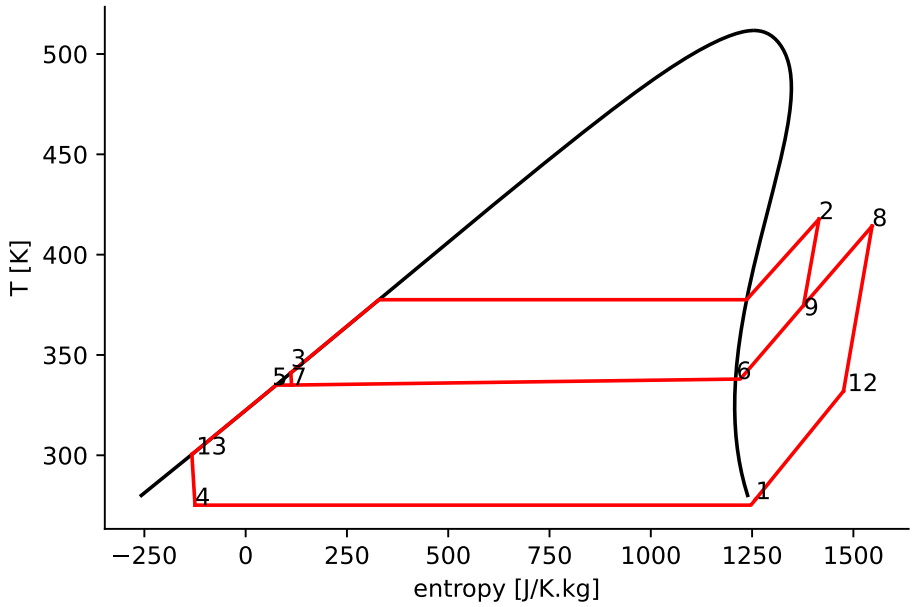

Figure A.11: T-s diagram of the cycle with recuperator

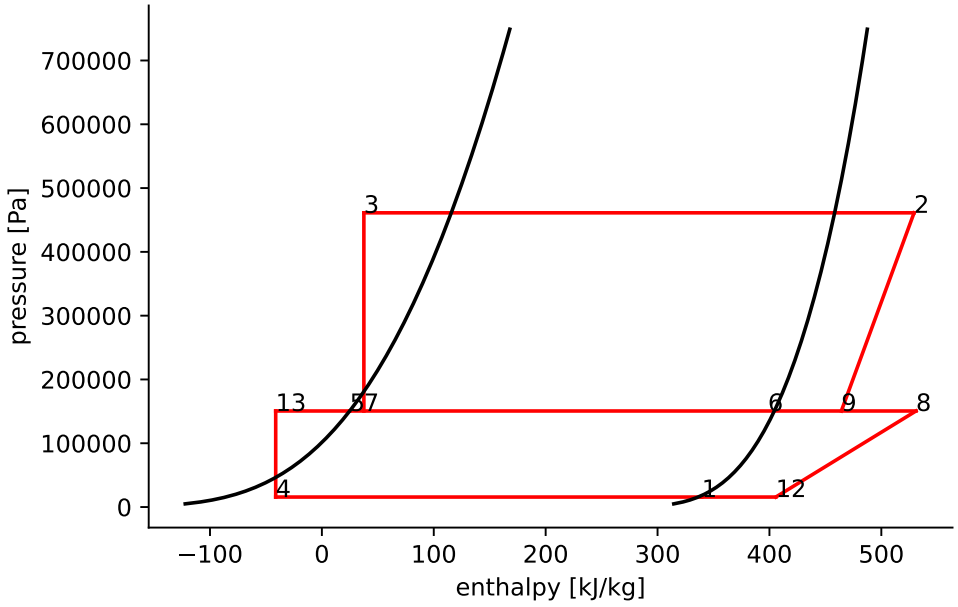

Figure A.12: p-h diagram of the cycle with recuperator

5.0 two HP in parallel

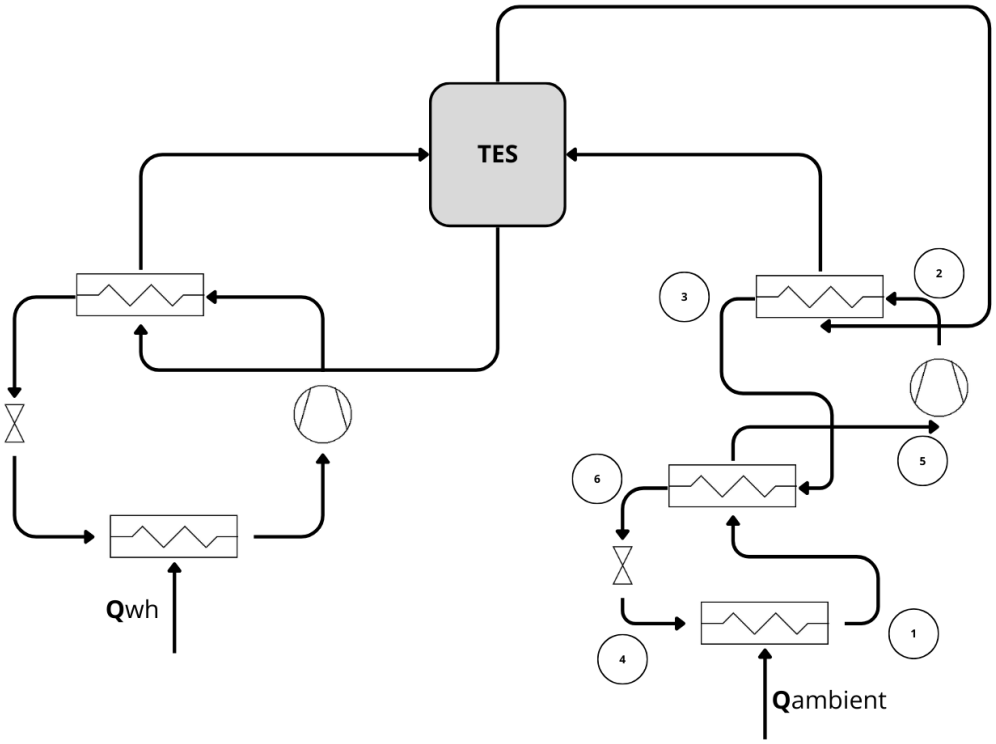

Figure A.13: Scheme of the DSHP with 2 HP in parallel and recuperator

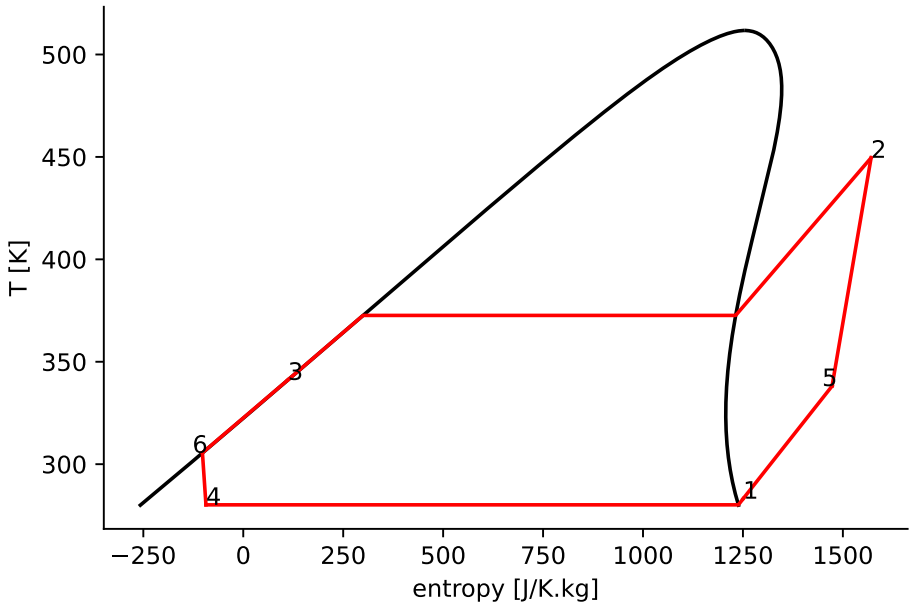

Figure A.14: T-s diagram of the cycle using the ambient air as source with recuperator

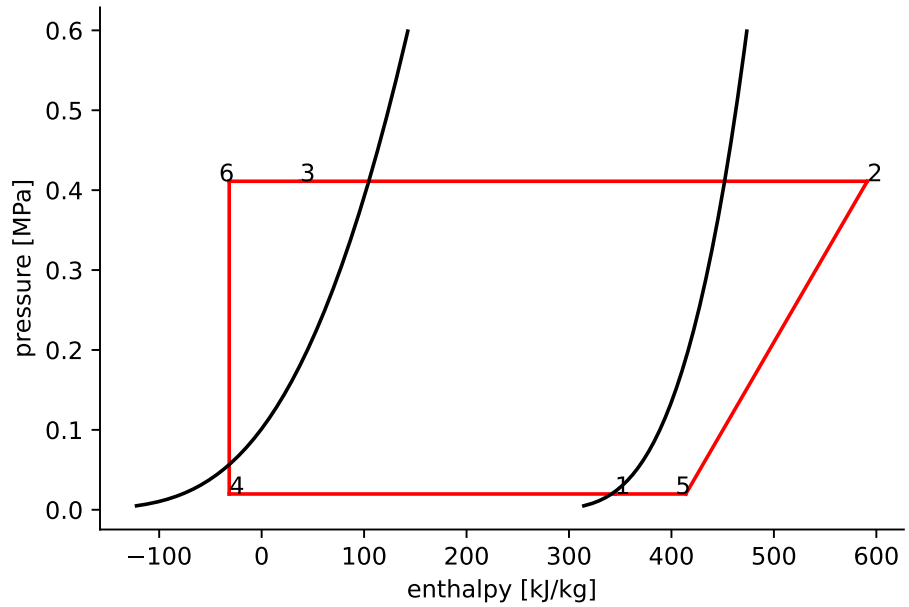

Figure A.15: p-h diagram of the cycle using the ambient air as source with recuperator

Appendix B

Thermodynamic analysis results

1.0 Carnot battery optimisation

As stated in the section 4.2, the Carnot battery dilemma is presented using two other ratios $E_{th,produced}/E_{wh}$. The figures are shown below for a ratio of 1.5 and 4.

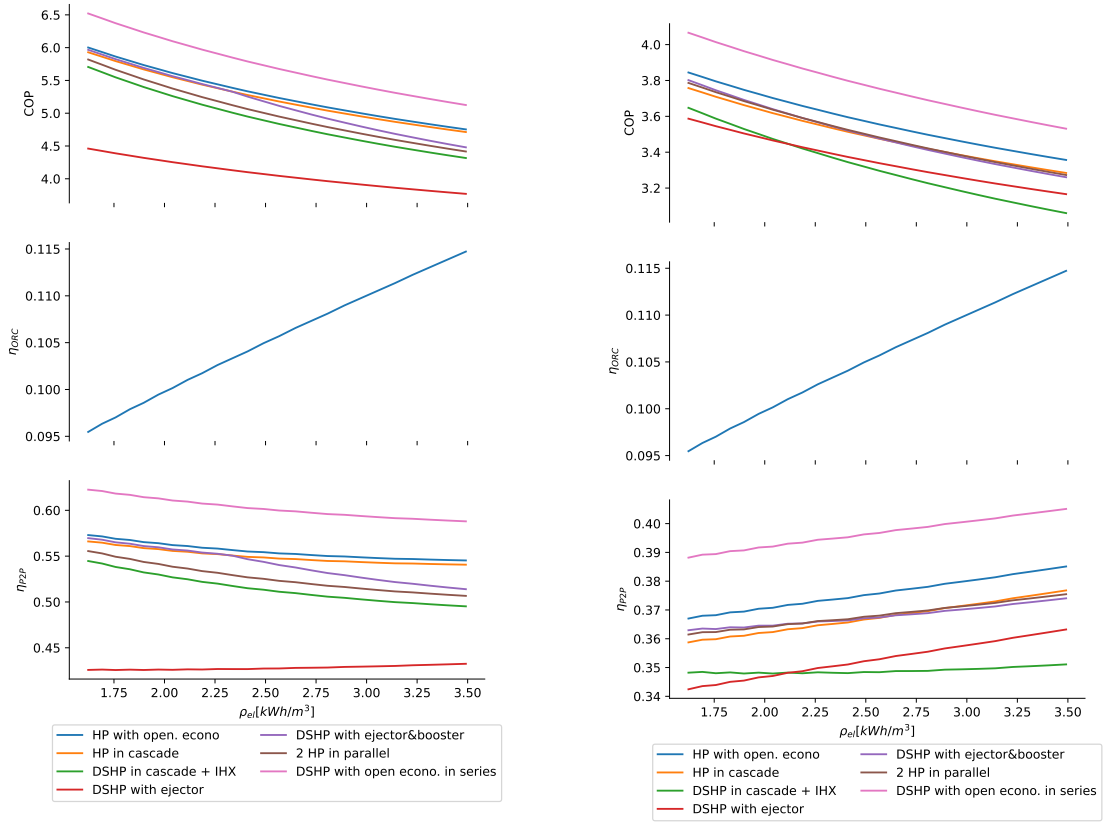

Figure B.1: Carnot battery dilemma with $E_{th,produced}/E_{wh}$ equal to 1.5 (left) and 4 (right).

2.0 Sensitivity analysis of $\eta_{c,is}, \eta_{t,is}, \eta_{p,i}$

Note: in the following graphs, we only consider one configuration for the ORC over all the density range which is the configuration without recuperator.

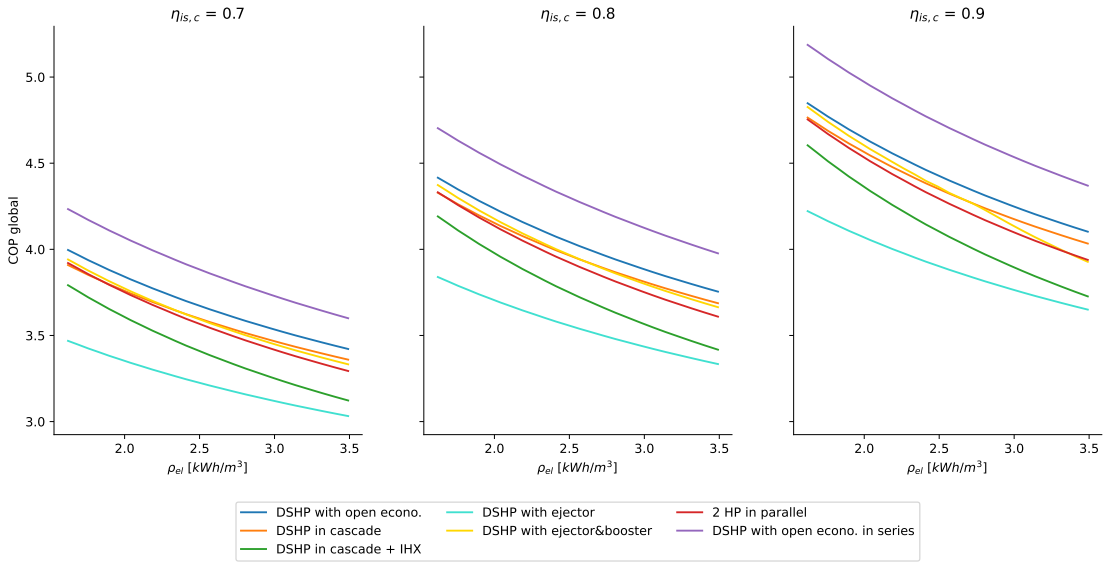

Figure B.2: COP sensitivity with different pinch point function of energetic density

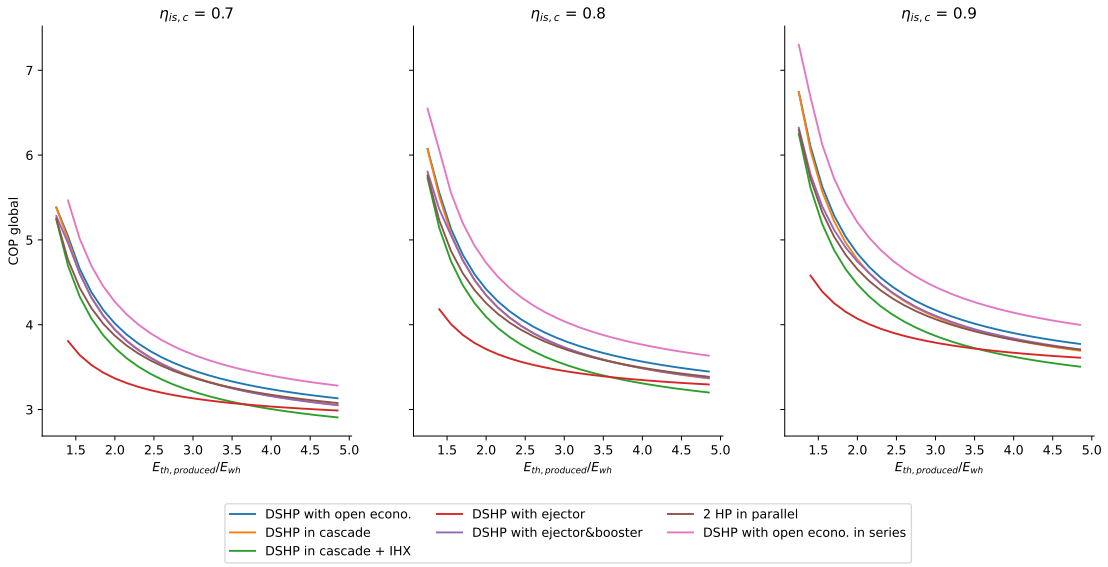

Figure B.3: COP sensitivity with different compressor efficiency function of ratio $E_{th,produced}/E_{wh}$.

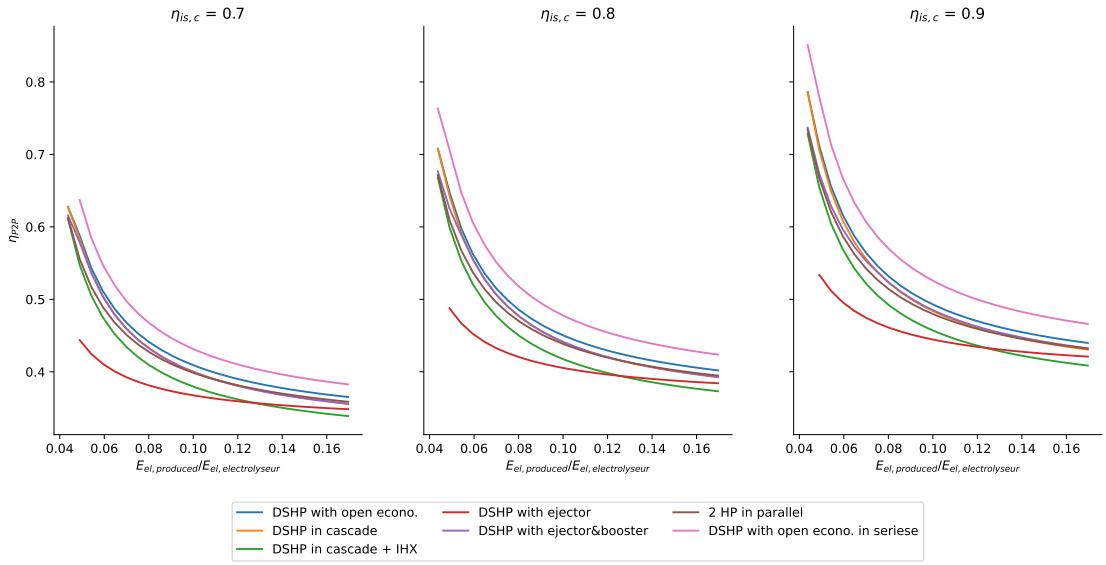

Figure B.4: η_{P2P} sensitivity with different compressor efficiency function of ratio $E_{el,produced}/E_{electro}$.

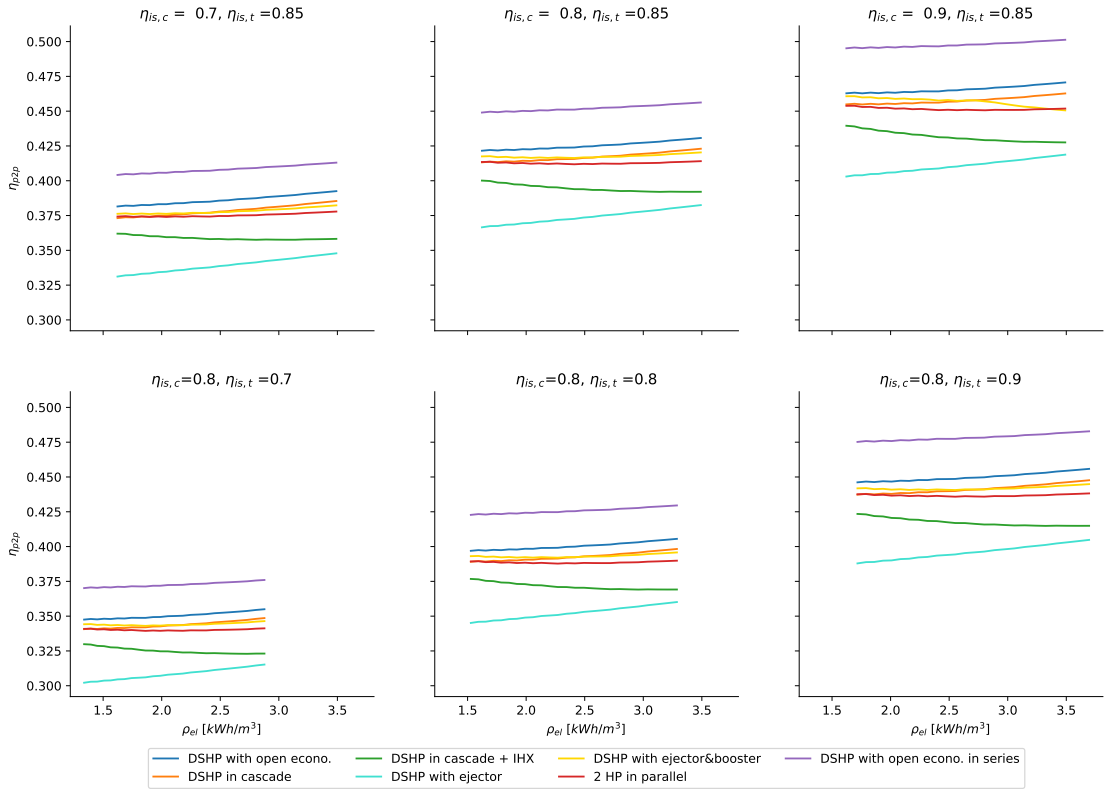

Figure B.5: η_{P2P} sensitivity with different compressor and expander efficiencies function of energetic density.

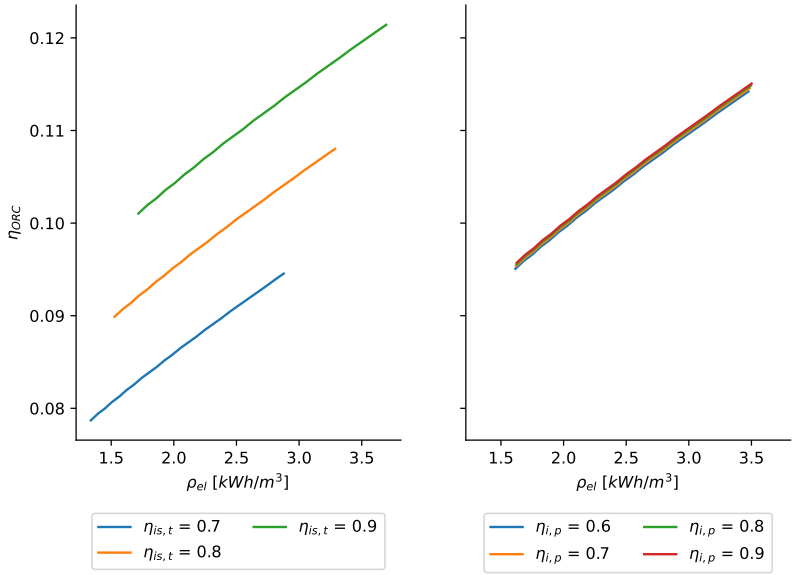

Figure B.6: η_{ORC} sensitivity with different expander and pump efficiencies function of energetic density.

3.0 Sensitivity analysis of pinch point

As a reminder, we are analysing the sensitivity of the temperature pinch at the dual-source HP-TES and TES-ORC heat exchangers.

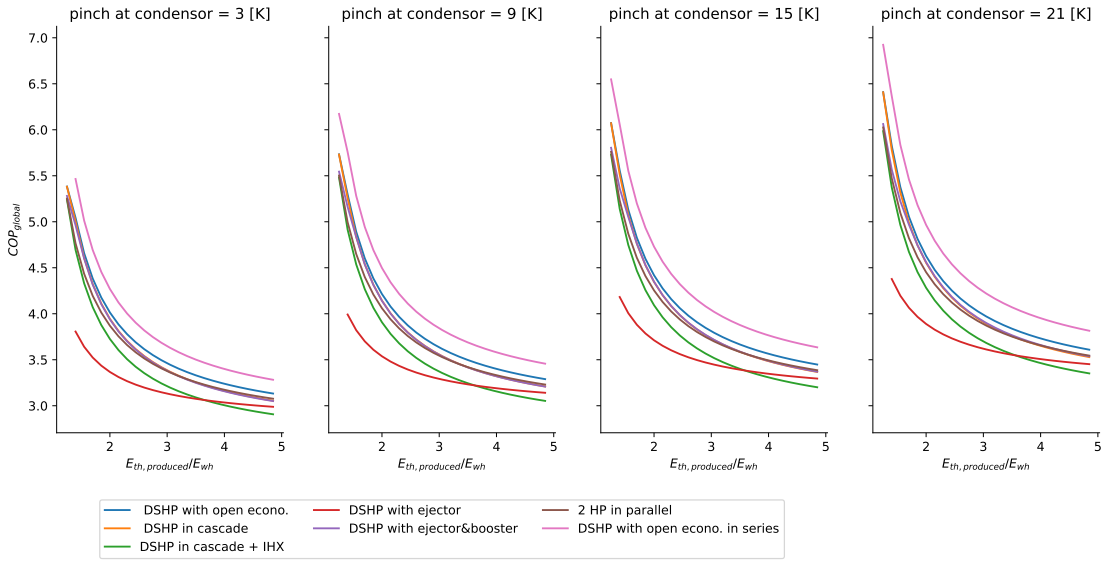

Figure B.7: COP sensitivity with different pinch point function of ratio $E_{th,produced}/E_{wh}$.

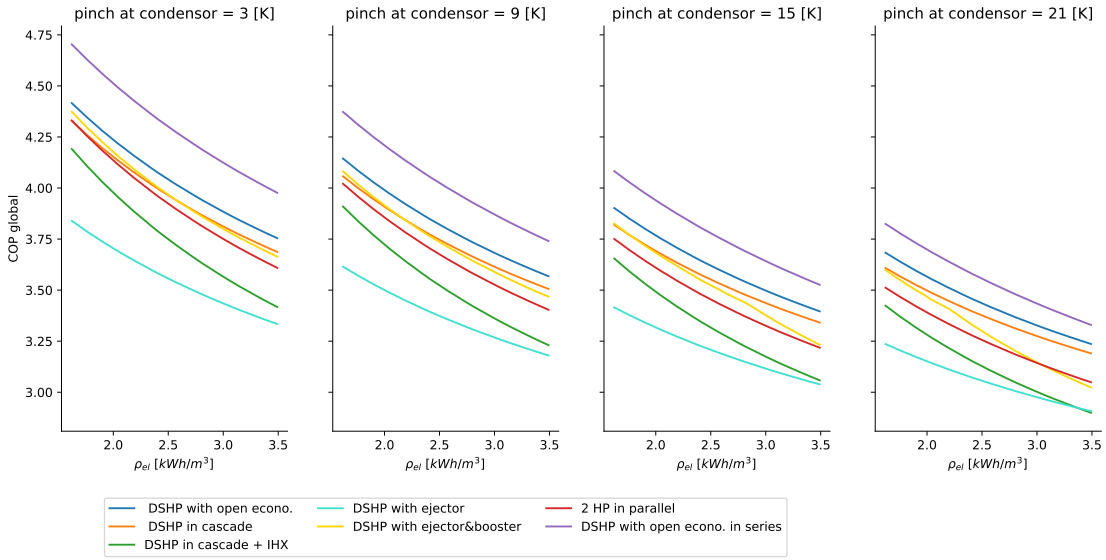

Figure B.8: COP sensitivity with different pinch point function of energetic density.

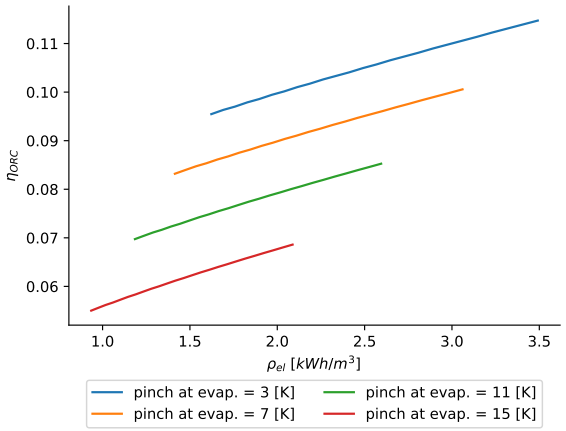

Figure B.9: η_{ORC} sensitivity with different pinch point function of energetic density.

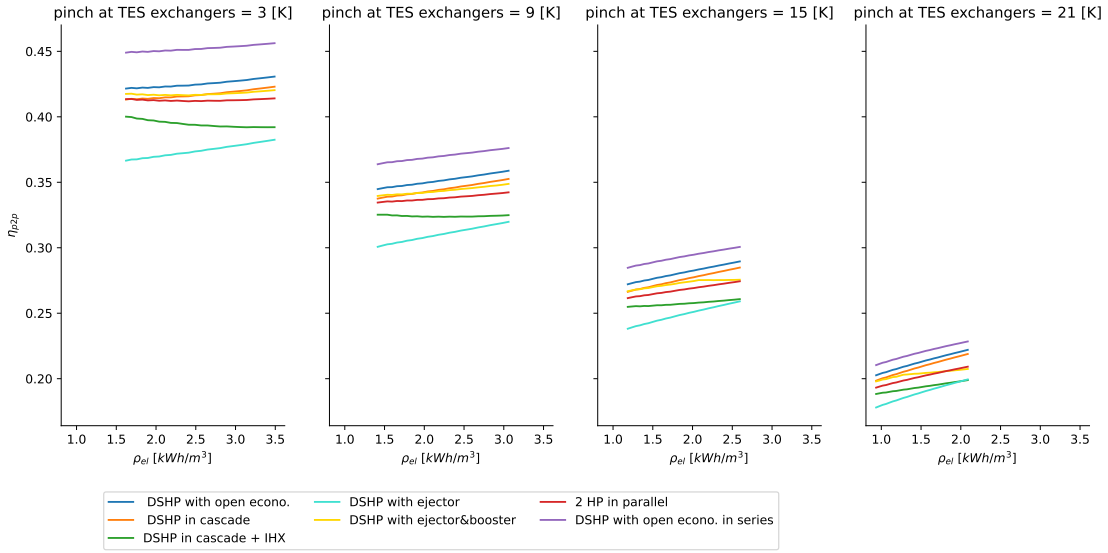

Figure B.10: η_{P2P} sensitivity with different pinch point function of energetic density.

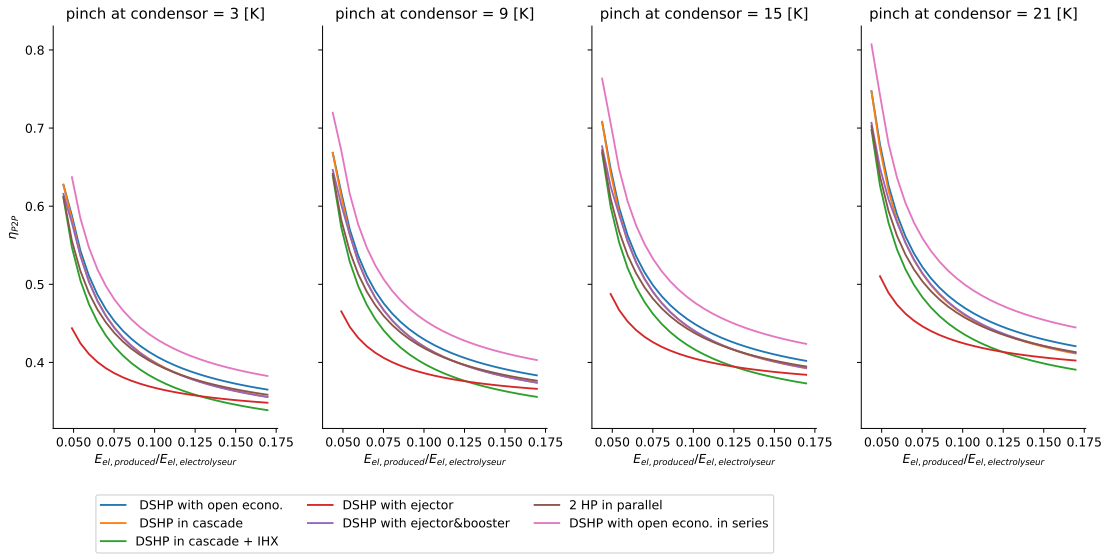

Figure B.11: η_{P2P} sensitivity with different pinch point function of ratio $E_{el,produced}/E_{electro}$.

Bibliography

[1] URL: https://s3.production.france-hydrogene.org/uploads/sites/4/2021/11/Fiche_201.3_20-_20d_C3_A9c._202020_20PM.pdf.

[2] URL: http://coolprop.org/index.html.

[3] *About self-discharge of lithium ion solar batteries*. URL: https://www.bsl-battery.com/about-self-discharge-of-lithium-ion-solar-batteries.html (visited on 05/16/2024).

[4] Jae Hwan Ahn et al. "Heating performance characteristics of a dual source heat pump using air and waste heat in electric vehicles". In: *Applied Energy* 119 (Apr. 15, 2014), pp. 1–9. ISSN: 0306-2619. DOI: 10.1016/j.apenergy.2013.12.065. URL: https://www.sciencedirect.com/science/article/pii/S0306261914000051 (visited on 02/16/2024).

[5] Alleau. *Production d'hydrogene par electrolyse de l'eau*. Sept. 2019.

[6] Laterre Antoine et al. "Systematic and multi-criteria optimisation of sub-critical thermally integrated carnot batteries (TI-PTES) in an extended domain". In: 2023.

[7] Tim Arthur, Graeme J. Millar, and Jonathan Love. "Integration of waste heat recovered from water electrolysis to desalinate feedwater with membrane distillation". In: *Journal of Water Process Engineering* 56 (Dec. 1, 2023), p. 104426. ISSN: 2214-7144. DOI: 10.1016/j.jwpe.2023.104426. URL: https://www.sciencedirect.com/science/article/pii/S2214714423009467 (visited on 05/24/2024).

[8] Tao Bai et al. "Theoretical Performance Analysis of an Ejector Enhanced High-Temperature Heat Pump with Dual-Pressure Condensation and Evaporation". In: *J. Therm. Sci.* 31.5 (Sept. 1, 2022), pp. 1367–1379. ISSN: 1993-033X. DOI: 10.1007/s11630-022-1588-7. URL: https://doi.org/10.1007/s11630-022-1588-7 (visited on 05/09/2024).

[9] Pal Bergan and Christopher Greiner. "A New Type of Large Scale Thermal Energy Storage". In: *Energy Procedia* 58 (Dec. 31, 2014). DOI: 10.1016/j.egypro.2014.10.422.

[10] Stefan Bertsch, Michael Uhlmann, and Andres Heldstab. “Heat Pump with Two Heat Sources on Different Temperature Levels”. In: (2014).

[11] Ramchandra Bhandari, Clemens A. Trudewind, and Petra Zapp. “Life cycle assessment of hydrogen production via electrolysis – a review”. In: *Journal of Cleaner Production*. Special Volume: Making Progress Towards More Sustainable Societies through Lean and Green Initiatives 85 (Dec. 15, 2014), pp. 151–163. ISSN: 0959-6526. DOI: 10.1016/j.jclepro.2013.07.048. URL: https://www.sciencedirect.com/science/article/pii/S095965261300509X (visited on 10/21/2023).

[12] *BiB Batteries - Bienvenue*. BiB Batteries. URL: https://bib-batteries.fr/ (visited on 05/24/2024).

[13] Samuel Boahen and Choi. “A Study on the Performance of a Cascade Heat Pump for Generating Hot Water”. In: *Energies* 12 (Nov. 12, 2019), p. 4313. DOI: 10.3390/en12224313.

[14] Jonas Bodner et al. “Analysis of low-temperature pumped thermal energy storage systems based on a transcritical CO2 charging process”. In: *Energy Science & Engineering* 11.9 (2023). _eprint: https://onlinelibrary.wiley.com/doi/pdf/10.1002/e pp. 3289–3306. ISSN: 2050-0505. DOI: 10.1002/ese3.1505. URL: https://onlinelibrary.wiley.com/doi/abs/10.1002/ese3.1505 (visited on 10/21/2023).

[15] Michele Bottarelli and Francisco Javier González Gallero. “Energy Analysis of a Dual-Source Heat Pump Coupled with Phase Change Materials”. In: *Energies* 13.11 (Jan. 2020). Number: 11 Publisher: Multidisciplinary Digital Publishing Institute, p. 2933. ISSN: 1996-1073. DOI: 10.3390/en13112933. URL: https://www.mdpi.com/1996-1073/13/11/2933 (visited on 02/16/2024).

[16] Alexander Buttler and Hartmut Spliethoff. “Current status of water electrolysis for energy storage, grid balancing and sector coupling via power-to-gas and power-to-liquids: A review”. In: *Renewable and Sustainable Energy Reviews* 82 (Feb. 1, 2018), pp. 2440–2454. ISSN: 1364-0321. DOI: 10.1016/j.rser.2017.09.003. URL: https://www.sciencedirect.com/science/article/pii/S136403211731242X (visited on 05/24/2024).

[17] C. Smith, Z. Nicholls, K. Armour, W. Collins, P. Forster, M. Meinshausen, M. Palmer et al. “The Physical Science Basis. Contribution of Working Group I to 878 the Sixth Assessment Report of the Intergovernmental Panel on Climate Change, 2021”. In: *Climate Change 2021*.

[18] Hanmin Cai et al. “Technical assessment of electric heat boosters in low-temperature district heating based on combined heat and power analysis”. In: *Energy* 150 (May 1, 2018), pp. 938–949. ISSN: 0360-5442. DOI: 10.1016/j.

energy.2018.02.084. URL: https://www.sciencedirect.com/science/article/pii/S0360544218303128 (visited on 11/10/2023).

[19] Jingyong Cai, Feng Zhang, and Jie Ji. "Comparative analysis of solar-air dual source heat pump system with different heat source configurations". In: *Renewable Energy* 150 (May 1, 2020), pp. 191–203. ISSN: 0960-1481. DOI: 10.1016/j.renene.2019.12.128. URL: https://www.sciencedirect.com/science/article/pii/S0960148119320002 (visited on 02/18/2024).

[20] Marcella Calabrese et al. "Hydrogen Safety Challenges: A Comprehensive Review on Production, Storage, Transport, Utilization, and CFD-Based Consequence and Risk Assessment". In: *Energies* 17.6 (2024). ISSN: 1996-1073. DOI: 10.3390/en17061350. URL: https://www.mdpi.com/1996-1073/17/6/1350.

[21] Nicolas Campion et al. "Techno-economic assessment of green ammonia production with different wind and solar potentials". In: *Renewable and Sustainable Energy Reviews* 173 (Mar. 2023), p. 113057. ISSN: 13640321. DOI: 10.1016/j.rser.2022.113057. URL: https://linkinghub.elsevier.com/retrieve/pii/S1364032122009388 (visited on 05/06/2024).

[22] Yan Cao, Towhid Parikhani, and Ammar M. Bahman. "Thermodynamic and thermoeconomic analyses of an ejector/booster enhanced heat pump system with zeotropic mixture". In: *International Journal of Energy Research* 45.3 (2021). _eprint: https://onlinelibrary.wiley.com/doi/pdf/10.1002/er.6114, pp. 4443–4465. ISSN: 1099-114X. DOI: 10.1002/er.6114. URL: https://onlinelibrary.wiley.com/doi/abs/10.1002/er.6114 (visited on 02/17/2024).

[23] Marcelo Carmo et al. "A comprehensive review on PEM water electrolysis". In: *International Journal of Hydrogen Energy* 38.12 (Apr. 22, 2013), pp. 4901–4934. ISSN: 0360-3199. DOI: 10.1016/j.ijhydene.2013.01.151. URL: https://www.sciencedirect.com/science/article/pii/S0360319913002607 (visited on 05/12/2024).

[24] *Carnot battery*. In: *Wikipedia*. Page Version ID: 1218010861. Apr. 9, 2024. URL: https://en.wikipedia.org/w/index.php?title=Carnot_battery&oldid=1218010861 (visited on 05/23/2024).

[25] *CFD Modeling and Experimental Validation of an Alkaline Water Electrolysis Cell for Hydrogen Production*. URL: https://www.mdpi.com/2227-9717/8/12/1634 (visited on 10/28/2023).

[26] *ChemiCal energy Storage*. URL: https://ease-storage.eu/wp-content/uploads/2016/03/EASE_TD_Hydrogen.pdf.

[27] *Fuel Cell TeChnology A Clean, Reliable Source of Stationary Power*. 2010. URL: https://www.cesa.org/wp-content/uploads/CESA-fuelcelltechnology-may2010.pdf.

[28] Wesley Cole and Akash Karmakar. "Cost Projections for Utility-Scale Battery Storage: 2023 Update". In: *Renewable Energy* (2023).

[29] Wikimedia Commons. *File:Absorption heat transformer process scheme.png — Wikimedia Commons, the free media repository*. [Online; accessed 24-May-2024]. 2023. URL: %5Curl%7Bhttps://commons.wikimedia.org/w/index.php?title=File:Absorption_heat_transformer_process_scheme.png&oldid=780226276%7D.

[30] Diederik Coppitters, Ward De Paepe, and Francesco Contino. "Surrogate-assisted robust design optimization and global sensitivity analysis of a directly coupled photovoltaic-electrolyzer system under techno-economic uncertainty". In: *Applied Energy* 248 (Aug. 15, 2019), pp. 310–320. ISSN: 0306-2619. DOI: 10.1016/j.apenergy.2019.04.101. URL: https://www.sciencedirect.com/science/article/pii/S0306261919307573 (visited on 05/15/2024).

[31] José M Corberán et al. "Dual source heat pump, a high efficiency and cost-effective alternative for heating, cooling and DHW production". In: *International Journal of Low-Carbon Technologies* 13.2 (June 1, 2018), pp. 161–176. ISSN: 1748-1317. DOI: 10.1093/ijlct/cty008. URL: https://doi.org/10.1093/ijlct/cty008 (visited on 02/16/2024).

[32] IBERDROLA CORPORATIVA. *Iberdrola builds the largest green hydrogen plant for industrial use in Europe*. Iberdrola. URL: https://www.iberdrola.com/about-us/what-we-do/green-hydrogen/puertollano-green-hydrogen-plant (visited on 05/16/2024).

[33] *Cours en ligne et simulateur de thermodynamique appliquée*. URL: https://direns.mines-paristech.fr/Sites/Thopt/fr/co/ejecteurs.html (visited on 04/22/2024).

[34] *Critical Minerals – Topics*. IEA. URL: https://www.iea.org/topics/critical-minerals (visited on 05/24/2024).

[35] O. Dumont and V. Lemort. "Mapping of performance of pumped thermal energy storage (Carnot battery) using waste heat recovery". In: *Energy* 211 (Nov. 15, 2020), p. 118963. ISSN: 0360-5442. DOI: 10.1016/j.energy.2020.118963. URL: https://www.sciencedirect.com/science/article/pii/S0360544220320703 (visited on 10/21/2023).

[36] Olivier Dumont et al. “Carnot battery technology: A state-of-the-art review”. In: *Journal of Energy Storage* 32 (Dec. 1, 2020), p. 101756. ISSN: 2352-152X. DOI: 10.1016/j.est.2020.101756. URL: https://www.sciencedirect.com/science/article/pii/S2352152X20315930 (visited on 10/21/2023).

[37] *Efficiency of batteries worldwide 2023*. Statista. URL: https://www.statista.com/statistics/1423012/efficiency-of-battery-energy-systems/ (visited on 05/16/2024).

[38] Giuseppe Emmi, Angelo Zarrella, and Michele De Carli. “A heat pump coupled with photovoltaic thermal hybrid solar collectors: A case study of a multi-source energy system”. In: *Energy Conversion and Management* 151 (Nov. 1, 2017), pp. 386–399. ISSN: 0196-8904. DOI: 10.1016/j.enconman.2017.08.077. URL: https://www.sciencedirect.com/science/article/pii/S0196890417308026 (visited on 02/18/2024).

[39] Lixin Fan, Zhengkai Tu, and Siew Hwa Chan. “Recent development of hydrogen and fuel cell technologies: A review”. In: *Energy Reports* 7 (Nov. 1, 2021), pp. 8421–8446. ISSN: 2352-4847. DOI: 10.1016/j.egyr.2021.08.003. URL: https://www.sciencedirect.com/science/article/pii/S2352484721006053 (visited on 05/24/2024).

[40] Guido Francesco Frate, Lorenzo Ferrari, and Umberto Desideri. “Multi-criteria investigation of a pumped thermal electricity storage (PTES) system with thermal integration and sensible heat storage”. In: *Energy Conversion and Management* 208 (Mar. 15, 2020), p. 112530. ISSN: 0196-8904. DOI: 10.1016/j.enconman.2020.112530. URL: https://www.sciencedirect.com/science/article/pii/S0196890420300662 (visited on 10/21/2023).

[41] Guido Francesco Frate, Lorenzo Ferrari, and Umberto Desideri. “Rankine Carnot Batteries with the Integration of Thermal Energy Sources: A Review”. In: *Energies* 13.18 (Jan. 2020). Number: 18 Publisher: Multidisciplinary Digital Publishing Institute, p. 4766. ISSN: 1996-1073. DOI: 10.3390/en13184766. URL: https://www.mdpi.com/1996-1073/13/18/4766 (visited on 05/14/2024).

[42] Guido Francesco Frate, Lorenzo Ferrari, and Umberto Desideri. “Techno-Economic Comparison of Brayton Pumped Thermal Electricity Storage (PTES) Systems Based on Solid and Liquid Sensible Heat Storage”. In: *Energies* 15 (Dec. 2022), p. 9595. DOI: 10.3390/en15249595.

[43] *Fuel Cell Benefits - Plug Power*. June 22, 2020. URL: https://www.plugpower.com/fuel-cell-power/fuel-cell-benefits/,%20https://www.plugpower.com/fuel-cell-power/fuel-cell-benefits/ (visited on 05/16/2024).

[44] Bourasseau Gracia Casero. *Energies | Free Full-Text | Use of Hydrogen in Off-Grid Locations, a Techno-Economic Assessment*. URL: https://www.mdpi.com/1996-1073/11/11/3141 (visited on 05/24/2024).

[45] *GSO power*. URL: https://www.gsopower.com/.

[46] Zongwei Han et al. "Simulation of a multi-source hybrid heat pump system with seasonal thermal storage in cold regions". In: *Applied Thermal Engineering* 116 (Apr. 1, 2017), pp. 292–302. ISSN: 1359-4311. DOI: 10.1016/j.applthermaleng.2017.01.057. URL: https://www.sciencedirect.com/science/article/pii/S1359431116327016 (visited on 02/16/2024).

[47] *Heat generation*. Home in the Earth. URL: https://www.homeintheearth.com/tech_notes/conventional-systems/hvac/heat-generation/ (visited on 11/11/2023).

[48] Florian Heberle, Christopher Schifflechner, and Dieter Brüggemann. "Life cycle assessment of Organic Rankine Cycles for geothermal power generation considering low-GWP working fluids". In: *Geothermics* 64 (Nov. 1, 2016), pp. 392–400. ISSN: 0375-6505. DOI: 10.1016/j.geothermics.2016.06.010. URL: https://www.sciencedirect.com/science/article/pii/S0375650516300669 (visited on 05/20/2024).

[49] Xander van Heule, Michel De Paepe, and Steven Lecompte. "Two-Phase Volumetric Expanders: A Review of the State-of-the-Art". In: *Energies* 15.14 (Jan. 2022). Number: 14 Publisher: Multidisciplinary Digital Publishing Institute, p. 4991. ISSN: 1996-1073. DOI: 10.3390/en15144991. URL: https://www.mdpi.com/1996-1073/15/14/4991 (visited on 11/15/2023).

[50] LE BOULZEC Hugo. "La production d'hydrogène «vert »". In: ().

[51] "Innovation outlook: Thermal energy storage". In: ().

[52] Fredrik Jonsson and Andrea Miljanovic. "UTILIZATION OF WASTE HEAT FROM HYDROGEN PRODUCTION". In: ().

[53] Hae Won Jung et al. "Performance comparison between a single-stage and a cascade multi-functional heat pump for both air heating and hot water supply". In: *International Journal of Refrigeration* (2013).

[54] Ali Kakavand et al. "Techno-economic assessment of green hydrogen and ammonia production from wind and solar energy in Iran". In: *International Journal of Hydrogen Energy* 48.38 (May 1, 2023), pp. 14170–14191. ISSN: 0360-3199. DOI: 10.1016/j.ijhydene.2022.12.285. URL: https://www.sciencedirect.com/science/article/pii/S0360319922061481 (visited on 05/15/2024).

[55] *La densité énergétique de l'hydrogène : une propriété unique*. Demaco Cryogenics. URL: https://demaco-cryogenics.com/fr/blog/la-densite-energetique-de-lhydrogene-une-propriete-unique/ (visited on 05/15/2024).

[56] Vincent Laguna Aguirrez. *Thermal integration of Carnot Batteries in energy systems*. 2022.

[57] Youcef Laouid et al. "Performance analysis and optimisation of a reheat organic Rankine cycle". In: *International Journal of Sustainable Energy* 41 (Oct. 2021). DOI: 10.1080/14786451.2021.1990294.

[58] Renato M. Lazzarin. "Dual source heat pump systems: Operation and performance". In: *Energy and Buildings* 52 (Sept. 1, 2012), pp. 77–85. ISSN: 0378-7788. DOI: 10.1016/j.enbuild.2012.05.026. URL: https://www.sciencedirect.com/science/article/pii/S0378778812002812 (visited on 10/21/2023).

[59] Jean Lemale. *LES POMPES À CHALEUR*. DUNOD, 2014.

[60] Matthieu Lerondeau. *Transport et stockage d'hydrogène*. Leonard, prospective et innovation par VINCI. May 1, 2021. URL: https://leonard.vinci.com/transport-et-stockage-dhydrogene/ (visited on 05/15/2024).

[61] Shengyu Li et al. "Performance assessment and working fluid selection for heat recovery ejector heat pump system in cold climatic conditions". In: *International Journal of Refrigeration* 158 (Feb. 1, 2024), pp. 313–328. ISSN: 0140-7007. DOI: 10.1016/j.ijrefrig.2023.12.012. URL: https://www.sciencedirect.com/science/article/pii/S0140700723004681 (visited on 04/18/2024).

[62] Fang Liu. "Review on Ejector Efficiencies in Various Ejector Systems". In: (2014).

[63] Fang Liu and Eckhard A. Groll. "Study of ejector efficiencies in refrigeration cycles". In: *Applied Thermal Engineering* 52.2 (Apr. 15, 2013), pp. 360–370. ISSN: 1359-4311. DOI: 10.1016/j.applthermaleng.2012.12.001. URL: https://www.sciencedirect.com/science/article/pii/S135943111200806X (visited on 04/18/2024).

[64] Daniel Maestre-Cambronel et al. "Thermoeconomic analysis of improved exhaust waste heat recovery system for natural gas engine based on Vortex Tube heat booster and supercritical CO2 Brayton cycle". In: *Sustainable Energy Technologies and Assessments* 47 (Oct. 1, 2021), p. 101355. ISSN: 2213-1388. DOI: 10.1016/j.seta.2021.101355. URL: https://www.sciencedirect.com/science/article/pii/S2213138821003659 (visited on 11/10/2023).

[65] Daniel Maraver et al. “Systematic optimization of subcritical and transcritical organic Rankine cycles (ORCs) constrained by technical parameters in multiple applications”. In: *Applied Energy* 117 (Mar. 15, 2014), pp. 11–29. ISSN: 0306-2619. DOI: 10.1016/j.apenergy.2013.11.076. URL: https://www.sciencedirect.com/science/article/pii/S0306261913009859 (visited on 05/14/2024).

[66] Stefania Marini et al. “Advanced alkaline water electrolysis”. In: *Electrochimica Acta*. ELECTROCHEMICAL FRONTIERS IN GLOBAL ENVIRONMENT AND ENERGY 82 (Nov. 1, 2012), pp. 384–391. ISSN: 0013-4686. DOI: 10.1016/j.electacta.2012.05.011. URL: https://www.sciencedirect.com/science/article/pii/S001346861200713X (visited on 10/10/2023).

[67] Konrad Meier. “Hydrogen production with sea water electrolysis using Norwegian offshore wind energy potentials”. In: *Int J Energy Environ Eng* 5.2 (May 13, 2014), p. 104. ISSN: 2251-6832. DOI: 10.1007/s40095-014-0104-6. URL: https://doi.org/10.1007/s40095-014-0104-6 (visited on 04/26/2024).

[68] Eric R. Morgan, James F. Manwell, and Jon G. McGowan. “Sustainable Ammonia Production from U.S. Offshore Wind Farms: A Techno-Economic Review”. In: *ACS Sustainable Chem. Eng.* 5.11 (Nov. 6, 2017). Publisher: American Chemical Society, pp. 9554–9567. DOI: 10.1021/acssuschemeng.7b02070. URL: https://doi.org/10.1021/acssuschemeng.7b02070 (visited on 05/15/2024).

[69] Hossein Nami, Peter V Hendriksen, and Henrik Lund Frandsen. “AEC- and SOEC-based routes to green ammonia”. In: ().

[70] *NSRDB*. URL: https://nsrdb.nrel.gov/ (visited on 05/24/2024).

[71] Torben Ommen et al. “Performance of ultra low temperature district heating systems with utility plant and booster heat pumps”. In: *Energy* 137 (Oct. 15, 2017), pp. 544–555. ISSN: 0360-5442. DOI: 10.1016/j.energy.2017.05.165. URL: https://www.sciencedirect.com/science/article/pii/S0360544217309544 (visited on 11/10/2023).

[72] Jean-François Oudkerk. “Modélisation, simulation et contrôle d’un cycle de Rankine organique en régime dynamique.” In: ().

[73] *Pinch analysis (2022)*. URL: https://www.ipieca.org/resources/energy-efficiency-database/pinch-analysis-2022#:~:text=A%20’pinch’%20occurs%20where%20the,cost%20and%20higher%20utility%20cost..

[74] *Processes | Free Full-Text | Comparison of the New Refrigerant R1336mzz(E) with R1234ze(E) as an Alternative to R134a for Use in Heat Pumps*. URL: https://www.mdpi.com/2227-9717/10/2/218 (visited on 02/17/2024).

[75] *Production d'hydrogène renouvelable : comment ça marche ? | ENGIE*. Engie.com. URL: https://www.engie.com/renouvelables/hydrogene/production-hydrogene-renouvelable (visited on 05/12/2024).

[76] Joris Proost. "State-of-the art CAPEX data for water electrolysers, and their impact on renewable hydrogen price settings". In: *International Journal of Hydrogen Energy*. European Fuel Cell Conference & Exhibition 2017 44.9 (Feb. 15, 2019), pp. 4406–4413. ISSN: 0360-3199. DOI: 10.1016/j.ijhydene.2018.07.164. URL: https://www.sciencedirect.com/science/article/pii/S0360319918324157 (visited on 05/23/2024).

[77] Fatemeh Rajaee et al. "Techno-economic evaluation of an organic rankine cycle-based multi-source energy system for 100%-renewable power supply: A rural case study". In: *Sustainable Cities and Society* 89 (Feb. 1, 2023), p. 104290. ISSN: 2210-6707. DOI: 10.1016/j.scs.2022.104290. URL: https://www.sciencedirect.com/science/article/pii/S2210670722005947 (visited on 05/20/2024).

[78] Krishnan Rajeshwar, Robert D. McConnell, and S. Licht, eds. *Solar hydrogen generation: toward a renewable energy future*. New York, NY: Springer, 2008. 318 pp. ISBN: 978-0-387-72809-4 978-0-387-72810-0.

[79] *Rankine - an overview ScienceDirect Topics*. URL: https://www.sciencedirect.com/topics/engineering/rankine (visited on 10/28/2023).

[80] *Réglementation des fluides frigorigènes*. Energie Plus Le Site. URL: https://energieplus-lesite.be/reglementations/climatisation-et-refrigeration3/reglementation-des-fluides-frigorigenes/ (visited on 05/30/2024).

[81] *Review of Carnot Battery Technology Commercial Development*. URL: https://www.mdpi.com/1996-1073/15/2/647# (visited on 10/28/2023).

[82] *Sensible heat storage - Norvento - Norvento*. URL: https://www.norvento.com/en/blog/sensible-heat-storage/ (visited on 05/20/2024).

[83] S. Shiva Kumar and V. Himabindu. "Hydrogen production by PEM water electrolysis – A review". In: *Materials Science for Energy Technologies* 2.3 (Dec. 1, 2019), pp. 442–454. ISSN: 2589-2991. DOI: 10.1016/j.mset.2019.03.002. URL: https://www.sciencedirect.com/science/article/pii/S2589299119300035 (visited on 05/12/2024).

[84] J. Siecker, K. Kusakana, and B. P. Numbi. "Optimal heat recovery during polymer electrolyte membrane electrolysis". In: *International Journal of Hydrogen Energy* 47.76 (Sept. 5, 2022), pp. 32692–32706. ISSN: 0360-3199. DOI: 10.1016/j.ijhydene.2022.07.169. URL: https://www.sciencedirect.com/science/article/pii/S0360319922032220 (visited on 05/24/2024).

[85] *Stockage par chaleur latente*. URL: http://www.recuperation-chaleur.fr/stockage-par-chaleur-latente (visited on 05/13/2024).

[86] *STOLECT teste le stockage par batterie de Carnot*. Techniques de l'Ingénieur. URL: https://www.techniques-ingenieur.fr/actualite/articles/stolect-teste-le-stockage-par-batterie-de-carnot-123251/ (visited on 05/23/2024).

[87] Francesco Superchi et al. "Development of a reliable simulation framework for techno-economic analyses on green hydrogen production from wind farms using alkaline electrolyzers". In: *Renewable Energy* 207 (May 1, 2023), pp. 731–742. ISSN: 0960-1481. DOI: 10.1016/j.renene.2023.03.077. URL: https://www.sciencedirect.com/science/article/pii/S0960148123003725 (visited on 05/24/2024).

[88] URL: https://sam.nrel.gov/.

[89] M. Tahir Erdinc et al. "Performance improvement potential of a PV/T integrated dual-source heat pump unit with a pressure booster ejector". In: *Thermal Science and Engineering Progress* 37 (Jan. 1, 2023), p. 101534. ISSN: 2451-9049. DOI: 10.1016/j.tsep.2022.101534. URL: https://www.sciencedirect.com/science/article/pii/S2451904922003407 (visited on 02/16/2024).

[90] Robin Tassenoy et al. "INTRODUCTION OF A HIGH-LEVEL, APPLICATION BASED SIZING METHODOLOGY FOR CARNOT BATTERIES". In: (2021).

[91] Robin Tassenoy et al. "Techno-economic assessment of Carnot batteries for load-shifting of solar PV production of an office building". In: *Renewable Energy* 199 (Nov. 1, 2022), pp. 1133–1144. ISSN: 0960-1481. DOI: 10.1016/j.renene.2022.09.039. URL: https://www.sciencedirect.com/science/article/pii/S0960148122013891 (visited on 05/20/2024).

[92] *Update on New Refrigerants Designations and Safety Classifications*. URL: https://www.ashrae.org/file%20library/technical%20resources/bookstore/factsheet_ashrae_english_november2022.pdf.

[93] Els Van Der Roest et al. "Utilisation of waste heat from PEM electrolysers – Unlocking local optimisation". In: *International Journal of Hydrogen Energy* 48.72 (Aug. 2023), pp. 27872–27891. ISSN: 03603199. DOI: 10.1016/j.ijhydene.2023.03.374. URL: https://linkinghub.elsevier.com/retrieve/pii/S0360319923015410 (visited on 05/24/2024).

[94] Kevin Verleysen, Alessandro Parente, and Francesco Contino. "How sensitive is a dynamic ammonia synthesis process? Global sensitivity analysis of a dynamic Haber-Bosch process (for flexible seasonal energy storage)". In: *Energy* 232 (Oct. 1, 2021), p. 121016. ISSN: 0360-5442. DOI: 10.1016/j.energy.

2021.121016. URL: https://www.sciencedirect.com/science/article/pii/S0360544221012640 (visited on 05/24/2024).

[95] Kevin Verleysen et al. "How can power-to-ammonia be robust? Optimization of an ammonia synthesis plant powered by a wind turbine considering operational uncertainties". In: *Fuel* 266 (Apr. 15, 2020), p. 117049. ISSN: 0016-2361. DOI: 10.1016/j.fuel.2020.117049. URL: https://www.sciencedirect.com/science/article/pii/S0016236120300442 (visited on 05/24/2024).

[96] Min Wang, Yue Cheng, and Jianlin Yu. "Analysis of a dual-temperature air source heat pump cycle with an ejector". In: *Applied Thermal Engineering* 193 (July 5, 2021), p. 116994. ISSN: 1359-4311. DOI: 10.1016/j.applthermaleng.2021.116994. URL: https://www.sciencedirect.com/science/article/pii/S1359431121004415 (visited on 02/16/2024).

[97] Maximilian Weitzer, Dominik Müller, and Jürgen Karl. "Two-phase expansion processes in heat pump – ORC systems (Carnot batteries) with volumetric machines for enhanced off-design efficiency". In: *Renewable Energy* 199 (Nov. 1, 2022), pp. 720–732. ISSN: 0960-1481. DOI: 10.1016/j.renene.2022.08.143. URL: https://www.sciencedirect.com/science/article/pii/S0960148122013222 (visited on 11/15/2023).

[98] Maximilian Weitzer et al. "Organic flash cycles in Rankine-based Carnot batteries with large storage temperature spreads". In: *Energy Conversion and Management* 255 (Mar. 1, 2022), p. 115323. ISSN: 0196-8904. DOI: 10.1016/j.enconman.2022.115323. URL: https://www.sciencedirect.com/science/article/pii/S0196890422001194 (visited on 10/21/2023).

[99] Alexander White, Geoff Parks, and Christos N. Markides. "Thermodynamic analysis of pumped thermal electricity storage". In: *Applied Thermal Engineering*. Includes Special Issue: PRO-TEM Special Issue 53.2 (May 2, 2013), pp. 291–298. ISSN: 1359-4311. DOI: 10.1016/j.applthermaleng.2012.03.030. URL: https://www.sciencedirect.com/science/article/pii/S1359431112002141 (visited on 05/13/2024).

[100] Wu Xu and Keith Scott. "The effects of ionomer content on PEM water electrolyser membrane electrode assembly performance". In: *International Journal of Hydrogen Energy*. VIII symposium of the Mexican Hydrogen Society 35.21 (Nov. 1, 2010), pp. 12029–12037. ISSN: 0360-3199. DOI: 10.1016/j.ijhydene.2010.08.055. URL: https://www.sciencedirect.com/science/article/pii/S0360319910016940 (visited on 05/24/2024).

[101] Claire Yu Yan. "6.2 Refrigerator and heat pump". In: (Sept. 1, 2022). Book Title: Introduction to Engineering Thermodynamics. URL: https://pressbooks.bccampus.ca/thermo1/chapter/6-2-refrigerator-and-heat-pump/ (visited on 05/23/2024).

[102] Michele Zehnder. “Efficient air-water heat pumps for high temperature lift residential heating, including oil migration aspects”. PhD thesis. Lausanne: EPFL, 2004. 257 pp. DOI: 10.5075/epfl-thesis-2998.

[103] Bo Zhang and Xiangji Guo. “Prospective applications of Ranque–Hilsch vortex tubes to sustainable energy utilization and energy efficiency improvement with energy and mass separation”. In: *Renewable and Sustainable Energy Reviews* 89 (June 1, 2018), pp. 135–150. ISSN: 1364-0321. DOI: 10.1016/j.rser.2018.02.026. URL: https://www.sciencedirect.com/science/article/pii/S1364032118300534 (visited on 12/02/2023).

[104] Jia-ling Zhu et al. “A thermodynamics comparison of subcritical and transcritical organic Rankine cycle system for power generation”. In: *J. Cent. South Univ.* 22.9 (Sept. 2015), pp. 3641–3649. ISSN: 2095-2899, 2227-5223. DOI: 10.1007/s11771-015-2905-z. URL: http://link.springer.com/10.1007/s11771-015-2905-z (visited on 05/24/2024).

[105] Emmanuel Zoulias et al. “A REVIEW ON WATER ELECTROLYSIS”. In: ().

[106] B. Zühlsdorf et al. “Improving the performance of booster heat pumps using zeotropic mixtures”. In: *Energy* 154 (July 1, 2018), pp. 390–402. ISSN: 0360-5442. DOI: 10.1016/j.energy.2018.04.137. URL: https://www.sciencedirect.com/science/article/pii/S0360544218307539 (visited on 11/10/2023).

UNIVERSITÉ CATHOLIQUE DE LOUVAIN
École polytechnique de Louvain
Rue Archimède, 1 bte L6.11.01, 1348 Louvain-la-Neuve, Belgique | **www.uclouvain.be/epl**